Dissertation der
Graduate School of Systemic Neurosciences der
Ludwig-Maximilians-Universität München

The role of pericytes in microcirculatory dysfunction after subarachnoid hemorrhage

Kathrin Nehrkorn (geb. Schüller)

25. April 2016

Dissertation at the
Graduate School of Systemic Neurosciences
Ludwig-Maximilians-Universität München
Munich, Germany

Graduate School of
Systemic Neurosciences
LMU Munich

The role of pericytes in microcirculatory dysfunction after subarachnoid hemorrhage

Kathrin Nehrkorn (née Schüller)

Submitted on 8th of April 2015

1st supervisor and reviewer

Prof. Dr. Nikolaus Plesnila

2nd reviewer

Prof. Dr. Martin Kerschensteiner

3rd reviewer

Fatima A. Sehba, PhD

Date of submission

8th of April 2015

Date of oral defense

25th of April 2016

Contents

A Abstract

Subarachnoid hemorrhage is a subtype of stroke that is caused by a bleeding into the subarachnoid space. Cerebral ischemia develops early after the bleeding and has a negative influence on outcome in patients. The underlying pathophysiology triggering early ischemia has not been characterized in detail. Suggested pathomechnisms are pial microvasospasm, endothelial dysfunction and microthrombosis. The aim of the current thesis was to characterize and reveal the pathophysiology of microcirculatory perfusion deficits early after subarachnoid hemorrhage. The main hypothesis was that pericytes constrict upon subarachnoid hemorrhage and thereby induce capillary spasm and hamper parenchymal blood flow dynamics.

We found that pial arterioles constrict in three different characteristic patterns and that spastic vessel segments were continuously covered with vascular smooth muscle cells. Superficial microvasospasm was associated with reduced blood flow velocity and significant reduction of endothelial intracellular Ca^{2+} concentration which may be a trigger for endothelial dysfunction. Reduced blood flow velocity in combination with reduced vessel diameter diminished total blood volume that reached the parenchymal microcirculation via penetrating arterioles. This led to a severe reduction of perfused capillary volume in the cortex. Leukocyte numbers that were sticking in capillaries and venules were increased after subarachnoid hemorrhage but their numbers were too low to explain severe perfusion deficits.

Capillaries revealed a significantly reduced vessel diameter after subarachnoid hemorrhage, however vessel narrowings were not co-localizing with sites where pericytes were associated to capillaries. Furthermore pericytes neither underwent cell death nor migrated away from capillaries within 24 hours after the bleeding.

In conclusion we showed that microvasospasm on the brain surface lead to severe perfusion deficits in the parenchyma. Microvasospasm are probably induced by vascular smooth muscle cells and are accompanied by reduced intracellular Ca^{2+} concentration in endothelial cells. Pericytes do not play a major role in the pathophysiology of early ischemia after subarachnoid hemorrhage: they neither migrate, nor die or induce capillary spasm.

B Introduction

1. Subarachnoid hemorrhage

1.1. Clinical features

1.1.1. Epidemiology

Subarachnoid hemorrhage (SAH) is a rather rare subtype of stroke. In 2005 the annual age adjusted incidence in Northern Americans was nine per 100,000.[1] With this incidence it accounts for about four percent of all stroke cases. However research in the field of SAH is urgently needed, as the case fatality rate is high varying between 23 and 67%.[2] 21% of patients die within the first day after the bleeding and 16% even before submission to hospital; the cumulative case fatality within the first month after the bleeding levels at 44%.[3] These numbers show that acute mortality after SAH accounts for half of the fatal cases and is therefore clinically highly relevant. Regarding the twelve month modified Rankin scale the overall clinical outcome of surviving patients is low.[4] As patients suffer from SAH at a relatively young age and during their productive phase the socio-economic cost of SAH is highly relevant. In Germany the five-year-cost of each SAH patient is 38 300 Euros.[5]

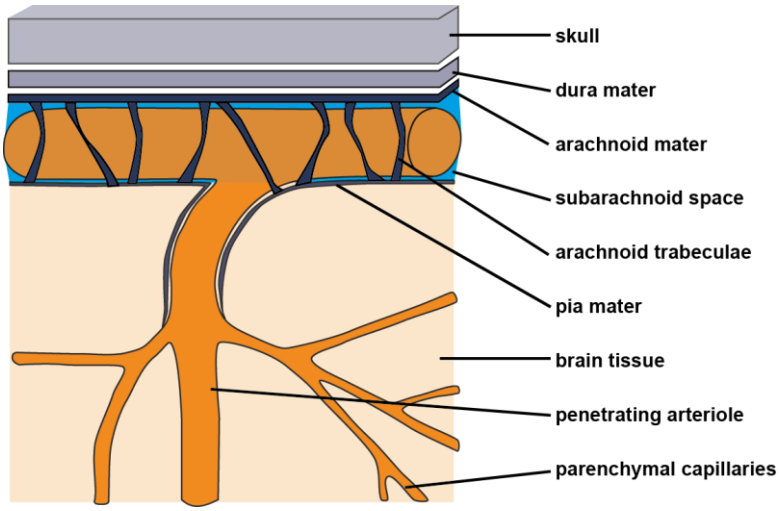

In 85% of SAH cases a bleeding into the subarachnoid space occurs due to the rupture of an aneurysm.[6] Aneurysms develop during the course of life and are present in two to three percent of healthy 50-year-old persons. The occurrence of aneurysms is associated with certain risk factors like a positive family history for SAH or polycystic kidney disease.[7] An association with atherosclerosis was suspected but could not be reproduced in a meta-analysis.[7] A connective tissue weakness may lead to a widening of cerebral arteries at locations of increased mechanical stress. Saccular vessel malformations develop primarily at branching points of the Circle of Willis,[8] an arterial

vessel ring located at the base of the brain. The wall of aneurysms is thin and thereby prone to rupture. Another more benign form of subarachnoid hemorrhage is perimesencephalic hemorrhage where the source of bleeding is presumably venous and subarachnoid blood is confined to small areas at the base of the brain without causing an increase of intracranial pressure (ICP). Hence the prognosis of perimesencephalic hemorrhage is much better than that of aneurysmal SAH.[9]

1.1.2. Symptoms

The cardinal symptom of patients with acute SAH is sudden headache that is described by patients as the worst pain of their lifetime. For half of the patients the onset headache is instantaneous and associated with exertion.[10] Headache is caused by irritation of the dura mater by subarachnoid blood and lasts for about two weeks with decreasing intensity. Neck stiffness is caused by irritation through blood products in the subarachnoid space and occurs within several hours after the bleeding. Another common symptom after SAH is depressed consciousness, which can result in coma. It may be the cause of an elevated ICP that results in a reduced cerebral perfusion pressure (CPP) and hence global cerebral ischemia.[11] Focal neurological deficits like aphasia or nerve palsy can occur when brain areas around the location of the vessel malformation are affected.[12] Generalized seizures occur in 7.8% of patients within one hour after onset of headache and are a predictor for high disability five weeks after SAH.[13] Nausea and vomiting is another common but unspecific symptom in SAH patients.[14] It may be caused by elevated ICP due to the volume effect of extravasated blood. A hydrocephalus develops when clotted blood plugs the arachnoid granulation, a structure derived from the dura mater which drains the CSF from the subarachnoid space into the venous sinus of the brain. Hydrocephalus symptoms range from a decline of consciousness to gaze impairment and non-reactive pupils.[15] It is a predictor for poor outcome twelve months after SAH.[16] SAH can be accompanied by retinal bleeding (Terson's syndrome)[17] which induces blurred vision. Alterations of the electrocardiogram reflect ischemic heart disease and are diagnosed in 90% of SAH patients within 24 hours after the bleeding.[18] Episodes of cardiac arrest occur in three percent of SAH patients and are associated with poor clinical outcome. Mortality of patients with cardiac arrest is significantly higher than of those without cardiac arrest.[19]

Rebleedings from the ruptured aneurysm occur in 14% of the patients within the first 24 hours after the bleeding.[20] During the first 21 days after the hemorrhage the cumulative risk for rebleeding is 39%. Rebleedings are often detrimental for patients and in 78% associated with poor outcome.[21] Rebleedings manifest in a sudden deterioration of clinical symptoms.

Delayed cerebral ischemia is a secondary event that develops four to 15 days after the initial bleeding in 27% of the patients.[22] The cumulative risk for delayed cerebral ischemia within 21 days after SAH is 34%.[23] It manifests in focal neurological deficits

and/or depressed consciousness.[24] Vessel spasm of big brain supplying arteries are held responsible for the occurrence of delayed cerebral ischemia after SAH.

1.1.3. Diagnosis

Subarachnoid blood can be identified in 98.5% of patients within the first six hours after the bleeding by computer tomography (CT). Over time subarachnoid blood is cleared and therefore not regularly detectable by CT, therefore the sensitivity of SAH diagnosis by CT drops to 90% when performed more than six hours after the bleeding.[25] False positive interpretation of CT scans may occur due to acute brain swelling, when congested blood in subarachnoid vessels may be misinterpreted as extravasated subarachnoid blood.[26] Acute hydrocephalus is diagnosed by ventricle measurement in repetitive CT scans. At late investigation time points magnetic resonance tomography (MRT) scans more sensitively portray subarachnoid blood. T2 scans reveal a sensitivity of 100% and FLAIR scans of 87% in the subacute phase after SAH.[27] When subarachnoid blood is found in the initial scan an angiography is performed to identify the location and size of aneurysm. The exact localization is needed for surgical obliteration of the bleeding site. Angiography can either be performed by catheter angiography or by CT and MR angiography.[28] The gold standard of aneurysm diagnosis is digital subtraction angiography as especially small aneurysms are not always detected by native imaging techniques.[29] A lumbar puncture of cerebrospinal fluid (CSF) is necessary for SAH diagnosis in patients with an uncertain CT scan. Only the detection of the hemoglobin breakdown product bilirubin in the CSF is conclusive as contaminations with hemoglobin occur in ten percent of lumbar punctures.[30] Therefore a puncture should be performed twelve hours after the onset of symptoms to allow the erythrocytes in the CSF to degenerate and form bilirubin.[31]

Vessel spasm of big brain supplying arteries and delayed cerebral ischemia can be detected by CT or conventional angiography combined with CT perfusion scan.[32] Transcranial Doppler sonography is a non-invasive indirect diagnostic method for vessel spasm which determines blood flow velocity in brain supplying arteries, mainly the Circle of Willis. Constricted vessel segments show an increased blood flow velocity.[33] However in the past years it became evident that vessel spasm do not seem to be the only cause of delayed cerebral ischemia. In one quarter to one third of delayed cerebral infarction in patients the common diagnostic imaging techniques are not able to predict infarction.[24] On the other hand a subset of patients develops delayed cerebral ischemia, which is independent of large artery spasm.[34] These numbers indicate that the pathophysiology of delayed cerebral ischemia cannot be confined to large vessel spasm. Accordingly the diagnosis of delayed cerebral ischemia after SAH needs to be adapted.

1.1.4. Therapy

The first treatment measures for SAH patients who arrive at the hospital are general intensive care procedures: Patients receive fluid by an intravenous line and the head is placed at an elevated position to enhance CSF drainage. Patients are intensively monitored for focal deficits and body temperature. Furthermore they are monitored with electrocardiography to detect and potentially treat cardiac complications. Extensive headache is treated with analgesics to comfort the patient and to keep blood pressure below 180 mmHg in order to avoid re-bleedings.[35]

The prevention of re-bleedings from the ruptured aneurysm is the primary goal of acute treatment after SAH. After identification of the bleeding site the aneurysm is surgically treated by clipping or coiling. Traditionally the ruptured aneurysm was obliterated by application of a clip at the aneurysm shaft. Therefore the skull has to be opened to make the aneurysm accessible for intervention. For coiling a small platinum coil is pushed into the aneurysm that triggers clot formation and its obliteration. The wire is applied by an endovascular approach[36] which makes coiling the less invasive technique. The decision which obliteration technique is employed depends on the size, shape and location of the aneurysm. An international trial comparing both techniques found an absolute risk reduction for poor outcome for coiling versus clipping.[37]

Patients who arrive at the hospital with depressed consciousness might suffer of global cerebral perfusion deficits due to elevated ICP. A conservative approach to reduce ICP is to administer hyperosmotic fluids which cause an osmotic gradient between the intravascular space and the brain parenchyma thereby reducing brain water content. In patients who do not respond to conservative therapy, an evacuation of the hematoma or a hemicraniectomy might be indicated to lower ICP. However a single center matched pair analysis between SAH patients that underwent decompressive craniectomy or conservative therapy revealed no difference in outcome between both treatments.[38]

A hydrocephalus may develop acutely after the hemorrhage due to plugging of the subarachnoid space with clotted blood. These clots can be lysed therapeutically by intraventricular application of recombinant tissue plasminogen activator.[39] Hydrocephalus resolves after successful clearance of the drainage system. If hydrocephalus persists CSF needs to be drained by lumbar puncture or ventricular catheterization.[35]

In the last decades many clinical trials were conducted in order to identify new drugs for the treatment of delayed cerebral ischemia and large vessel spasm: Ca^{2+} antagonists, namely Nimodipine, reduce the absolute risk of poor outcome during delayed cerebral ischemia by 5.3%.[40] In Germany 91% of surveyed centers use Nimodipine orally for prevention and treatment of delayed cerebral ischemia.[41] The endothelin-1 receptor antagonist Clazosentan significantly resolved angiographic vasospasm,[42] however, it

did not improve delayed cerebral ischemia and patient outcome.[43] Statins are discussed to improve vascular reactivity via cholesterol dependent mechanisms and restoration of endothelial function.[44] Pravastatin was suggested to reduce vasospasm and mortality associated to delayed cerebral ischemia.[45] However subsequent trials could not confirm the protective results of statins after SAH.[46, 47] Magnesium sulphate is thought to inhibit voltage gated Ca^{2+} channels thereby reducing contraction of vascular smooth muscle cells (VSMC). So far, however, clinical trials investigating the potential effect of magnesium after SAH were inconclusive. Thus no proof of a beneficial effect of magnesium on delayed cerebral ischemia exists.[48] Despite negative or inconclusive trails magnesium and statins are commonly used in clinical practice for the treatment of cerebral vasospasm due to the lack of alternatives and a reasonable safety profile.[41] A different therapeutic approach for delayed cerebral ischemia is the so-called triple H therapy that aims to facilitate cerebral perfusion by hemodilution, hypervolaemia and hypertension.[49] However a prospective clinical trial on triple H therapy has never been conducted. Potential negative side effects like pulmonary edema or renal dysfunction have to be kept in mind when evaluating the triple H therapy.[50] In clinical practice a targeted mean arterial blood pressure of 90 to 110 mmHg is achieved by administration of Norepinephrine and hypervolaemia/hemodilution is achieved by additional intravenous fluid administration of one to three liters electrolyte solution per day.[41]

Furthermore vessel spasm may be mechanically dilated by angioplasty or balloon vasodilatation using an endovascular approach. The endovascular balloon dilatation of spastic vessel segments was first described by Zubkov et al.[51] The combination of the endovascular dilation approach together with local application of vasodilative substances shows promising results for the opening of spastic vessel segments. However vasodilation by local application of papaverine did not sustain until the next day after intervention.[52]

In conclusion validated treatment options after SAH are rare. Nimodipine is to date the only therapy for delayed cerebral ischemia that proved efficacy in a prospective randomized trial. The most striking finding is that Clazosentan resolved vessel spasm but does not have a beneficial effect on delayed cerebral ischemia. The result of the trial indicates that delayed cerebral ischemia is probably multifactorial and cannot be narrowed down to cerebral large artery spasm.[53, 54] It implies that large vessel spasm might not be the correct therapeutic target for treatment of delayed cerebral ischemia. Research on the complex pathophysiology after SAH will have to be performed to identify new therapeutic targets.[55]

1.2. Animal models

In the past most experimental SAH studies have been conducted in larger laboratory animals such as dogs or rabbits. The double injection dog SAH model was a widely used animal model for the investigation of delayed cerebral ischemia and vasospasm.[56]

In the past years large laboratory animal research declined; today most of SAH research is performed in rodents like rats and mice.[56] Mice have the advantage that transgenic animals are available. The design of genetically modified mice offers new opportunities for experimental research but also the challenge to adopt microsurgically demanding animal models to these rather small rodents. At present a couple of different mouse SAH models exist where blood is either injected into the subarachnoid space or a subarachnoid vessel is perforated. The SAH blood injection model in rodents was first described by Solomon et al.[57] Autologous arterial blood withdrawn from a peripheral vessel is injected into the cisterna magna. This method is fast and relatively easy to perform. Animals develop an increased ICP, neurological deficits and delayed vasospasm.[58] However, the site of injection does not correspond to the clinical situation where bleeding mostly occurs at the Circle of Willis. Therefore another injection model has been established where the blood is applied into the prechiasmatic cistern[59] which corresponds to the usual bleeding site in patients. A drawback of the prechiasmatic injection model is that a needle needs to be pushed through the brain in order to reach the skull base. The biggest advantages of injection models are that the amount of injected blood can be controlled and that the effect of blood can be distinguished from the volume effect of saline injection in the sham situation. A drawback of the injection model is, however, that a vessel injury/rupture cannot be mimicked. An alternative approach for bleeding induction is to perforate a brain-supplying vessel and thereby induce a local bleeding. This can be achieved for example by intracisternal vein transection technique. A vein at the base of the brain is opened and allows a venous blood spill into the subarachnoid space.[60] However in the clinical condition SAH is mostly caused by an arterial bleeding which reveals a different blood pressure situation than veins. The vein transection technique therefore rather mimics the situation of a perimesencephalic SAH. In order to model the pathophysiology of an artery rupture the endovascular perforation model was developed.[61] This model was first described in rats by Bederson et al.[62] and Veelken et al.[63] A stiff filament is inserted into the left external carotid artery and advanced to the skull base via the internal carotid artery. At the bifurcation of the middle cerebral artery the filament perforates the Circle of Willis which initiates blood extravasation into the subarachnoid space.[64] This model reflects the clinical feature of a vessel injury and can also exhibit rebleedings, which occur in 39% of patients within 3 weeks after SAH.[21] The endovascular perforation model was adapted to mice by Kamii et al.[65] and Parra et al.[66] Provided that a standardized anesthesia protocol is used and ICP and CBF are monitored the mouse endovascular perforation model is highly reproducible and suited to investigate early brain injury after SAH.[67]

1.3. Pathophysiology

1.3.1. Delayed brain injury

Traditionally SAH research was primarily focused on delayed cerebral ischemia rather than early pathophysiologic events. Therefore to date most of mechanistic insights and therapeutic studies are based on delayed brain injury. Since the first description of large vessel constrictions after SAH in 1951[68] it was believed that artery spasm induce delayed cerebral ischemia. Vessel spasm of big brain supplying arteries are mediated by contraction of VSMC. Muscle fiber contraction is induced by Ca^{2+} influx through voltage dependent Ca^{2+} channels and a subsequent increase of the free intracellular Ca^{2+} concentration. Elevated Ca^{2+} levels initiate phosphorylation of myosin light chains and subsequent contraction.[69] After SAH contracted cerebral arteries tend to have a higher amount of phosphorylated myosin light chain than arteries of controls.[70]

Another potential pathomechanism of delayed vessel spasm is that hemoglobin in the subarachnoid space scavenges nitric oxide (NO), a potent soluble vasodilator. NO which is released from endothelial cells induces relaxation of VSMC via cyclic guanylatcyclase signaling.[71] When NO is bound by hemoglobin the expression levels of soluble cyclic guanylatcyclase is reduced and the endothelium dependent relaxation of cerebral vessels is impaired.[72] In this context also the production of reactive oxygen species after SAH plays a role. The conversion of hemoglobin to oxyhemoglobin releases superoxides, which together with NO form peroxynitrite, a neurotoxic substance.[73] If the free radical scavenging system is therapeutically enhanced by induction of the enzyme superoxide dismutase the production of superoxide can be diminished and vasospasm can be ameliorated.[65] The concept that free radicals play a role in the formation of vasospasm is strengthened by a study that shows amelioration of vasospasm under treatment with melatonin, a free radical scavenger and stimulator of antioxidant enzymes.[74]

Endothelin-1 is a potent vasoconstrictive peptide that is found in high concentration in the human CSF after SAH.[75] Continuous endothelin-1 infusion leads to sustained arterial constriction.[76] Endothelin-1 is overexpressed in endothelial cells and smooth muscle cells during superfusion with oxyhemoglobin and induces arterial narrowing.[77] Neutrophils infiltrating the brain parenchyma after SAH may be a source of increased endothelin-1 production.[78] Experimental data suggests that vessels become more sensitive to endothelin-1 after SAH and are thereby more prone to constrict in its presence.[79]

However the whole concept that spasm of cerebral arteries induce secondary brain infarction after SAH has been challenged by the results of the endothelin-1 antagonist Clazosentan trial. Despite successful reopening of the vessels the clinical outcome after SAH was not improved.[43] This study initiated research and discussion about different

mechanisms for the development of delayed brain injury. One proposed alternative pathomechanism for large vessel spasm is microthrombosis that induces disturbance of the microcirculation and hence delayed cerebral ischemia.[80] Recently other dysfunctions of the cerebral microcirculation like glial swelling and edema have been suggested to be causative for delayed cerebral ischemia.[81]

Another potential trigger for delayed cerebral ischemia is cortical spreading depression (CSD). It describes a mass depolarization of neurons and glia cells which is initiated by a massive efflux of K^+ into the extracellular space.[82] The cation derangement induces enhanced release of the excitatory neurotransmitter glutamate that triggers depolarization. The depolarization is self-propagating and induces increased CBF via neurovascular coupling in the healthy brain.[83] However when brain slices are superfused with hemolysis products, cortical depolarization leads to a vasoconstriction rather than a vasodilatation.[84] This finding initiated studies on CSD in SAH patients. Cortical electrical activity, partial pressure of oxygen and CBF were recorded on the surface of the cortex after SAH. Spreading depolarization occurred in 12 of 13 patients and were in 5 patients associated with local reduction of CBF and hypoxia.[85] These findings were confirmed by another study in which electrocorticography and oxygen pressure measurements were performed during aneurysm clipping.[86] The area of spreading depolarization co-localized with brain regions that later developed delayed cerebral ischemia.[87] However CSD alone is not likely to induce cerebral infarction because increased neuronal activity induces functional hyperemia in a healthy brain. Accordingly, CSD only leads to a relative lack of oxygen and glucose when functional hyperemia is impaired. Another hypothesis is that cortical spreading depression in combination with vessel spasm and formation of microemboli induces cerebral ischemia.[88]

1.3.2. Early brain injury

Early brain injury describes the pathophysiological changes that occur in the brain during the first three days after the bleeding.[89] Clinicians and researchers became aware that this period is particularly relevant for the pathogenesis of SAH when reversal of delayed vasospams with Clazosentan did not result in improvement of delayed cerebral ischemia and patient outcome. Therefore pathomechanisms of early brain injury have only recently moved into the focus of SAH research. Early brain injury is initiated by the impact of bleeding and composed of different key factors: These include the rise of ICP and subsequent drop of CPP as well as early cerebral ischemia, formation of brain edema, inflammation and neuronal cell death.[90]

1.3.2.1. Intracranial pressure

Upon aneurysm rupture the extravasating blood is filling the subarachnoid cisterns. The spill of blood out of the vessel staunches when a blood clot forms at the site of injury.

The volume effect of extravasated blood leads to an increase of ICP to values close to the systemic blood pressure[91] and compresses vessels which are located in the subarachnoid space.[92] In most cases ICP stabilizes within minutes at values slightly above normal. In other cases ICP remains elevated due to formation of a large hematoma, development of hydrocephalus or brain edema.[93] A mean ICP above 20 mmHg during the first seven days after the bleeding is associated with high mortality.[94] However the initial peak of ICP seems to be important to stop the bleeding from the ruptured aneurysm. A study that investigated ICP during rebleedings in patients under early decompressive management shows that these patients show repetitive pressure peaks.[91] This finding has recently been affirmed by a study on decompressive craniectomy in a mouse model of SAH. A craniectomy that is performed before bleeding induction mimics initial decompressive management and leads to massive hematoma and recurrent bleedings.[95]

1.3.2.2. Acute cerebral ischemia

Rise of ICP leads to an immediate global reduction of CBF[58] because the CPP drops to values close to zero.[62] This acute and transient cessation of blood flow leads to global ischemia as demonstrated by absolute measurements of CBF performed 15 and 90 minutes after endovascular perforation in rats.[96] As global cerebral ischemia is an important component of early brain injury after SAH the pathophysiology of both diseases overlap.[97, 98] Interestingly cerebral perfusion is further diminished even when the CPP rises to values close to 70 mmHg several minutes after the bleeding.[62] It means that the CBF is still disturbed even if ICP drops and the improved CPP theoretically allows cerebral reperfusion. These findings indicate that acute cerebral ischemia is not only caused by elevated ICP but is multifactorial. Importantly it was shown that the reduction of regional CBF 60 min after SAH predicts the 24 hour mortality in rats.[99] This indicates that acute ischemia after SAH might be one of the key predictors in outcome after SAH. Experimental results on early cerebral ischemia are also supported by clinical data. In a xenon contrast study it became evident that patients suffer of global cerebral ischemia within twelve hours after the insult. Ischemia was present in all parts of the brain but brain areas close to the bleeding site were more severely affected. Interestingly the extent of ischemia correlated with the clinical score of patients indicating that early ischemia plays a significant role in outcome after SAH.[100, 101] A more recent study investigated the correlation of ischemic lesions depicted by MRI within three days after the insult with neurological status, delayed ischemia and three-month outcome. Two third of investigated patients show perfusion deficits early after the insult. Early ischemia is indeed related with neurological dysfunction, the development of delayed ischemia and a poor three-month outcome.[102]

Cerebral ischemia after SAH induces a series of pathological events in the brain. These include among others cell death, brain edema and inflammation.

1.3.2.2.1. Necrosis

Necrosis describes a cell death pathway that is energy independent. Brain areas that are not perfused reveal a severe lack of oxygen and ATP and can therefore not initiate programmed cell death.[103] Brain pathology samples from patients that died after SAH show clusters of necrosis in the cortex.[104] Necrotic processes are not only limited to neuronal tissue. A rat SAH study revealed that myonecrosis of smooth muscle cells occurs 48 hours after the bleeding. Mostly cells of the medial layer next to the elastic lamina were affected.[58] High mobility group box 1 is a DNA binding protein, which is released from necrotic cells and acts as a pro-inflammatory cytokine by activating microglia.[105] High mobility group box 1 is increased in patients after SAH and correlates with poor outcome.[106]

1.3.2.2.2. Apoptosis

Apoptosis is an energy consuming programmed cell death mechanism that is initiated by different signaling pathways such as caspases and pro-apoptotic bcl-2 family members.[107] Some apoptosis related proteins were shown to be enhanced after SAH: The concentration of caspase three and eight, cytosolic p53, AIF and cytosolic cytochrome C are increased 24 hours after SAH compared to sham condition.[108] 24 hours after SAH caspase three and TUNEL positive cells indicate apoptotic processes histologically. Apoptosis was primarily shown in endothelial cells and hippocampal neurons; only little apoptosis was found in the cerebral cortex.[109] The amount of apoptotic cells in the hippocampus is higher because hippocampal neurons are more sensitive to ischemic conditions than cortical neurons. Endothelial cells are directly affected by decreased blood supply and may thereby die first. At ten minutes after SAH ten percent of endothelial cells are positive for TUNEL. By 24 hours the number of TUNEL positive endothelial cells is reduced to three percent. The time course for TUNEL positive neurons shows an opposite pattern with four percent TUNEL positive cells at ten minutes and 14% TUNEL positive cells at 24 hours after SAH.[110] These data implicate that first endothelial cells undergo apoptosis and neurons become apoptotic at later time points. The degree of acute cerebral ischemia correlates with the extent of apoptosis at two and seven days after SAH. Therefore it is likely that acute rather than delayed cerebral ischemia is responsible for apoptotic cell death that is observed after SAH.[111]

1.3.2.2.3. Metabolic derangement

A reduction in blood flow induces a metabolic disturbance by impairing the oxidative energy metabolism. Primarily in the acute phase of global cerebral ischemia the metabolism after SAH is heavily impaired. Oxygen tension is reduced immediately after SAH to values around 40% of baseline and only slowly increases during the first 90 minutes after SAH.[96] The extracellular glutamate level raises six-fold within 30 minutes

after the insult and is accompanied by a drop of glucose concentration indicating increased energy consumption. Additionally lactate concentration, a product of anaerobic metabolism is increased 60 minutes after SAH. The increase of lactate levels combined with an increase of the lactate pyruvate ratio indicate sustained metabolic imbalance.[112] This imbalance has further implications for the survival of neurons and brain edema formation.

1.3.2.2.4. Brain edema

Two different types of brain edema exist: the cytotoxic and vasogenic edema. In the cytotoxic form the influx of water into the brain is mediated by swelling of cells as a consequence of early global ischemia and metabolic derangement.[113] In contrast vasogenic edema is caused by a breakdown of the blood brain barrier (BBB).[114] Although both kinds of edema are present after SAH the vasogenic edema seems to play the major role. Bovine serum albumin used as a marker of BBB breakdown starts extravasating in the ipsilateral hemisphere six hours after the hemorrhage and reaches peak values after 48 hours.[115] Apoptosis of endothelial cells leads to a leakage of fluid and small molecules into the brain parenchyma.[109] Microvascular collagenase activity is increased at three, six and 24 hours after SAH and returns to baseline levels at 48 hours after the bleeding.[116] One day after the bleeding immunostaining and western blot reveal a reduction of collagen VI, a component of the basal lamina.[115] Collagen VI is also degraded by matrix metalloproteinases (MMP), a proteinase family that is modulating the extracellular matrix.[117] In MMP 9 knockout mice formation of brain edema is reduced compared to wildtype controls, indicating that MMP 9 is contributing to microvascular damage after SAH.[118] Importantly the extent of brain edema development correlates with the clinical outcome[119] indicating that brain edema plays an important role in the early pathophysiology after SAH.

1.3.2.2.5. Inflammation

Inflammatory processes after SAH are induced in patients and manifest in increased levels of pro-inflammatory cytokines in the CSF:[120] Tumor necrosis factor α (TNFα) is a proinflammatory cytokine that is upregulated after SAH.[120] It initiates immune cell trafficking and the release of other proinflammatory cytokines. The inhibition of TNFα by application of a specific antibody after SAH reduces apoptosis.[121] Interleukin 6 is another proinflammatory cytokine that is secreted in the CSF up to 10,000 fold after SAH compared to healthy controls.[120] Importantly the regional upregulation of proinflammatory cytokines in the brain corresponds with areas of enhanced apoptosis after SAH.[122]

SAH animal models reveal that macrophages and leukocytes accumulate in the subarachnoid space after the bleeding. Macrophages are significantly increased in the subarachnoid space from day two to seven compared to sham. T cells are found in

significantly higher numbers from day one to three after the bleeding.[123] Infiltrating immune cells most probably clear extravasated blood and its degradation products.[58] Leukocytes do not only infiltrate the subarachnoid space but also accumulate close to cerebral vessels and in the brain parenchyma. Significant numbers of leukocytes adhere to the endothelium and start infiltrating into the brain already ten minutes after the bleeding; thereafter the total number of adherent and infiltrating leukocytes decreases.[124] These findings indicate that inflammatory processes are induced immediately after SAH.

Beside immune cell infiltration into the brain SAH may induce a systemic inflammatory response syndrome. A systemic inflammatory response is associated with high mortality and morbidity in SAH patients.[125]

1.4. Microcirculation

Big brain supplying arteries do not show vessel spasm in the early phase after SAH, therefore early cerebral ischemia is probably occurring on the level of the cerebral microcirculation. Few studies on the microcirculation after SAH have already been performed in the 70ies. A severe bleeding led to a complete non-perfusion of the parenchymal microcirculation three hours after the insult in a dog SAH model.[126] The no-reflow phenomenon was believed to be caused by obstructions of the vessel lumen e.g. plugging with microthrombi or leukocytes.[127] Obstruction of the capillary lumen may also occur when the blood flow velocity drops below a certain threshold that increases blood viscosity and thereby leads to obstruction and microthrombosis.[128] Furthermore it was shown that a local superfusion with blood constricts pial vessels.[129] Therefore it is likely that subarachnoid vessels that come into direct contract with extravasated blood will constrict acutely.

However the focus of clinical research was always more on large artery spasm. The reason for this may be that the microvasculature cannot be depicted with clinical imaging techniques. Thus investigations of microvascular changes in patients are difficult to perform. Only when early brain injury and especially early cerebral ischemia after SAH moved into the focus of research the microcirculation could no longer be ignored.

New imaging techniques like two-photon microscopy with its deep penetration depth now make investigations of small vessels possible. With this technique blood flow and perfusion parameters can be investigated in detail. The importance of small vessels, which supply most of the parenchyma with blood becomes evident in *in vivo* studies on CBF. The occlusion or a hemorrhage of small vessels was modeled *in vivo* and revealed interesting insights on the pathomechanism of neuronal damage.[130] Special attention has to be drawn to penetrating arterioles because they represent a bottleneck in blood supply to superficial layers of the cortex.[131] With these tools in hand the

hemodynamic impact of superficial vessel pathology on the cerebral microcirculation can be investigated in detail.

Disturbances of blood flow in the microcirculation can either be induced by endothelial dysfunction, platelet and leukocyte adhesion or by an active constriction of vessels.

1.4.1. Endothelial dysfunction

Endothelial cells coat the inner vessel lumen and thereby come into direct contact with blood components. Hence endothelial cells are directly affected by disruption of CBF after SAH. Especially the basal lamina of parenchymal microvessels is affected early after SAH. When collagen VI is stained in capillaries 24 hours after SAH a decrease of area and length of stained vessels can be observed.[132] The disruption of the basal lamina seems to be induced by reduced blood flow in the capillaries. One suggested pathomechanism causing decreased microvascular perfusion after SAH is a lack of the vasodilator NO.[133] An experimental study of cortical perfusion in rabbits shows that an increase of the mean blood transit time correlates with decreased plasma NO levels. NO substitution has been shown to be beneficial for brain perfusion as early as one day after the bleeding.[134] These findings are supported by a study where an NO donor is applied systemically directly after the bleeding. Application of an NO donor leads to a significant increase in regional CBF compared to a saline treated control.[135] Hence early NO depletion in the vasculature is a potential pathomechanism of acute cerebral ischemia. NO concentration may be reduced after SAH because free hemoglobin in the subarachnoid space scavenges NO.[136] A lack of NO comes together with reduced expression levels of soluble cyclic guanylatcylase, which mediates the endothelium dependent relaxation of cerebral microvessels.[137] These findings strengthen the role of NO for endothelial survival and function after SAH.

1.4.2. Platelet aggregation

Blood platelets form aggregates when blood flow velocity is reduced below a certain threshold. Aggregates may trigger thrombosis and induce endothelial damage[138] as well as scattered ischemia.[139] Platelet aggregates in the microcirculation occur as early as ten minutes after the bleeding and show a biphasic occurrence. Platelet aggregation diminishes from one hour to six hours after SAH and peaks again at 24 hours after SAH. At 48 hours after SAH no more platelet aggregation is detectable.[140] It has also been shown that platelet aggregates co-localize with constricted vessel segments, regional loss of collagen VI and extravasation ten minutes after SAH. These findings indicate that platelet aggregates contribute to endothelial and BBB dysfunction after SAH.[141] Importantly the number of microthrombi correlates with the number of apoptotic cells in the cortex, indicating that microthrombi formation is relevant for neuronal cell death.[139]

1.4.3. Leukocyte-endothelium interaction

After SAH the expression of endothelial adhesion molecules is enhanced. 48 hours after the bleeding the protein levels of toll-like receptor 4, nuclear factor kappa b and intracellular adhesion molecule-1 are significantly upregulated.[142] Adhesion molecules mediate rolling and sticking of leukocytes to the endothelium before they transmigrate into the parenchyma. The number of adherent and rolling leukocytes was increased significantly at eight hours after the bleeding.[143] When leukocytes stick in the capillaries they may obstruct the vessel lumen and thereby reduce CBF. This no-reflow phenomenon was described in global and focal cerebral ischemia.[127] Whether parenchymal capillaries are similarly plugged by activated leukocytes after SAH has never been investigated *in vivo*.

1.4.4. Neurovascular coupling

Neurovascular coupling (NVC) describes the adaptation of blood flow to the metabolic needs of neuronal tissue. Activated neurons give metabolic signals via astrocytes to VSMC that are located around penetrating arterioles. Long known metabolic signals are for example glutamate for vasodilation and ATP and O_2 for vasoconstriction. Subsequently vessels dilate in case of high-energy demand and constrict when energy consumption is low.[144] Neural activity also induces Ca^{2+} dependent release of vasodilatory substances at the neurovascular unit.[144] One vasodilatory pathway is mediated by large conductance Ca^{2+} waves which activate K^+ channels on astrocytic endfeet. The increased extracellular K^+ concentration leads to vasodilation.[145] After SAH however this mechanism is inverted, so that an increased extracellular K^+ concentration induces vasoconstriction instead of vasodilation.[146] An inversion of NVC is important for the pathophysiology of SAH because an already existing metabolic derangement may be further aggravated.

1.4.5. Microvasospasm

The term microvasospasm describes a vessel narrowing in superficial cerebral arteries that are located within the subarachnoid space. These characteristic vessel spasm were first described in human patients that underwent aneurysm clipping within three days after the bleeding by orthogonal polarization spectral imaging.[147] Microvasospasm occur in 50% of superficial arteries and exhibit a mean vessel diameter reduction of 30%. Simultaneously the pial capillary density after SAH is reduced significantly.[147] Another study in patients using the same imaging technique confirmed the initial findings. In this study the vessel reactivity during hyperventilation of the patient was observed. In 60% of patients the vessels contracted in a pearl-string fashion, which were irresponsive to the endogenous vasodilator CO_2.[148] Similar vasoconstrictions of superficial arteries could be reproduced in a rat cisterna magna injection model. Spasm of pial arterioles as well as a reduction of venular vessel diameter were described. The microvascular

alterations occured in combination with decreased blood flow velocity.[149] Microvasospasm was also found in the mouse endovascular perforation model. Spastic arterioles were detected as early as three hours after the hemorrhage and vessels stayed spastic up to three days after the bleeding. The spasm was more severe at early time points and in smaller vessels. Furthermore microthrombi were found exclusively in vessels that were spastic.[150] Interestingly these microvasospasm were not reactive to hyper- or hypoventilation. The vasodilatory and hyperemic effect of CO_2 is not present in vessels that exhibit spasms.[151]

The hemodynamic consequences of superficial microvasospasm for parenchymal perfusion have not been investigated to date. However one may assume that a vessel narrowing of superficial brain supplying arteries will impact blood flow in parenchymal capillaries. Therefore one aim of the thesis was to characterize microcirculatory disturbance that emerges from superficial microvasospasm after SAH.

In addition the question arises whether also parenchymal vessels constrict in response to SAH. Parenchymal capillaries are the vessel segments where metabolites cross the BBB and are therefore functionally highly relevant. They have to date not been studied *in vivo* after SAH. Therefore we aimed to investigate whether capillaries in the brain parenchyma constrict after SAH and which cell type might mediate vessel narrowing.

2. Pericytes

2.1. Characterization

2.1.1. Morphology

Pericytes were first described in 1873 by Rouget as contractile cells surrounding capillary endothelial cells. The former definition could not sustain until today because newer insights revealed that different cell types surround the capillary endothelium.[152] The current morphological definition of a pericyte is a cell that is embedded within the vascular basement membrane.[153] Accordingly pericytes are completely surrounded by the basement membrane with one layer towards endothelial cells and one layer as a demarcation to astrocytic endfeet and the perivascular space.[154] Pericytes belong to the vascular wall[154] and are found in the capillary bed of the whole body. The number of pericytes is highest in retina and brain, followed by lung tissue.[155] In the brain pericytes cover up to 30% of the capillary surface.[156] Three different subtypes of pericytes were distinguished by Zimmermann in 1923:[157] Type I is found at the so-called middle capillaries. Cells have an elongated cell body with long primary processes that stretch along the vessel. One pericyte can span two to four endothelial cells.[158] From the processes small secondary finger-like branches wrap around the capillary and stretch to neighboring pericytes. Processes can overlap and form several layers or contact neighboring capillaries.[158] Type II pericytes cover precapillary arterioles. They have

rather big processes that cover the vessel almost completely. Type III pericytes exhibit a big cell body and short processes and are located along postcapillary venules.

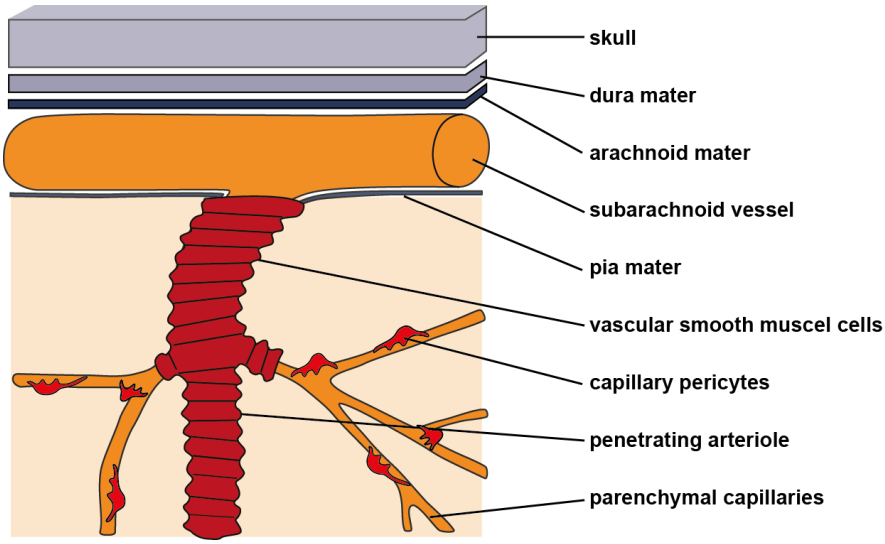

2.1.2. Immunohistochemical characterization

The characterization of pericytes and their discrimination to other perivascular cell types is not always easy. The current definition of a pericyte is based on its location and morphology: a pericyte is a cell that surrounds the endothelium and is located within the same basement membrane.[153] A practical problem emerges from this definition: This morphological feature can only be seen by electron microscopy, a technique that is not always available. A drawback of electron microscopy is that only a tiny tissue area can be visualized. Furthermore tissue needs to be treated massively, which makes stainings hardly possible. In order to overcome this issue many immunohistochemical markers for pericytes have been identified. Unfortunately none of the markers is specific for pericytes or stably expressed in the different pericyte subtypes. Hence always a combination of different markers has to be considered and combined with morphological examinations to allow a statement about the cell type investigated.[159] The discrimination to endothelial cells can easily be made because pericytes are negative for van Willebrand factor and platelet endothelial cell adhesion molecule (PECAM-1), both commonly used antigens for endothelium staining.[160] Neurons can be distinguished morphologically, by location and by staining for specify neuronal markers like NeuN (neural nuclei). Challenging is the discrimination of VSMC and pericytes because both cell types are suspected to emerge from the same progenitors. In a vessel-remodeling situation and in cell culture pericytes can become VSMC and VSMC in turn can differentiate into pericytes.[161] Precapillary arteriolar and postcapillary venular pericytes robustly express the contractile element αSMA which is a commonly used marker for VSMC and exhibit contractile functions.[162] Neural-glial antigen 2 (NG2), a membrane spanning chondroitin sulfate proteoglycan is expressed by capillary

pericytes[163] and by VSMC in the periphery.[164] The intermediate filament protein desmin is expressed in VSMC and pericytes.[161] A discrimination between pericytes and VSMC is therefore primarily possible by their location, as VSMC are located outside the basement membrane and separated from the endothelium by an additional layer of mesenchymal cells.[165] Another challenging discrimination is between pericytes and fibroblasts. A useful marker for the identification of brain pericytes is platelet derived growth factor receptor β (PDGF Rβ), which is expressed by pericytes. No expression of PDGF Rβ was found in neurons, astrocytes or endothelium.[166] However mesenchymal stem cells and myofibroblasts express PDGF Rβ.[167] In conclusion, none of the discussed markers is specific and thus always a combination of different markers has to be used to identify pericytes.[168]

2.1.3. Pericytes within the neurovascular unit

The neurovascular unit (NVU) is composed of endothelial cells, pericytes and astrocytes. The term already implies that cells of the NVU exhibit intense crosstalk and are interdependent in several functions.

Endothelial cells are spindle shaped cells that coat the vessel lumen. They form the BBB, a stringently selective barrier between brain vessels and the brain parenchyma. The BBB is formed by extensive tight junctions between endothelial cells which are composed of cadherins, claudins, occludin and junctional adhesion molecules.[169] The endothelium is absent of fenestrations in most parts of the brain, therefore nutrients and other metabolites have to be transported actively by transporters and endocytosis.[170] The choroid plexus and circumventricular organs however have fenestrated endothelium which is more permeable.

Pericytes are closely attached to endothelial cells. Gap junctions[171], adhesion plaques and peg-and-socket junctions ensure a tight connection between endothelial cells and pericytes. These connections are composed of extracellular matrix proteins like fibronectin.[153] The active contribution of pericytes in the formation of a functional BBB has long been neglected. An *in vitro* study shows that pericytes induce the expression of basement membrane proteins in endothelial cells.[172] Studies on pericyte-deficient mouse strains reveal the crucial role of pericytes in the formation and regulation of the BBB. Heterozygous PDGF Rβ knockout mice exhibit a leakage of the BBB for molecules up to 500.000 kD size. It means that in pericyte deficiency molecules like fibrin and thrombin can migrate into the brain and accumulate there.[173] Another study investigating the underlying mechanism of BBB leakage finds an alteration of endothelial gene expression patterns and enhanced transcytosis in pericyte deficient mice.[174] Furthermore pericytes are actively forming the basement membrane by synthesizing collagen VI, laminin and glycosaminoglycans.[154]

Pericytes and endothelial cells are coated by astrocytic endfeet. These endfeet are astrocytic processes that cover brain capillaries almost completely and contain increased number of water and potassium channels. They are attached to the basement membrane by dystroglycan structures.[170] Astrocytic endfeet are believed to mediate communication between neurons and the endothelial cell and pericytes, however little is known about the underlying mechanisms.[175]

2.2. Functions of pericytes

2.2.1. Communication between endothelial cells and pericytes

Endothelial cells and pericytes are interdependent and communicate closely. The only separation between them is a thin basement membrane, which allows direct contact of both cell types.[171] Pericytes and endothelial cells communicate via different growth factors like transforming growth factor β (TGF β), platelet derived growth factor b (PDGF b), sphingosin-1 phosphate, angiopoietins and notch three.[176, 177] These factors are especially important for the maturation of vessels during angiogenesis[165] and for the maintenance of the BBB.[178]

TGF β signaling between pericytes and endothelial cells is important for a functional vascular development. TGF β secreted by pericytes induces endothelium maturation and BBB formation. TGF β secreted by endothelial cells in turn induces extracellular matrix production and contractile protein expression in pericytes.[179]

PDGF b is essentially needed for the proliferation, migration and maturation of pericytes and endothelial cells. PDGF b knockout animals lack pericytes and develop cylindrical capillary dilations and microaneurysms that rupture during gestation.[180] Soluble PDGF b binds to the PDGF Rβ that is expressed on pericytes and VSMC and induces their proliferation and migration towards the vessel.[181] PDGF Rβ knockouts are prenatally lethal due to vascular dysfunction composed of a complete lack of pericytes combined with endothelial hyperplasia.[182] Heterozygous animals show an age dependent progressive loss of pericytes that induces cerebral hypoperfusion and hypoxia.[173] For maturation and attachment of pericytes to the endothelium a steep gradient of PDGF b is needed[183] which is created by a positively charged C terminal sequence. The positive charge interacts with the negatively charged extracellular matrix and leads to retention of PDGF b.[181] The retention motive has been a target for the creation of genetically modified animals because the full PDGF b knockout is embryonically lethal.[180] In PDGF b retention motif knockouts (PDGF b $^{ret/ret}$) primarily the maturation and convergence of pericytes to the endothelium is disturbed. Mice survive but exhibit less functional pericytes and a phenotype, which is associated to a disturbed BBB.[183] PDGF b $^{ret/ret}$ knockout mice are important for investigations on the role of pericytes in health and disease.

2.2.2. Contractility

Already Rouget suggested a contractile function for pericytes in his first characterization of the cell type. The location of pericytes along vessels that do not exhibit a smooth muscle cell layer as well as their vessel-wrapping morphology made this assumption reasonable. Later the evidence that pericytes express contractile elements like smooth muscle myosin and tropomyosin strengthened this hypothesis.[184, 185] However the expression of contractile elements seems to be heterogeneous in different pericyte subtypes. Differential histological staining of retinal pericytes subgroups indicated that mid-capillary pericytes in contrast to pre- and postcapillaries do not express the contractile form of smooth muscle actin.[162] A more recent study however claims an expression of αSMA even in mid-capillaries.[186] Furthermore pericytes express receptors for vasoactive substances like catecholamines[187] and vasopressin.[188] Especially interesting in the context of SAH is that pericytes express endothelin-1 receptors.[189] Endothelin-1 induces a reorganization of contractile filaments in vitro and leads to contraction in cultured retinal pericytes.[189] If the contraction mechanisms are alike in the brain, pericytes might be susceptible for increased endothelin-1 levels after SAH and contribute to pathological vasoconstriction.[81] Interestingly dilation of pericytes might be mediated by NO that is secreted by the endothelium.[190] Thus also in the context of decreased NO levels after SAH a pathomechanistic role of pericytes can be suspected.

Direct evidence for pericytes constriction has to date primarily been shown *in vitro*. Experimental evidence for pericyte contraction and dilation upon superfusion with vasoactive substances exists in different cell culture studies.[191] Pericytes that are cultured three dimensionally in a collagen gel constrict upon exposure with acetylcholine and noradrenaline. In turn they relax upon superfusion with papaverine, a potent smooth muscle cell dilator.[192] Pericytes that are cultured on a deformable silicone substrate show a wrinkling response that is mediated by actomyosin and is great enough to affect underlying material.[193] Evidence for pericyte contraction *in vivo* however is sparse. A study on cochlear pericytes shows that they constrict in response to increased extracellular Ca^{2+} and K^{+} but not noradrenaline.[194] The functional evidence of pericyte constriction *in vivo* is technically demanding and therefore remains a phenomenon that needs further investigations.

2.2.2.1. Neurovascular coupling

It is still under debate whether pericytes are involved in NVC response although they have long been suspected to be involved in the adaptation of CBF to neuronal activity. Today increasing evidence supports that pericytes actively regulate capillary diameter. The metabolic state of surrounding neuronal tissue affects pericyte tone.[195] Pericytes constrict and narrow the vessel lumen in response to superfusion with ATP and noradrenaline which is reversible by superfusion with glutamate.[196] These experimental data are supported by the finding that pericyte-deficient mice show an attenuated CBF

response to neuronal activity.[173] An *in vivo* study shows that capillaries dilate similar to penetrating arterioles in response to increased neuronal activity by forepaw stimulation.[197] Recently a study on the time course of vasodilation of different vessel categories during whisker stimulation was published.[198] They found that capillaries dilate first, even before penetrating arterioles, and that the sites of vasodilation co-localized with pericytes location.[198] However a conflicting *in vivo* study suggests that pericytes were able to regulate the vessel diameter but that they were not mediating the physiological NVC response. Superfusion with a thromboxane A2 analogue constricted pericytes but seizure like neuronal activity did not dilate them. The authors conclude that pericytes can regulate the vessel diameter but are primarily involved under pathological condition and rather do not mediate physiological hyperemia.[199] These conflicting results show that the role of pericytes in NVC response is difficult to tackle and that further studies are needed to find conclusive answers.

2.2.2.2. Ca^{2+} signaling in pericytes

As pericytes express contractile elements and have the ability to constrict the question arises how tonicity of pericytes is mediated. In VSMC signaling cascades that induce cell constriction and dilation are well characterized:[200] An elevated intracellular Ca^{2+} concentration leads to an activation of myosin light chain kinase which induces phosphorylation of the myosin light chain and initiates its contraction. A relaxation of VSMC in turn is mediated by low intracellular Ca^{2+} levels and a low activity of myosin light chain kinase. Superfusion of cultured pericytes with acetylcholine induces a sustained increase in Ca^{2+}.[192] Another study identified triggers of increased cytosolic Ca^{2+} in pericytes: The Ca^{2+} ionophore A23187 as well as high concentration of K^+, tetraethylammonium and charbybdothoin significantly increased Ca^{2+} concentration in pericytes. Conversely the vasoactive substances angiotensin 2, acetylcholine and endothelin-1 cause a biphasic intracellular Ca^{2+} response.[201] These data indicate that a physiological as well as a potential pathological pericyte constriction might be mediated by increased intracellular Ca^{2+} concentration.

2.3. Pericytes in ischemia

The role of cerebral pericytes in ischemia has only recently moved into the focus of research.[202] Studies that are performed *in vivo* are sparse and reveal conflicting results. Therefore the role of pericytes in ischemic brain conditions needs to be further elucidated. To date three different pathophysiological reactions of pericytes to ischemia have been identified: constriction, migration/plasticity and cell death:

After transient ischemia reperfusion of cerebral capillaries is impaired even if the big brain supplying arteries are reopening. This phenomenon is known as the no-reflow phenomenon.[128] Recently experimental evidence on the contribution of pericytes to disturbed reperfusion of cerebral capillaries emerged. Yemisci et al. found that oxidative

stress induced pericyte constriction upon ischemia. It led to capillary narrowing that obstructed the flow of red blood cells. The suppression of the oxidative stress alleviated pericyte contraction and preserved the microcirculation.[203] However this study was not performed *in vivo*, which makes morphological findings difficult to interpret. A recent study shows that pericytes constrict after onset of ischemia and subsequently die in rigor mortis. This rigor further strangulates vessel volume.[198] This study was performed in cerebellar slices in the condition of oxygen-glucose deprivation, which might exhibit different pathophysiology than ischemic condition *in vivo*. Therefore *in vivo* studies in the cerebral cortex are needed to confirm pericyte constriction upon ischemia.

These data indicate that pericytes are susceptible to ischemic conditions[204] and might undergo early cell death upon cerebral ischemia. A study investigated pericyte survival 24 hours after ischemia. Dying cells were labeled with IB_4 and propidium iodide and revealed that about 70% of pericytes died early after focal cerebral ischemia.[198] Another study confirms pericyte death on day one to three after ischemia.[205]

Interestingly pericytes migrate away from the vessel during postischemic hypoperfusion within 24 hours after ischemia.[206] In an ultrastructural study of pericytes in hypoxic condition pericytes show characteristic cell protrusions that are directed towards the parenchyma. After two hours of hypoxia every third pericyte starts to migrate from its original location, leaving a thickened basal lamina.[207] A more recent ultrastructural study shows that hypothermia delays pericyte migratory behavior after transient cerebral ischemia.[208] Pericyte migration might disrupt the BBB thereby increasing vascular permeability.[209] The triggers and purpose of pericyte migration are still unknown.

Proliferation of pericytes in the ischemic core has been suggested after experimental stroke. An upregulation of the vascular expression of PDGF Rβ was found 48 hours after transient middle cerebral artery occlusion.[210] Another study investigating plasticity of pericytes after ischemia finds that pericytes proliferate and migrate upon distal permanent ischemia. At seven days after stroke the number of pericytes is ten-fold in the peri-ischemic area compared to the contralateral side. These activated parenchymal pericytes express microglial marker and show a transcription pattern similar to microglial cells.[211] Therefore they might take over immune function.[212] Another recent study claims that perivascular stromal cells change their phenotype and are involved in scar formation after cerebral ischemia. These cells are PDGF $R\beta^+$ and $CD105^+$ and originate from the NVU.[205]

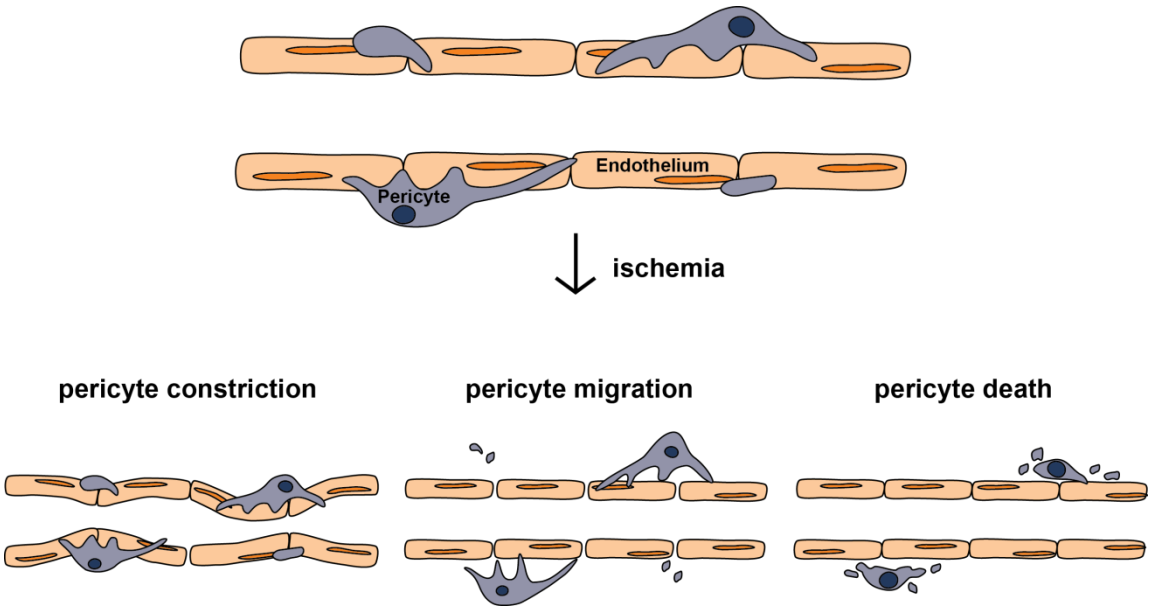

In summary the literature on the role of pericytes in ischemia is heterogeneous and pericyte pathophysiology therefore needs to be further investigated in more detail. *In vivo* studies will help to elucidate the dynamics and fate of pericytes in ischemia.

The role of pericytes after SAH has not been investigated to date. As SAH and ischemic stroke share common pathophysiologies e.g. tissue hypoxia it is likely that pericytes react to SAH in a similar way as observed in focal cerebral ischemia. Therefore one aim of the current thesis was to characterize the reaction of pericytes to SAH *in vivo*. Pericyte survival as well as a possible migratory behavior were addressed. However most interesting for the early pathophysiology after SAH is the involvement of pericytes in the formation of vessel spasm. If capillaries constrict after SAH, pericytes are the associated contractile cell type that can mediate vessel constrictions.

A murine model of subarachnoid hemorrhage

Aim of the study:

The endovascular filament perforation model is the animal model which resembles the pathophysiological situation in SAH patients most closely.[213] It has been invented by Bederson et al. and Veelken et al.[62, 63] and primarily used and optimized in rats, a laboratory animal frequently used in medical science. Since studies on transgenic animals were moving into the focus of biomedical research, mice were replacing rats as experimental animals. Subsequently researchers had to adopt animal models from rats to mice. Especially the SAH model was not easily applicable in mice because of the small body size and blood volume. The size of the filament that perforates the vessel as well as adequate physiological monitoring are crucial for successful SAH induction.[61] Although the endovascular filament perforation model was described in mice[65, 66] it was rarely used in SAH research. Instead alternative SAH models like the blood injection model were employed because they are quick and easy to perform. However investigations on the pathophysiology of a disease should always be performed in the animal model that resembles the situation in patients best. Therefore we decided to further standardize the model and publish a methodological video publication. Guidelines for the monitoring of physiologic conditions during SAH induction and exemplary data are provided.

Moreover the distribution of extravasated blood inside the subarachnoid space after filament perforation is described. Blood distribution after SAH has never been investigated in mice but might be relevant for the pathophysiology because free hemoglobin is suspected to be involved in the formation of early brain injury.[133] Furthermore the blood distribution pattern in the perivascular space might have implications on pial vessel pathology and microthrombosis.

Subarachnoid blood distributes in the subarachnoid space primarily along superficial arterioles i.e. branches of the middle cerebral artery. Moreover perivascular blood stretches on the brain surface as far as to the dorsal cortices. This finding is relevant for subsequent studies where the cortical microcirculation after SAH is investigated *in vivo*.

A murine model of subarachnoid hemorrhage

Journal of Visualized Experiments (JoVE), November 2013
doi: 10.3791/50845

Kathrin Schüller[1], Dominik Bühler[1], Nikolaus Plesnila[1]

[1] Institute for Stroke and Dementia Research (ISD), University of Munich Medical School

Author contributions: KS and NP planned experiments, KS and DB acquired data, KS and DB analyzed data, KS and NP wrote manuscript

Keywords: Subarachnoid hemorrhage (SAH), mouse model, filament perforation, intracranial pressure monitoring, blood distribution, surgical technique

Short Abstract

A standardized mouse model of subarachnoid hemorrhage by intraluminal Circle of Willis perforation is described. Vessel perforation and subarachnoid bleeding are monitored by intracranial pressure monitoring. In addition various vital parameters are recorded and controlled to maintain physiologic conditions.

Long Abstract

In this video publication a standardized mouse model of subarachnoid hemorrhage (SAH) is presented. Bleeding is induced by endovascular Circle of Willis perforation (CWp) and proven by intracranial pressure (ICP) monitoring. Thereby a homogenous blood distribution in subarachnoid spaces surrounding the arterial circulation and cerebellar fissures is achieved. Animal physiology is maintained by intubation, mechanical ventilation, and continuous on-line monitoring of various physiological and cardiovascular parameters: body temperature, systemic blood pressure, heart rate, and hemoglobin saturation. Thereby the cerebral perfusion pressure can be tightly monitored resulting in a less variable volume of extravasated blood. This allows a better standardization of endovascular filament perforation in mice and makes the whole model highly reproducible. Thus it is readily available for pharmacological and pathophysiological studies in wildtype and genetically altered mice.

Introduction

SAH is the stroke subtype with the least beneficial outcome for patients: 40% of the patients die within a month after the bleeding[1] and survivors rarely have a clinically favorable outcome.

The large majority of spontaneous SAHs (80%) are caused by rupture of intracranial aneurysms which are mostly located along the anterior and posterior communicating artery, the basilar artery, and middle cerebral artery (MCA)[2].

Such aneurysms are difficult to model in animals and therefore animal models of SAH are either performed by injection of blood into the subarachnoid space/cerebral ventricles or by

endovascular perforation of a subarachnoid vessel.

Autologous blood injection into the cisterna magna is easy to perform and reproducible as the blood volume can be directly controlled[3]. Unfortunately some aspects of the SAH pathophysiology, *e.g.* the vessel injury, cannot be modeled by this procedure. Another technical approach for induction of SAH is the opening of an intracisternal vein[4].

However, the intraluminal CWp at the MCA branch appears to be the procedure that models the pathophysiology in humans most closely[5]. The method was developed and first described in rats by Bederson and colleagues and at the same time by Veelken and colleagues[6, 7]. Later the intraluminal perforation model was adapted to mice[8, 9]. A filament is inserted into the external carotid artery (ECA) and advanced to the skull base via the internal carotid artery (ICA). At the branching point of the MCA the filament perforates the vessel and induces a bleeding into the subarachnoid space at the skull base. The blood then distributes into the remaining subarachnoid space along fissures and blood vessels. Bleeding is stopped by clot formation at the site of perforation but re-bleedings, which are often detrimental in patients[10], can occur. Accordingly, the endovascular filament model became a widely used SAH model during the past few years. The most frequently mentioned drawback of the filament perforation model is that bleeding volume cannot be directly controlled and may therefore be variable. This variability can significantly be reduced by tight control of animal physiology and post-hemorrhagic ICP.

Mice have the great advantage that a large number of genetically modified strains are available. However, due to their small size surgical procedures tend to be more complex than in larger species, *e.g.* rats or rabbits. Therefore the downscaling of techniques developed for rats to mice often does not lead to the desired results, *e.g.* as mice have a very limited body weight and blood volume non-invasive techniques for blood pressure and blood gas analysis as well as for hemoglobin saturation and heart rate monitoring have to be applied whenever possible.

Accordingly, the aim of the current publication is to describe the filament perforation model for SAH in mice and to demonstrate how this model can be performed in a standardized and highly reproducible manner.

Protocol Text

All surgical procedures were subjected to ethical review and approved by the government of Upper Bavaria (reference number: 55.2-1-54-2532.3-13-13 and -2532-136-11). Animals are male C57BL/6 mice with a body weight of approximately 25 g.

1. Animal preparation

1.1) Induce anesthesia by putting the mouse into a chamber. Flush the chamber with 5% isoflurane until the animal loses consciousness.

1.2) Inject premixed anesthetics intraperitoneally: fentanyl (0.05 mg/kg), midazolam (5 mg/kg) and medetomidine (0.5 mg/kg).Check reflexes before and regularly during the procedure. Reinject one third of the initial amount hourly to maintain anesthesia.

1.3) Intubate oro-tracheally with a tube made from a 20G venous catheter[11]. For intubation fix the animal on a slanted platform (30°), retract the tongue with bent forceps, visualize the vocal cords under an operation microscope and insert the tube into the trachea during inspiration.

1.4) Place the mouse in a prone position and check the correct placement of the tube with a piece of cotton or a microcapnograph.

1.5) Connect the intubation tube to the respirator. Ventilate the mouse with room air supplemented with 25% oxygen with a frequency of 180- 220 breaths/min and a stroke volume of 200- 250 µl.

1.6) Connect the intubation tube to the microcapnograph. Maintain the endexpiratory pCO_2 at 30 mmHg by adjusting the ventilation frequency.

1.7) Insert a rectal temperature probe and place the animal on a heating pad in order to maintain 37°C core body temperature.

1.8) Apply the annular pulsoximeter sensor on the right hind paw.

1.9) Open the skin above the skull with a pair of scissors. The incision should be approximately 0.5 cm long and between ear and eye.

1.10) Dissect the left temporal muscle with a scalpel from the temporal bone.

1.11) Glue the laser Doppler flowmeter (LDF) probe onthe left temporal bone. Hold the probe in a fixed position until the glue hardens.

1.12) Drill a hole of approximately 1.5 mm diameter with a dental drill into the left temporal bone. Cool the bone with saline to prevent heat damage.

1.13) Insert the ICP probe into the cranial cavity. Push forward as dorsally as possible to prevent brain tissue damage and bleeding.

1.14) If the probe is at the right position, fix and seal it with cement. Let the cement dry for 5 min.

1.15) Turn the mouse carefully to a supine position.

1.16) For continuous blood pressure monitoring catheterize the left femoral artery.

1.17) Connect the femoral catheter to the blood pressure monitoring device.

2. **SAH induction**

2.1) Open the skin with a pair of scissors from sternum to chin. Dissect the connective tissue bluntly and push the salivary glands aside.

2.2) Expose the left common carotid artery (CCA) and mobilize it. Preserve the vagal nerve which runs in the same connective tissue sheath as the CCA. Move cranial and expose and mobilize the ICA and the ECA using the same technique.

2.3) Ligate the ECA as far cranially as possible.

2.4) Prearrange two more ligations for the filament around the ECA.

2.5) Occlude the CCA and the ICA temporarily with microclips. Position the microclips with a microclip applicator. Make sure the clips are applied correctly by gently pulling them back.

2.6) Cut a hole for the filament insertion into the ECA with a vessel scissors.

2.7) Insert a Prolene 5-0 filament with 12mm length into the ECA.

2.8) Close the insertion site with one prearranged ligation.

2.9) Remove the microclips with a microclip applicator from the CCA and the ICA.

2.10) Advance the filament with a forceps into the ICA until the ICP rises. A sudden rise of the ICP indicates bleeding induction.

2.11) Withdraw the filament immediately and ligate the ECA by closing both prearranged ligations consecutively. This prevents bleeding out of the insertion site.

2.12) Suture the skin wound.

2.13) Monitor the physiologic parameters of the animal for another 20 min.

2.14) Remove ICP and LDF probes and suture the skin wound.

3. End of experiment

3.1) Perfuse the animal transcardially with 20 ml of saline (room temperature) followed by 20 ml of 4 % PFA in PBS (4°C).

3.2) Dissect the brain out of the skull. Cut the skull in the midline and between the orbital cavities. Then peel the bone from the brain.

3.3) Evaluate the blood distribution in the subarachnoid space.

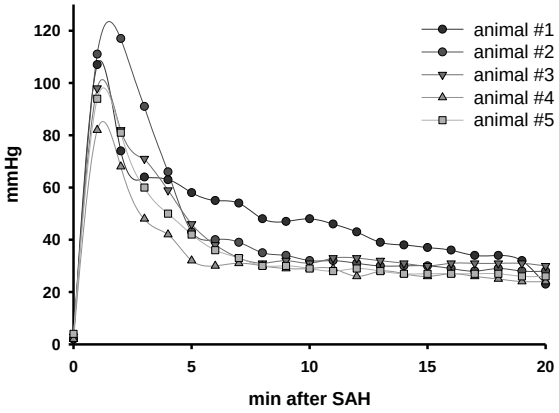

***Figure 1**: Representative ICP values of 5 animals after SAH.*

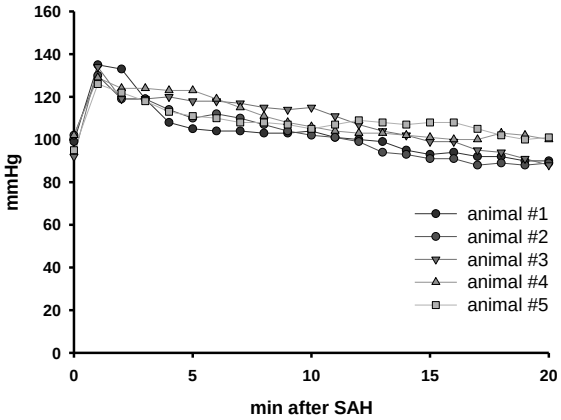

***Figure 2**: Representative blood pressure values of 5 animals after SAH.*

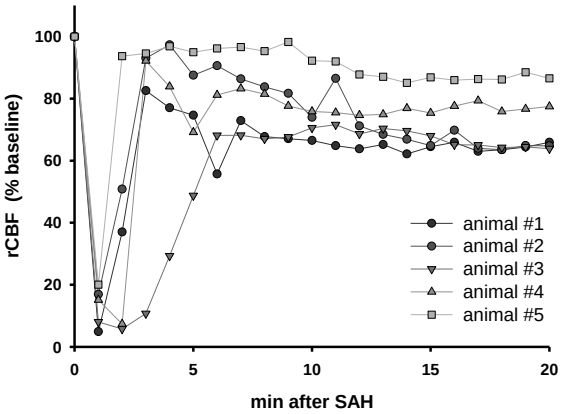

***Figure 3:** Representative laser Doppler flowmeter values of 5 animals after SAH.*

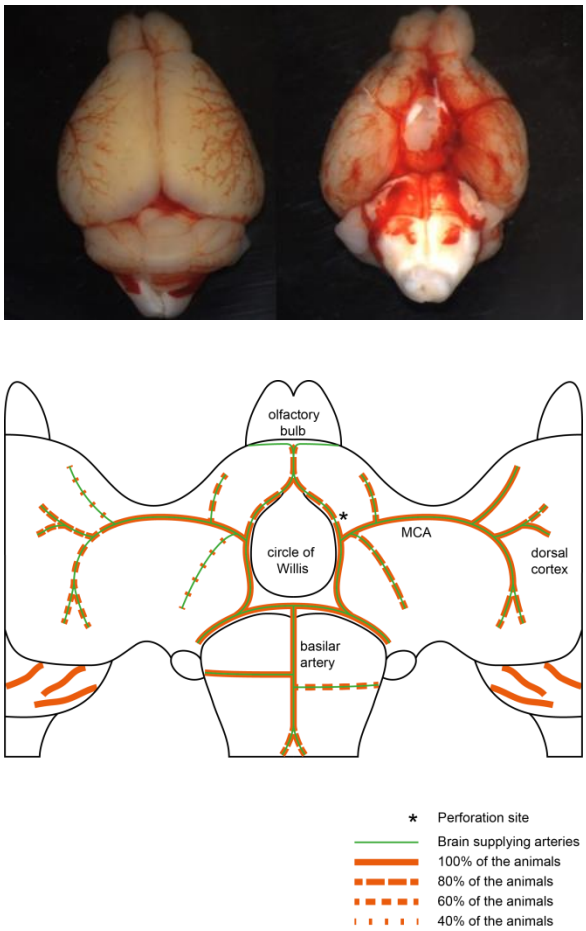

***Figure 4:** Blood distribution along brain supplying arteries. Representative blood distribution of 5 animals after SAH. Red lines indicate blood distribution along brain supplying arteries.*

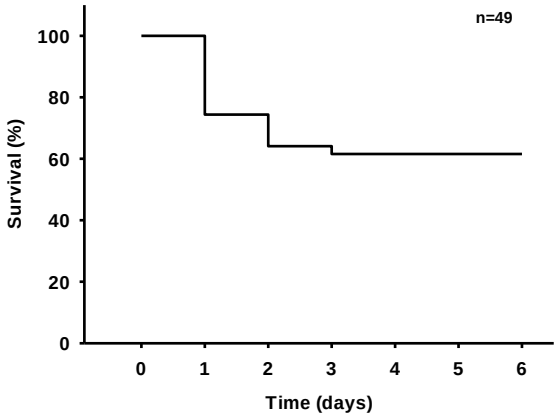

Figure 5: *Survival curve after SAH. Survival curve following SAH in 49 male C57BL/6 mice.*

Results

Mortality

Once the surgery technique is mastered the procedure does not elicit any intraoperative mortality. Also bleeding can be achieved in virtually all animals. Postoperative mortality is 30-40 % with most animals dying on day 1 after surgery (Fig.5).

ICP values after SAH

The ICP before bleeding is around 4 mmHg. Bleeding results in a sharp increase of the ICP up to 120 mmHg. ICP values then stabilize within 5 min at approximately 30 mmHg (Fig.1). At 24 hrs after bleeding the ICP is still slightly elevated to 10 mmHg[5].

Blood pressure after SAH

Blood pressure rises immediately after bleeding induction (Fig.2). This is due to the Cushing reflex which is initiated by elevated ICP.

Cerebral perfusion after SAH

After bleeding induction a dramatic decrease of cerebral perfusion can be monitored. Reperfusion to an individually different level occurs within 5 min after the insult (Fig.3).

Blood distributes along brain supplying arteries and cerebellar fissures

We perfused animals 3 hrs after SAH transcardially with 20 ml of saline followed by 20 ml of chilled 4 % PFA. The brain was carefully removed and blood distribution in the subarachnoid space was observed. Blood distributes along the perivascular space of brain supplying arteries towards the dorsal cortex. In all cases the extravasated blood covered the MCA up to the second branching. The side ipsilateral to the hemorrhage was covered with more blood than the contralateral hemisphere (Fig.4).

Blood distribution does not correlate with ICP rise

In 5 animals we investigated whether the rise of the ICP during SAH has an impact on blood distribution in the subarachnoid space. One hypothesis was that animals which show only a moderate ICP rise during SAH might exhibit less extravasated blood which then does not distribute to the dorsal parts of the cortex. We found that only the size of the hematoma at the skull base seems to correlate with the ICP rise. Blood distribution along the brain supplying arteries did not differ between animals with different ICP peak values.

Discussion

Treatment options after SAH are scarce and mostly inefficacious. Therefore the pathophysiology of post-hemorrhagic brain damage needs to be further understood in order to identify new therapeutic targets and develop novel therapeutic approaches. Standardized and well reproducible animal models in genetically modified animals, *i.e.* mice, are crucial for such investigations. The CWp model has become a widely used model for SAH as it resembles the pathophysiology in humans closely; however, its use in mice is hampered by low reproducibility and a high interpersonal variability. Variations of the model are caused by different anesthetic protocols which alter physiologic conditions. The amount of bleeding varies between animals due to vessel reactivity, blood pressure and coagulation differences[12]. Thus it is important to monitor physiologic conditions throughout the procedure and to establish surgical and

monitoring protocols which reduce the variability of this model.

Blood distribution after SAH may be different between species. In the rat model blood seems to be equally distributed across both cerebral hemispheres[6]. As human brains show a gyrencephalic architecture the blood is likely to distribute mainly along brain sulci and not primarily along vessels. On the other hand brain supplying arteries run in those sulci *e.g.* the MCA in the lateral sulcus. Thus vessel pathologies might be similar in rodent animal models and the human brain.

In our laboratory we use a combination of fentanyl, medetomidine and midazolam as described above for surgical anesthesia. This combination has a relatively small effect on blood pressure and vessel reactivity[11]. In contrast, isoflurane, a widely used anesthetic in SAH research, leads to peripheral vasodilation, severely impaired cerebral autoregulation[13], and low blood pressure immediately after SAH[12, 13], findings which are not regularly associated with the early pathophysiology of SAH in humans. Hence, the use of an anesthetic protocol which does not disturb post-hemorrhagic pathophysiology is an important prerequisite for a valid experimental SAH model.

The amount of bleeding depends on the vessel lesion and varies therefore with filament size[14]. Another crucial step of the model is the withdrawal of the filament after vessel perforation. Blood flow in the ICA is disrupted by the filament and a delayed withdrawal may result in smaller bleedings. Accordingly, it is crucial to standardize the time between vessel perforation and filament withdrawal. This is of course only possible if the time point of vessel perforation can be determined with high temporal precision. In our set-up this is achieved by continuous measurement of ICP. A sharp increase in ICP indicates successful vessel perforation and allows thereby the standardization of filament withdrawal and hence bleeding intensity. In addition, ICP-controlled vessel perforation prevents that the filament is advanced too far thereby preventing brain tissue damage. Accordingly, continuous ICP measurement is an excellent technique to minimize the variability of the murine SAH model.

Acknowledgements

The current research is funded by the Solorz-Zak Research Foundation.

Disclosures

Authors have nothing to disclose.

References

1. Cahill, J. & Zhang, J.H. Subarachnoid hemorrhage: is it time for a new direction? *Stroke* **40**, S86-7 (2009).
2. van Gijn, J., Kerr, R.S. & Rinkel, G.J. Subarachnoid haemorrhage. *Lancet* **369**, 306-18 (2007).
3. Lin, C.L. et al. A murine model of subarachnoid hemorrhage-induced cerebral vasospasm. *J Neurosci Methods* **123**, 89-97 (2003).
4. Altay, T. et al. A novel method for subarachnoid hemorrhage to induce vasospasm in mice. *J Neurosci Methods* **183**, 136-40 (2009).
5. Feiler, S., Friedrich, B., Scholler, K., Thal, S.C. & Plesnila, N. Standardized induction of subarachnoid hemorrhage in mice by intracranial pressure monitoring. *J Neurosci Methods* **190**, 164-70 (2010).
6. Bederson, J.B., Germano, I.M. & Guarino, L. Cortical blood flow and cerebral perfusion pressure in a new noncraniotomy model of subarachnoid hemorrhage in the rat. *Stroke* **26**, 1086-91; discussion 1091-2 (1995).
7. Veelken, J.A., Laing, R.J. & Jakubowski, J. The Sheffield model of subarachnoid hemorrhage in rats. *Stroke* **26**, 1279-83; discussion 1284 (1995).
8. Kamii, H. et al. Amelioration of vasospasm after subarachnoid hemorrhage in transgenic mice overexpressing CuZn-superoxide dismutase. *Stroke* **30**, 867-71; discussion 872 (1999).
9. Parra, A. et al. Mouse model of subarachnoid hemorrhage associated cerebral vasospasm: methodological analysis. *Neurol Res* **24**, 510-6 (2002).
10. Broderick, J.P., Brott, T.G., Duldner, J.E., Tomsick, T. & Leach, A. Initial and recurrent bleeding are the major causes of death following subarachnoid hemorrhage. *Stroke* **25**, 1342-7 (1994).
11. Thal, S.C. & Plesnila, N. Non-invasive intraoperative monitoring of blood pressure and arterial pCO2 during surgical anesthesia in mice. *J Neurosci Methods* **159**, 261-7 (2007).
12. Hockel, K., Trabold, R., Scholler, K., Torok, E. & Plesnila, N. Impact of anesthesia on pathophysiology and mortality following subarachnoid hemorrhage in rats. *Exp Transl Stroke Med* **4**, 5 (2012).
13. Wang, Z., Schuler, B., Vogel, O., Arras, M. & Vogel, J. What is the optimal anesthetic protocol for measurements of cerebral autoregulation in spontaneously breathing mice? *Exp Brain Res* **207**, 249-58 (2010).
14. Schwartz, A.Y., Masago, A., Sehba, F.A. & Bederson, J.B. Experimental models of subarachnoid hemorrhage in the rat: a refinement of the endovascular filament model. *J Neurosci Methods* **96**, 161-7 (2000).

Impairment of the parenchymal cerebral microcirculation after subarachnoid hemorrhage

Aim of the study:

Cerebral ischemia, which correlates with the clinical score of patients, occurs early after SAH.[100] The underlying pathomechanism is not clear to date but two different concepts for the formation of cerebral ischemia after SAH are discussed: One hypothesis is that parenchymal vessels are obstructed due to leukocyte-endothelium interactions or formation of microthrombi that plug the vessel lumen. The so called no-reflow phenomenon, which is observed after focal ischemia hampers reperfusion of capillaries.[127] A second hypothesis is that vessels constrict acutely in response to SAH.[99] In patients as well as in a mouse model of SAH pearl-string like microvasospasm of superficial brain supplying arteries evolve early after the bleeding.[147-150]

We address the question whether vessel spasm on the surface of the brain have a negative impact on blood flow dynamics of capillaries in the brain parenchyma. The parenchyma is the localization where blood gases and nutrients cross the blood brain barrier to provide neurons and glia cells with energy and metabolites. It is also the location where actual brain damage after SAH occurs.[214] Therefore it is important to know whether vascular dysfunction on the brain surface also manifests deep in the cortex. To address this question we made use of two-photon microscopy after SAH. Vessel diameter was reduced by 23% in superficial vessels and three different types of superficial vessel constrictions were identified. In addition to pearl-string like constrictions global vessel constrictions over long vessel segments as well as bottleneck constrictions, which are more pronounced in distal vessel areas were identified. The reduction of vessel diameter was accompanied by reduced blood flow velocity in superficial vessels. Taken together the data shows that less blood volume passes superficial arteries and eventually reaches the cerebral microcirculation. It manifests in a reduction of perfused vessel volume of parenchymal capillaries after SAH. In order to test the occurrence of the no-reflow phenomenon after SAH we further investigated whether perfusion deficits are caused by plugging of vessels with leukocytes. SAH induced a five-fold increase in leukocyte-endothelium interactions but absolute numbers were too low to explain the severe reduction of perfused microvessels.

This study shows that the cortical microcirculation is affected early after SAH and that superficial microvasospasm are the suggested pathomechanism. However it needs to be further addressed whether the reduction of vessel diameter and blood flow velocity on the brain surface alone trigger parenchymal perfusion deficits or whether also capillaries constrict after SAH.

Impairment of the parenchymal cerebral microcirculation after subarachnoid hemorrhage

Kathrin Schüller [1,2], Uta Mamrak [1], Nikolaus Plesnila [1,2,3]

[1] Institute for Stroke and Dementia Research, University of Munich Medical Center, Munich, Germany

[2] Graduate School of Systemic Neurosciences, Ludwig-Maximilians-Universität, Munich, Germany

[3] Cluster of Systems Neurology (Synergy), Munich, Germany

Autor contributions: KS and NP planned experiments, KS and UM acquired data, KS analyzed data, KS and NP wrote manuscript

Key words: subarachnoid hemorrhage, ischemia, microvasospasm, leukocyte plugging, cerebral blood flow

Abstract

The outcome after subarachnoid hemorrhage (SAH) depends on the occurrence of early cerebral ischemia. Spasms of arteries in the subarachnoid space are a suggested mechanism. However, if these spasms also influence microperfusion in the brain parenchyma, where the actual damage occurs, remains unclear. The aim of the current study is therefore to investigate the parenchymal microcirculation after SAH using two-photon *in vivo* microscopy.

Vessel diameter and blood flow velocity in pial and parenchymal microvessels as well as perfused vessel volume were measured by two-photon microscopy three hours after SAH. Leukocyte plugging and microthrombi formation was investigated in a separate group of experiments using Rhodamine 6G as a leukocyte marker.

Arteriolar diameter and blood flow velocity in the pial microcirculation decreased by 23% and 54%, respectively. At the same time the volume of perfused microvessels in the cerebral parenchyma dropped by 68% indicating severe parenchymal perfusion deficits. The number of leukocytes plugging in parenchymal microvessels increased five-fold.

The current study demonstrates that SAH-induced microvasospasm of pial arterioles are associated with a severe reduction of parenchymal perfusion. Hence, alterations of the pial and parenchymal microcirculation may together be responsible for the ischemic brain damage observed after SAH. The cerebral microcirculation represents therefore a promising target for the development of novel therapeutic strategies to prevent brain injury after SAH.

Introduction

Subarachnoid hemorrhage (SAH) describes a bleeding into the subarachnoid space, the cerebrospinal fluid filled volume between the arachnoid membrane and the pia mater which hosts the large brain supplying arteries before they enter the brain parenchyma. SAH accounts for about 3 to 6% of all strokes, but it has a high socio-economic burden that almost equals that of ischemic stroke since it affects younger patients.[1] Over all, SAH has a mortality of 50% with 21% of patients dying within the first 24 hours after the bleeding.[2]

In most cases SAH is caused by a rupture of an aneurysm at the base of the brain.[3] Vessel rupture and the evolving hematoma cause high intracranial pressure (ICP) leading to the reduction of cerebral blood flow (CBF) and eventually to global cerebral ischemia.[4] Patients reaching the hospital after this acute phase often suffer also from focal cerebral ischemia[5] which further aggravates global ischemia-induced brain damage. Early ischemia has a negative impact on three-month outcome after SAH.[6]

The mechanisms underlying early focal cerebral ischemia after SAH are poorly understood. They may include acute spasms of large cerebral vessels as seen in histological examinations after experimental SAH[7] or acute spasms and microthrombosis of the pial microcirculation described in SAH patients[8, 9] and experimentally in mice.[10] The functional consequence of these spasms is largely unknown, i.e. whether constrictions of pial arterioles result in disturbance of circulation in the brain parenchyma, the area where post-hemorrhagic ischemia and brain damage actually occur. Accordingly, the aim of the current study was to visualize the parenchymal microcirculation *in vivo* by two-photon microscopy and to investigate the effect of SAH on parenchymal microvascular perfusion.

Material and Methods

C57Bl6 mice obtained from Charles River (Sulzfeld, Germany) were used for the current study. Mice were group housed in individually ventilated cages with access to food pellets and water ad libitum. Experiments are approved by the Government of Upper Bavaria.

Anesthesia

Anesthesia was induced in a chamber with increasing isoflurane concentrations to a maximum of 5% and maintained by intraperitoneal injection of 0.05 mg/kg fentanyl (Janssen- Cilac, Neuss, Germany), 0.5 mg/kg medetomidine (Pfizer, USA), and 5 mg/kg midazolam (Braun, Germany). Afterwards animals were placed on a feedback controlled heating pad for maintenance of body temperature at 37°C. Mice received 4 mg/kg carprofen (Pfizer, USA) subcutaneously for preoperative analgesia and were intubated and mechanically ventilated (Minivent 845, Hugo Sachs, Germany). A microcapnograph (Model 340, Hugo Sachs, Germany) was used to adjust the ventilation frequency to keep blood gases within the physiological range during the experiment. A pulsoximeter sensor (MouseSTAT, Kent Scientific, USA) was placed at the right hind paw and peripheral oxygen saturation as well as heart rate were continuously monitored during anesthesia. Surgical anesthesia was maintained by regular reinjection of anesthetics.

SAH model

SAH was is induced by endovascular perforation of the Circle of Willis as described previously.[11] Briefly, an intracranial pressure probe (Codman, Johnson & Johnson, UK) was implanted into the epidural space and a laser Doppler probe (Periflux 5000, Perimed, Sweden) was fixed on the temporal bone. The mouse was placed in a supine position and the left carotid arteries were exposed. A prolene filament (5-0) was inserted into the external carotid artery and advanced through the internal carotid artery towards the Circle of Willis until ICP rose sharply indicating

SAH induction. The filament was withdrawn immediately and the external carotid artery was sutured. Animals were monitored for 20 minutes, wounds were sutured and surgery was terminated by a subcutaneous injection of 1.2 mg/kg naloxone (Actavis, Ireland, USA), 0.5 mg/kg flumazenil (Inresa, Germany) and 2.5 mg/kg atipamezole (Pfizer, USA). In sham operated animals the filament was advanced up to the Circle of Willis without vessel perforation.

Two-photon microscopy

After topic application of lidocaine (2% HCl) the bone of the parietal cortex was thinned[12] or a glass window (four x four mm) was prepared as previously described.[13] Mice were fixed in a nose clamp (David Kopf instruments, USA) and placed under a Zeiss LSM 7 microscope equipped with a Li:Ti laser (Chameleon, Coherent, USA) and a 20x water immersion objective (Plan Apochromat, NA 1.0, Zeiss, Germany). Fluoreszeinisothiocyanate (FITC) dextran (0.5% in saline Sigma Aldrich, USA) or tetramethylrhodamine (TMRM) (0.5% in saline, Sigma Aldrich, USA) was injected via the tail vein or into the femoral catheter to stain the blood plasma. Rhodamine 6G (0.5% in saline, Sigma Aldrich, USA) was used to stain nucleated blood cells. Excitation wavelength was 800 nm for FITC and TMRM and 840 nm for FITC and Rhodamine 6G respectively. Fluorescence emission was detected using GaAsP-NDD detectors and 500-550 nm band pass filters for green fluorescence and 565-610 nm band pass filters for red fluorescence. Z-stacks (one µm step distance) of four randomly chosen regions of interest (ROI) with a size of 609 x 609 µm were obtained with 0.7x zoom up to a targeted minimum depth of 150 µm or 400 µm. For the measurement of blood flow velocity line scans were performed along randomly chosen pial arteries with a diameter of 12-60 µm. Each vessel was scanned 1000 times with maximum speed over a length of 50-100 µm. At the end of each experiment brains were kept for histological analysis.

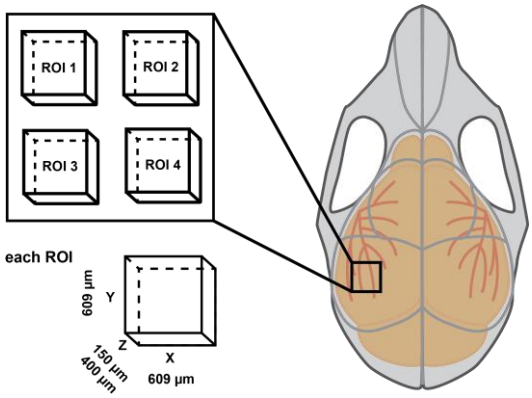

Figure 1
Sketch of a cranial window on the left parietal cortex. Four randomly chosen ROI within the cranial window were investigated by two-photon microscopy.

Experimental groups

Two experimental groups were investigated: In group one two-photon imaging was performed before and three hours after SAH. In group two plugging of pial and parenchymal microvessels by leukocytes was investigated three hours after SAH.

Quantification of data obtained by two-photon imaging

Vessel diameter was assessed by measuring the maximal vessel diameter in a given Z-stack. Maximal vessel diameter was measured at five positions along randomly selected vessel segments of 60-80 µm lengths. At least three vessel segments were measured in each ROI, which resulted in 12 vessel segments per experiment. In total 89 vessel segments were measured in sham condition and 109 vessel segments in SAH condition.

In order to obtain a value for the amount of perfused microvessels in a given volume of brain tissue, a crop (150 x 150 µm) of one ROI was subjected to 3D reconstruction (Imaris, Bitplane AG, Switzerland) and the absolute volume of all pixels stained with TMRM or FITC dextran was calculated. Perfusion deficits induced by SAH were quantified by comparing the total number of reconstructed dye-containing pixels. Superficial vessels including penetrating arterioles and the

parenchymal microcirculation were analyzed separately.

Blood flow velocity was calculated by dividing the travelled distance (µm) by the respective travel time (msec) and expressed as % of baseline values.

Sticking/plugging leukocytes were defined as red signals larger than 5 µm size which were immobile within 10 min. Leukocytes were quantified separately in pial venules and in parenchymal capillaries.

Statistical analysis

Statistical tests were performed with the SigmaPlot 12.0 software package (Systat Software Inc., USA). Groups were compared with the Mann Whitney U test. Differences of $p < 0.05$ were considered as statistically significant. Data are shown in mean ± standard deviation (SD) unless indicated otherwise.

	sham	SAH
et pCO_2 (mmHg)	25.6 ± 1.6	26.5 ± 1.5
blood pressure (mmHg)	86 ± 11	84 ± 16
temperature (°C)	37.5 ± 0.1	37.4 ± 0.2
heart rate (beats/min)	274 ± 63	306 ± 51
oxygen saturation (%)	97.5 ± 1.6	96.8 ± 1.5

Table 1 *Physiological monitoring during in vivo microscopy*

Results

During imaging systemic blood pressure, core body temperature, heart rate, and systemic hemoglobin oxygen saturation were within the physiological range and did not differ between mice subjected to SAH or sham surgery (Table 1). In order to control and maintain a physiologic arterial pCO_2, one of the main parameters determining cerebral vessels diameter, endexpiratory CO_2 was continuously measured by microcapnometry and kept constant by adjusting the ventilation frequency. This resulted in physiological arterial pCO_2 values.

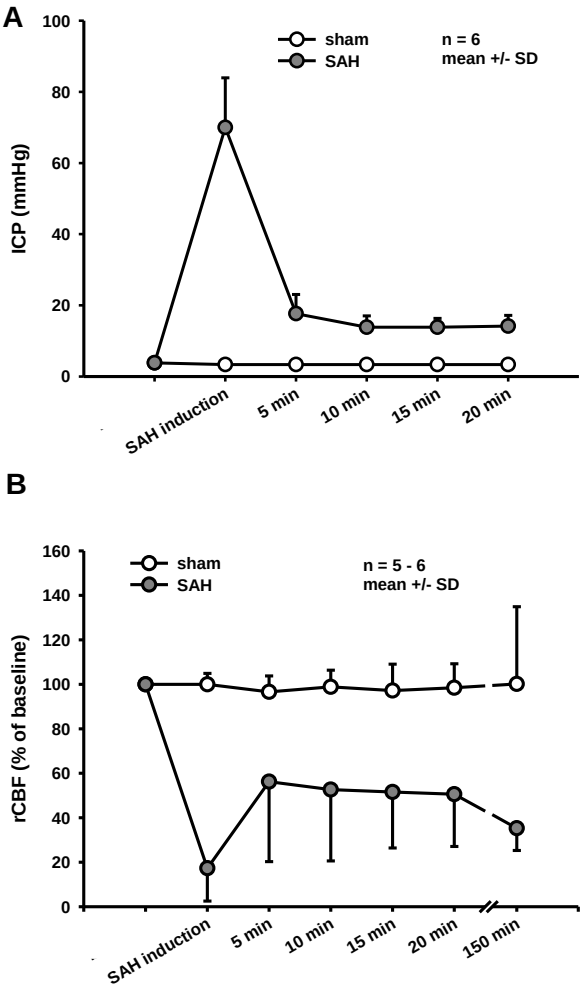

Figure 2

A *ICP measurement in mmHg during SAH/sham induction. SAH induction leads to a sharp increase of the ICP and stabilizes within five minutes at values around 14 mmHg. In sham condition ICP stays at baseline levels of four mmHg throughout the procedure.* ***B*** *rCBF values are shown in % of baseline. SAH induction leads to a drop in regional perfusion which does not recover even when ICP values stabilize.*

Physiological monitoring

SAH induced a sharp increase of ICP to values above 60 mmHg. After cessation of hemorrhage ICP dropped to mean values of 14 mmHg (Fig. 2A). Due to the reduction of cerebral perfusion pressure (CPP) the initial ICP peak was accompanied by a drop of regional cerebral blood flow (rCBF) in the hemisphere ipsilateral to the hemorrhage down to ischemic levels (Fig. 2B). Hence, animals suffer global cerebral ischemia for a few minutes. Despite recovery of ICP and the subsequent normalization of CPP rCBF

remained reduced after SAH. This suggests that mechanisms independent of CPP, i.e. spasms of the cerebral microcirculation, are responsible for post-hemorrhagic oligemia or ischemia.

Microvasospasms of the pial arterioles after SAH

The mean diameter of pial arterioles is significantly reduced by 23% after SAH (Fig. 3). 71% of measured vessel segments were spastic. When looking at the vessel morphology after SAH in detail three different vessel constriction types were distinguishable (Fig. 4A). 68% of observed vessel segments revealed pearl-string like constrictions as shown previously by pial vessel imaging after SAH.[10] However we detected two other constriction patterns. 21% of vessels showed an overall reduced vessel diameter over a long distance without additional focal constrictions (Fig. 4A and B, global constriction). A third type of spasms was characterized by an unchanged vessel diameter in proximal areas and an almost obliterated vascular lumen in more distal segments (Fig. 4A and B, bottleneck constriction). In order to further characterize the vessel constriction types we calculated a vessel constriction index, which describes the normalized range of vessel diameter within one vessel segment (see legend for details). The vessel constriction index is doubled after SAH (Fig. 4C).

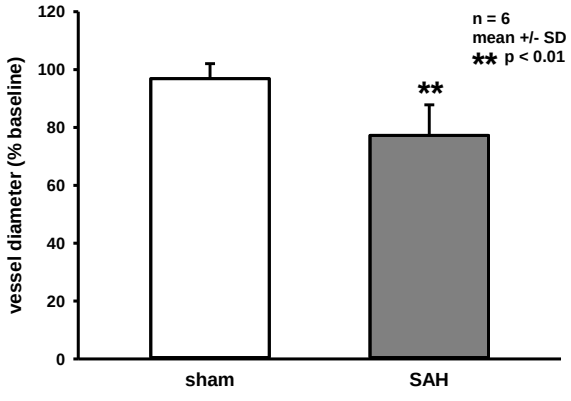

Figure 3
Measurement of vessel diameter after SAH/sham. Vessel diameter after SAH is significantly ($p < 0.01$) reduced compared to sham condition.

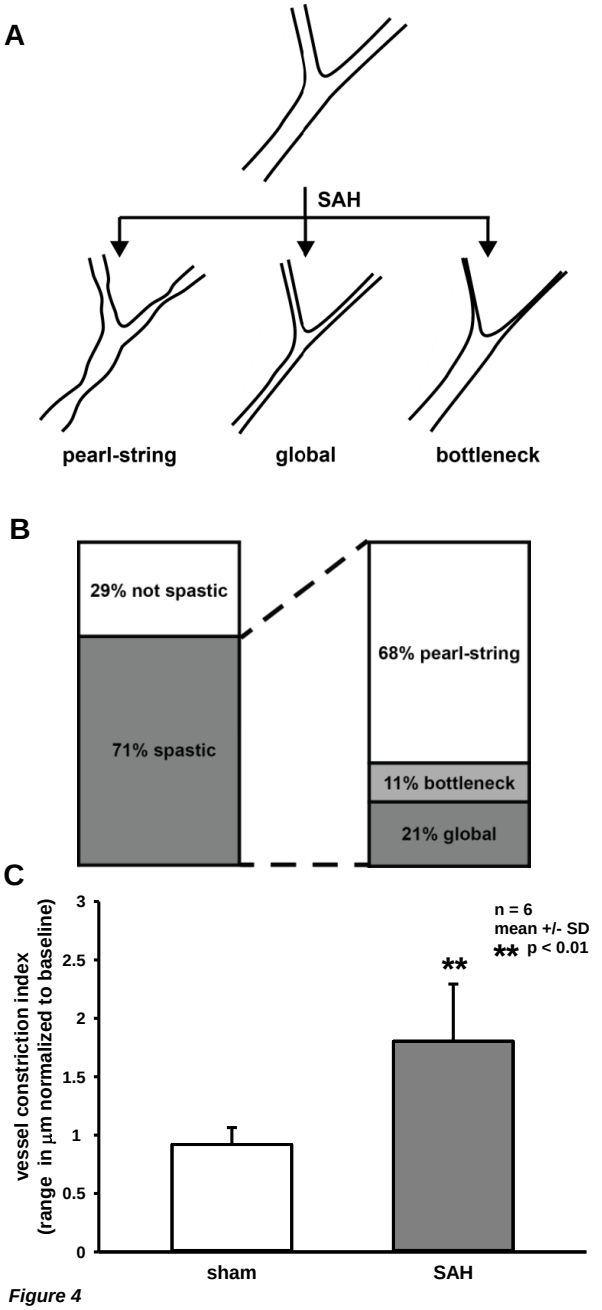

Figure 4

A *SAH induced different vessel constriction types: pearl-string constriction, global constriction and bottleneck constriction types were found in superficial arteries. Pearl-string constrictions were classified as vessel segments that had a 20% mean reduction of vessel diameter and a 30% diameter variability within the segment. The global constriction type was classified as a vessel segment that showed a reduction of vessel diameter of 20% and a variability within the segment of less than 30%. The bottleneck constriction type was characterized by more than 20% reduction and 30% variability of vessel diameter in conjunction with a decreased vessel diameter in distal segments.* ***B*** *After SAH 71% of the vessels were spastic with a mean diameter reduction of 20%. Of spastic vessels 68% showed a pearl-string constriction, 11% a bottleneck constriction and 21% a global constriction.* ***C*** *The vessel constriction index describes the range*

of vessel diameters measured within one segment normalized to the baseline condition. The vessel constriction index was significantly ($p < 0.01$) increased after SAH.

Reduction of blood flow velocity after SAH

Vasoconstriction could in theory be compensated by an increased blood flow velocity in order to maintain tissue perfusion. Therefore we measured blood flow velocity in pial arterioles after SAH. Instead of a compensatory increase in blood flow velocity we detected a reduction of blood flow velocity (Fig. 5B). Blood flow velocity in arterioles was reduced by 54% after SAH (Fig. 5B). When plotting the reduction of blood flow velocity against the degree of constriction only a weak correlation is found (Fig. 5C), suggesting that constriction of vessels is not exclusively responsible for the reduction of pial blood flow velocity after SAH. Other mechanisms like microthrombosis or plugging of capillaries by leukocytes may be involved.

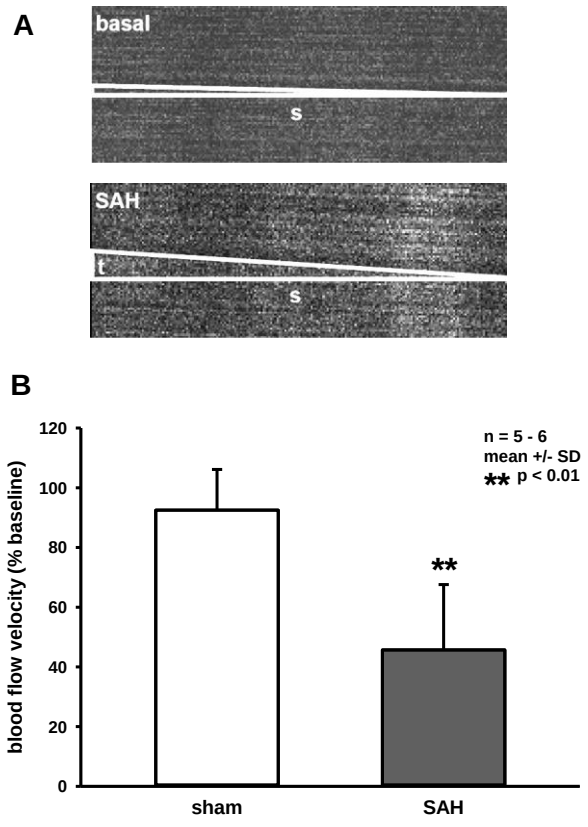

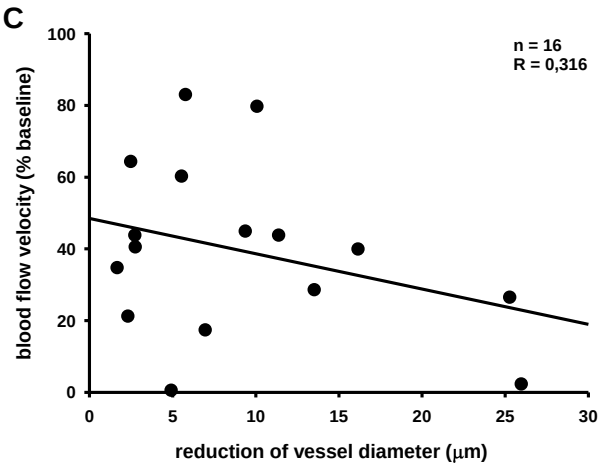

Figure 5
A *Example of repetitive line scans for blood flow velocity measurement.* ***B*** *Blood flow velocity is shown in % of baseline in corresponding vessel segments. Blood flow velocity is significantly ($p < 0.01$) reduced after SAH compared to the sham situation.* ***C*** *Correlation of reduction of blood flow velocity (in %) and reduction of vessel diameter (in µm).*

Perfusion of parenchymal vessels after SAH

After showing that SAH results in spasms of pial microvessels, which are located in the subarachnoid space and come into contact with blood, we wanted to know if these spasms result in impaired perfusion of downstream vessel branches, i.e. penetrating arterioles and the parenchymal microcirculation, which actually deliver oxygen and nutrients to brain tissue. To receive a value representing total perfusion in a given tissue volume, we stained the intravascular space with a fluorescent plasma marker, recorded the fluorescence by two-photon microscopy and counted fluorescent pixels in 3D (Fig. 6A). Since we previously observed that microvasospasms are more pronounced in small arterioles,[10] we analyzed pial vessels and penetrating arterioles separately from the perfused parenchymal microvessels. This analysis demonstrates that only 57% of all superficial and penetrating arterioles are still perfused after SAH (Fig. 6B). In the parenchymal microcirculation only 32% of the pre-hemorrhagic microvascular volume is still perfused after SAH (Fig. 6C), a value well in line with reduction of rCBF obtained by cortical laser Doppler measurements.

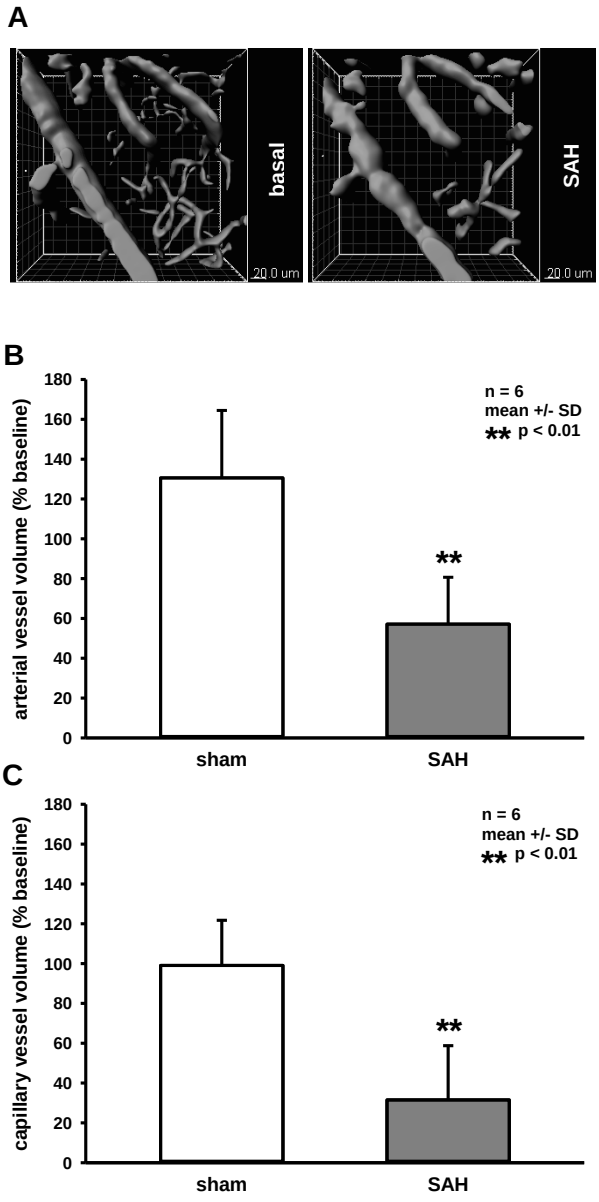

Figure 6

***A** Example of 3D vessel reconstruction with Imaris software after SAH. Large parts of the parenchymal microcirculation are not perfused after SAH. **B** Perfused arterial vessel volume is shown in % of baseline. Perfused arterial volume is significantly ($p < 0.01$) reduced after SAH compared to the sham situation. **C** Perfused capillary vessel volume is shown in % of baseline. Perfused capillary volume is significantly ($p < 0.01$) reduced after SAH compared to the sham situation.*

Leukocyte adhesion and plugging after SAH

Activated endothelium after SAH expresses adhesion molecules[14] which results in rolling and sticking of leukocytes in post-capillary venules. If capillaries are constricted above a certain degree, leukocytes may get stuck and block perfusion, a process called leukocyte plugging.[15] In the current study we investigated leukocyte adhesion in post-capillary venules and leukocyte plugging in capillaries in order to evaluate if the cerebrovascular endothelium gets activated and if leukocyte plugging may represent a possible mechanism for the loss of microcirculatory perfusion after SAH. After sham surgery little sticking or plugging leukocytes were detected (Fig. 7B, white bars). Three hours after SAH, when adhesion molecules start to be expressed on activated endothelium, multiple sticking (Fig. 7A arrowhead) and plugging (Fig. 7A arrow) leukocytes were found in the cerebral microcirculation. As compared to sham operated mice the number of leukocytes sticking in post-capillary venules and capillaries increased five-fold after SAH (Fig. 7B, gray bars). Since most capillaries which were occluded by leukocytes were also filled with the plasma marker FITC-dextran, the plugging must have occurred after injection of the plasma and leukocyte marker. Accordingly, we may have missed leukocytes already sticking in the microcirculation before this time window. The current data suggest that plugging leukocytes may contribute to the microvascular perfusion deficit observed after SAH.

Discussion

In the current study we examined the mechanism responsible for early cerebral ischemia after SAH and found that SAH induces arteriolar constrictions in pial arterioles and that these microvasospasms are associated with a heavily reduced perfusion of parenchymal microvessels. To explore for the mechanisms of parenchymal perfusion deficits we observed that the number of leukocytes plugging parenchymal capillaries increased five-fold after SAH. However, since the absolute number of plugged capillaries was too low to fully explain the severe perfusion deficits, we conclude that microvasospasms in pial arterioles are the main factor resulting in reduced cortical perfusion following SAH.

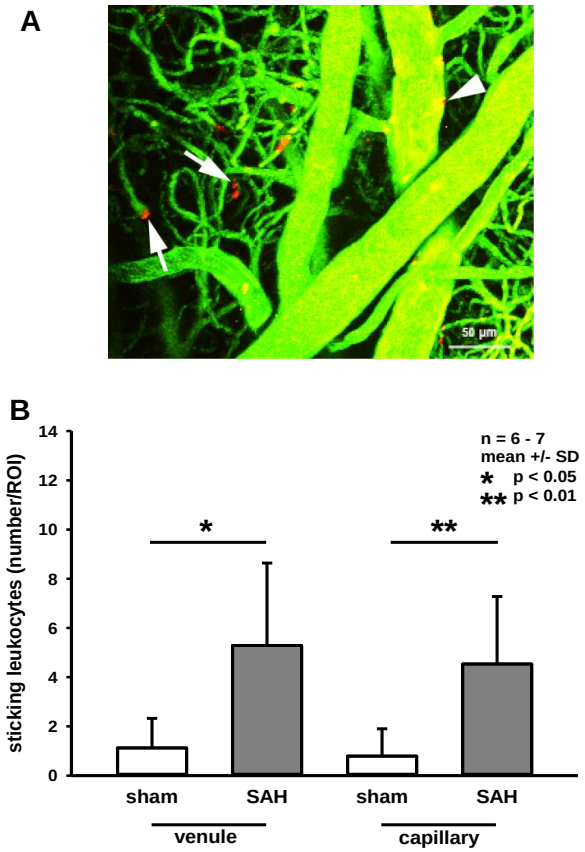

Figure 7
A *Example of projected microcirculation after SAH with sticking leukocytes (red) in parenchymal vessels and superficial venules. Arrows indicate sticking leukocytes in capillaries and arrowhead shows a sticking leukocyte in a venule.* ***B*** *Leukocyte-endothelium interactions are enhanced after SAH. In average 5 sticking leukocytes can be found in superficial venules of each ROI. 5 adherent leukocytes could be detected in the capillaries in a brain volume of 0.19 mm³. After SAH leukocyte-endothelium interactions are significantly increased ($p < 0.05$ and $p < 0.01$ respectively) compared to the sham situation in capillaries and venules.*

Experimental approach

In the current study we used the endovascular filament technique to induce SAH as it resembles the pathophysiology of SAH in patients most closely.[16] However, when using this model a comprehensive physiological monitoring is crucial to obtain a standardized bleeding induction. Especially the measurement of ICP, as performed in the current study, is important to ensure a standardized bleeding.[17] An important parameter which needs to be monitored and adjusted when studying the cerebral vasculature *in vivo* is the arterial pCO_2, since CO_2 is a strong and selective dilator of cerebral vessels. Therefore changes in pCO_2 due to variations in respiration may influence and bias measurement of cerebral vessel diameter. Experiments in the current study were performed on intubated and ventilated mice under real-time measurement of endexpiratory pCO_2 by microcapnometry in order to keep the arterial pCO_2 in a physiological range.

Cerebral blood flow after SAH

So far it was known from experimental studies that acutely after SAH the sudden rise in ICP to values near the systemic blood pressure results in a severe drop of CPP and subsequent global ischemia.[18] Within two to three minutes after SAH the ICP drops to about 20 mmHg and, hence, CCP returns to almost normal values. However, despite restoration of CPP CBF remains reduced after SAH.[18] In the current study we demonstrate that the post-hemorrhagic reduction in CBF last for 3 hours after SAH and becomes more severe over time. The fact that the cerebral perfusion is significantly reduced at almost normal CCP values following SAH together with the observation that spasms of the large intracranial arteries occur mostly later than five days after SAH suggest that constrictions or obstructions of cerebral vessels on the level of pial arterioles or below are responsible for the observed reduction of cerebral blood flow after SAH.[18, 19] Since these vessels are below the resolution of clinical CT and MR scanners it becomes clear why the contribution of this vascular compartment to the pathogenesis of SAH remained yet mostly unnoticed.

The pial microcirculation after SAH

The arterial cerebral microcirculation consists of three major compartments: pial arterioles feeding the pial microcirculation on the surface of the brain and draining into penetrating arterioles, penetrating arterioles which dive into the brain parenchyma, and parenchymal capillaries which deliver nutrients and oxygen to the brain parenchyma. In principle constriction or occlusion at all three levels of the cerebral microcirculation

could result in cerebral hypoperfusion or ischemia. The pial vasculature is the only compartment of the cerebral microcirculation investigated so far following SAH *in vivo*. In single patients as well as in experimental animals we and others demonstrated that pial arterioles show characteristic, pearl-string like constrictions following SAH.[8, 10, 20] In mice these arterial microvasospasm last for up to three days after hemorrhage. In addition to microvasospasm 30% of these arterioles were occluded by microthrombosis.[10] In the current study using two-photon microscopy we confirmed our previous results and were able to demonstrate that in total 71% of vessels are spastic after SAH. By using two-photon microscopy and line scanning we could also demonstrate that spasms of pial arterioles are hemodynamically relevant. Pial arterioles showed a reduction in blood flow velocity of 54% thereby proving that spasms of pial arterioles are not epiphenomena but indeed directly involved in the reduction of cerebral perfusion after SAH. So far the mechanisms causing post-hemorrhagic vasospasms are not completely clear. Recently we demonstrated that pial arterioles and cerebral blood flow following SAH in mice are not responsive to CO_2,[21] a selective cerebral vasodilator which exerts its activity through vascular and neuronal nitric oxide (NO).[22, 23] Accordingly, the lack of CO_2 reactivity after SAH suggests that perivascular blood blocks NO signaling thereby causing vasoconstriction. Further studies, however, need to clarify whether this conclusion can be proven experimentally and whether influencing NO signaling may represent a therapeutic option after SAH.

The parenchymal microcirculation after SAH

As mentioned above, the lack of high-resolution deep brain imaging technology did not allow studying the effect of SAH and pial artery spasms on the parenchymal microcirculation so far. Accordingly, it was not known if SAH has an effect on parenchymal microperfusion. Our current experiments demonstrate that the parenchymal microcirculation is severely affected after SAH. The arterial volume is reduced to 57% after SAH. When investigating the parenchymal microcirculation this fraction of no longer perfused vessels is even 68%. These data demonstrate that not only the pial but also the parenchymal microperfusion is severely compromised after SAH and that the microcirculation plays an important role for the pathogenesis of post-hemorrhagic ischemia. As discussed for pial microvessels above, also the mechanisms for the lack of perfusion of parenchymal microvessels is largely unknown. One obvious possibility is that the constrictions and microthrombi observed in pial arterioles restrict blood flow to the brain parenchyma thereby causing the reduction of parenchymal perfusion. Complete occlusion of one single penetrating arteriole on the pial surface has already effects on the capillary perfusion in its territory.[24] Accordingly, our data suggest that subarachnoid blood after SAH constricts pial arterioles and this may result in wide spread loss of parenchymal perfusion. Another possible mechanism for the lack of parenchymal perfusion may be leukocytes that interact with the endothelium after SAH.[25] This is a likely event, since it is well known that leukocytes sticking in brain capillaries contribute to the “no-reflow” following focal cerebral ischemia.[15] Accordingly, it could well be that the observed changes in the cerebral microcirculation after SAH are caused by the initial post-hemorrhagic global ischemia and are not secondary to changes in the pial microcirculation. If this was true, we should be able to detect a considerable amount of leukocytes obstructing parenchymal capillaries in our experiments. In fact, we found a five-fold increase of the number of leukocytes sticking in parenchymal microvessels after SAH as compared to sham. When considering that extremely few leukocytes stick to capillaries in normal brain and when looking at the absolute number of sticking cells, i.e. five sticking leukocytes in a volume of 0.19 mm^3, it becomes obvious that despite this significant increase of the number of sticking leukocytes, the biological relevance of leukocytes obstructing parenchymal microvessels after SAH

is most likely negligible. Since plugging leukocytes are characteristic for microvascular no-reflow after global ischemia our data suggest that the perfusion deficits in parenchymal microvessels observed in the current study are most likely not a consequence of global post-hemorrhagic ischemia. Further studies, however, are needed to establish a firm cause-effect relationship between pial spasms and loss of parenchymal perfusion after SAH.

Taken together, this is the first study to investigate the parenchymal microcirculation after SAH *in vivo*. In addition to a better characterization of pial spasms, the main finding of our study is that SAH causes a severe loss of microperfusion in the brain parenchyma. Since no biologically relevant plugging of leukocytes was observed, we conclude that the mechanisms underlying the loss of parenchymal perfusion are spasms of pial arterioles. The current study establishes the massive lack of parenchymal microperfusion as a likely mechanism for cerebral ischemia observed in SAH patients before the occurrence of delayed large artery spasms and may thereby pave the way for novel therapeutic concepts for treatment of early cerebral ischemia following SAH.

References

1. Johnston, S.C., Selvin, S. & Gress, D.R. The burden, trends, and demographics of mortality from subarachnoid hemorrhage. *Neurology* **50**, 1413-8 (1998).
2. Pobereskin, L.H. Influence of premorbid factors on survival following subarachnoid hemorrhage. *J Neurosurg* **95**, 555-9 (2001).
3. van Gijn, J., Kerr, R.S. & Rinkel, G.J. Subarachnoid haemorrhage. *Lancet* **369**, 306-18 (2007).
4. Jackowski, A., Crockard, A., Burnstock, G., Russell, R.R. & Kristek, F. The time course of intracranial pathophysiological changes following experimental subarachnoid haemorrhage in the rat. *J Cereb Blood Flow Metab* **10**, 835-49 (1990).
5. Schubert, G.A., Seiz, M., Hegewald, A.A., Manville, J. & Thome, C. Acute hypoperfusion immediately after subarachnoid hemorrhage: a xenon contrast-enhanced CT study. *J Neurotrauma* **26**, 2225-31 (2009).
6. Frontera, J.A. et al. Acute ischaemia after subarachnoid haemorrhage, relationship with early brain injury and impact on outcome: a prospective quantitative MRI study. *J Neurol Neurosurg Psychiatry* **86**, 71-8 (2015).
7. Bederson, J.B. et al. Acute vasoconstriction after subarachnoid hemorrhage. *Neurosurgery* **42**, 352-60; discussion 360-2 (1998).
8. Uhl, E., Lehmberg, J., Steiger, H.J. & Messmer, K. Intraoperative detection of early microvasospasm in patients with subarachnoid hemorrhage by using orthogonal polarization spectral imaging. *Neurosurgery* **52**, 1307-15; disacussion 1315-7 (2003).
9. Pennings, F.A., Bouma, G.J. & Ince, C. Direct observation of the human cerebral microcirculation during aneurysm surgery reveals increased arteriolar contractility. *Stroke* **35**, 1284-8 (2004).
10. Friedrich, B., Muller, F., Feiler, S., Scholler, K. & Plesnila, N. Experimental subarachnoid hemorrhage causes early and long-lasting microarterial constriction and microthrombosis: an in-vivo microscopy study. *J Cereb Blood Flow Metab* **32**, 447-55 (2012).
11. Schuller, K., Buhler, D. & Plesnila, N. A murine model of subarachnoid hemorrhage. *J Vis Exp*, e50845 (2013).
12. Nakamura, T. et al. Acute CO2-independent vasodilatation of penetrating and pre-capillary arterioles in mouse cerebral parenchyma upon hypoxia revealed by a thinned-skull window method. *Acta Physiol (Oxf)* **203**, 187-96 (2011).
13. Schwarzmaier, S.M. et al. In vivo temporal and spatial profile of leukocyte adhesion and migration after experimental traumatic brain injury in mice. *J Neuroinflammation* **10**, 32 (2013).
14. Wang, Z. et al. Progesterone administration modulates cortical TLR4/NF-kappaB signaling pathway after subarachnoid hemorrhage in male rats. *Mediators Inflamm* **2011**, 848309 (2011).
15. del Zoppo, G.J., Schmid-Schonbein, G.W., Mori, E., Copeland, B.R. & Chang, C.M. Polymorphonuclear leukocytes occlude capillaries following middle cerebral artery occlusion and reperfusion in baboons. *Stroke* **22**, 1276-83 (1991).
16. Kooijman, E. et al. The rodent endovascular puncture model of subarachnoid hemorrhage: mechanisms of brain damage and therapeutic strategies. *J Neuroinflammation* **11**, 2 (2014).
17. Feiler, S., Friedrich, B., Scholler, K., Thal, S.C. & Plesnila, N. Standardized induction of subarachnoid hemorrhage in mice by

intracranial pressure monitoring. *J Neurosci Methods* **190**, 164-70 (2010).
18. Bederson, J.B., Germano, I.M. & Guarino, L. Cortical blood flow and cerebral perfusion pressure in a new noncraniotomy model of subarachnoid hemorrhage in the rat. *Stroke* **26**, 1086-91; discussion 1091-2 (1995).
19. Plesnila, N. Pathophysiological Role of Global Cerebral Ischemia following Subarachnoid Hemorrhage: The Current Experimental Evidence. *Stroke Res Treat* **2013**, 651958 (2013).
20. Sun, B.L. et al. Dynamic alterations of cerebral pial microcirculation during experimental subarachnoid hemorrhage. *Cell Mol Neurobiol* **29**, 235-41 (2009).
21. Friedrich, B. et al. CO2 has no therapeutic effect on early microvasospasm after experimental subarachnoid hemorrhage. *J Cereb Blood Flow Metab* **34**, e1-6 (2014).
22. Iadecola, C. & Zhang, F. Nitric oxide-dependent and -independent components of cerebrovasodilation elicited by hypercapnia. *Am J Physiol* **266**, R546-52 (1994).
23. Niwa, K., Lindauer, U., Villringer, A. & Dirnagl, U. Blockade of nitric oxide synthesis in rats strongly attenuates the CBF response to extracellular acidosis. *J Cereb Blood Flow Metab* **13**, 535-9 (1993).
24. Nishimura, N., Rosidi, N.L., Iadecola, C. & Schaffer, C.B. Limitations of collateral flow after occlusion of a single cortical penetrating arteriole. *J Cereb Blood Flow Metab* **30**, 1914-27 (2010).
25. Ishikawa, M. et al. Platelet and leukocyte adhesion in the microvasculature at the cerebral surface immediately after subarachnoid hemorrhage. *Neurosurgery* **64**, 546-53; discussion 553-4 (2009).

The role of pericytes on microcirculatory dysfunction after subarachnoid hemorrhage

Aim of the study:

Pericytes are a perivascular cell type that expresses contractile elements[186] and covers up to 30% of cerebral capillary surface.[156] Their ability to constrict and thereby potentially control blood flow in the cerebral microcirculation has long been discussed. Recent data supports that pericytes are involved in the regulation of vessel diameter and blood flow during neurovascular coupling.[198] Whether they influence cerebral blood flow under pathological conditions is under debate and studies which were performed after cerebral ischemia suggest different potential pathomechanisms of pericytes.

In an ultrastructural study pericytes were shown to detach from the endothelium and migrate towards the parenchyma after brain hypoxia.[207] Perivascular stromal cells that migrate upon focal ischemia from vessels into the ischemic tissue might be involved in scar formation.[205] Furthermore it has been shown that pericyte numbers decline after ischemia indicating early death of pericytes in ischemic conditions.[198] Last but not least pericyte have been shown to constrict after ischemia due to oxidative stress thereby inducing capillary narrowing.[203] Because one major hallmark of early brain injury after SAH is cerebral ischemia, we hypothesized that pericytes may play a crucial role in the pathophysiology after SAH.

Pericyte survival was examined by platelet derived growth factor beta (PDGF Rβ) staining and revealed that pericytes do not undergo cell death three and 24 hours after SAH. Furthermore potential pericyte constriction after SAH and its involvement in the formation of microvasospasm was investigated by two-photon microscopy. For that purpose a transgenic mouse line which expresses a fluorescent marker under control of the neural/glial antigen 2 (NG2) promotor was used.[215] Perivascular expression of NG2 was characterized by immunohistochemistry with different cell markers. $NG2^+$ cells that were associated to vessels bigger than 10 µm co-localized with αSMA and confluently covered the vessel indicating that these cells are vascular smooth muscle cells. Vascular smooth muscle cells co-localized with superficial microvasospasm after SAH. $NG2^+$ cells associated to capillaries co-stained with PDGF Rβ and revealed pericyte morphology. Therefore we identify those cells as mid-capillary pericytes. When comparing capillary diameter after SAH at sites where pericytes are associated to vessels with sites where no pericyte is present no significant difference was found. Therefore we conclude that pericytes are not involved in capillary narrowing after SAH. Other components of the neurovascular unit will have to be investigated in detail to reveal the pathomechanism of capillary narrowing after SAH.

The role of pericytes on microcirculatory dysfunction after subarachnoid hemorrhage

Kathrin Schüller [1,2], Matilde Balbi [1,2], Nikolaus Plesnila [1,2,3]

[1] Institute for Stroke and Dementia Research, University of Munich Medical Center, Munich, Germany

[2] Graduate School of Systemic Neurosciences, Ludwig-Maximilians-Universität, Munich, Germany

[3] Cluster of Systems Neurology (Synergy), Munich

Author contributions: KS and NP planned experiments, KS and MB acquired data, KS analyzed data, KS and NP wrote manuscript

Key words: pericyte, subarachnoid hemorrhage, ischemia, migration, cell death, constriction

Abstract

Microvasospasms of pial vessels occur after subarachnoid hemorrhage in humans as well as in mice and are suspected to be involved in the development of early cerebral ischemia. The underlying pathomechanisms of early vessel spasm are not known. In this study we investigate the transgenic pericyte reporter mouse line NG2 DsRed in a model of subarachnoid hemorrhage to investigate the role of pericytes in the formation of vessel spasms. Vessel diameter in conjunction with pericyte location was evaluated by two-photon microscopy.

The expression of the red fluorescent protein (DsRed) under the neural/glial antigen 2 (NG2) promotor was characterized by immunohistochemistry for different cell markers. Pericyte survival and migration was investigated three and 24 hours after subarachnoid hemorrhage by staining for platelet derived growth factor receptor β.

$NG2^+$ cells covering arteries and arterioles express α-smooth muscle actin and are negative for pericyte markers suggesting that these cells are vascular smooth muscle cells. $NG2^+$ cells located on capillaries express platelet derived growth factor receptor β and are therefore presumably pericytes. Cell counts of $NG2^+$ cells at three and 24 hours after subarachnoid hemorrhage did not reveal pericyte death or migratory behavior in the cortex, hippocampus or striatum. Arterioles as well as capillaries showed a significantly reduced vessel diameter three hours after subarachnoid hemorrhage. Constricted arterioles were covered with vascular smooth muscle cells. The capillary vessel diameter however was continuously narrowed and constrictions were not restricted to sites where $NG2^+$ cells were located.

We conclude that the localization and the viability of pericytes are not altered three and 24 hours after subarachnoid hemorrhage. Arterioles as well as capillaries exhibit a reduced vessel diameter after SAH. Pericytes however do not seem to be involved in the formation of capillary spasm after SAH.

Introduction:

Subarachnoid hemorrhage (SAH) is a devastating subtype of stroke that is associated with a high 30 days mortality. 21% of case fatalities occur within 24 hours after the bleeding.[1] Early brain injury describes acute pathological consequences of the bleeding into the subarachnoid space. They are multifactorial and induced by increased intracranial pressure (ICP), cerebral ischemia, brain edema, early cell death and inflammatory processes.[2] Early cerebral ischemia predicts the 24 hour mortality in a rat SAH model[3] and negatively influences three-month outcome of SAH patients.[4] The underlying mechanisms of early cerebral ischemia are not clear to date. Pearl-string like constrictions of superficial arteries arise in humans[5, 6]as well as in mice[7, 8] early after SAH. In the SAH mouse model superficial microvasospasms are present from three to 72 hours after the bleeding and induce microthrombosis in pial vessels.[7] Moreover a subsequent reduction of blood flow velocity as well as deep parenchymal cerebral perfusion deficits are related to microvasospasms. To date the underlying pathophysiology of acute vessel spasm formation is not clear. The extravasated subarachnoid blood is suspected to play a role in the development of arteriolar spasm. Imaging data in humans indicate that early ischemia after SAH is more pronounced in regions which are in close proximity to the aneurysm rupture.[9] It is suggested that free hemoglobin that is released into the subarachnoid space scavenges nitric oxide (NO), an endothelial vasodilator. A reduction of endothelial NO leads to a vessel narrowing that can be resolved by the application of a NO donor.[10]

Whether also capillaries in the parenchyma, which do not come in direct contact with subarachnoid blood, constrict in response to SAH is not clear. The cell type of the neurovascular unit that may induce spasm at the level of the capillaries are contractile pericytes. Increasing evidence indicates that pericytes regulate capillary diameter in health and disease.[11] Pericytes were shown to constrict upon cerebral ischemia and thereby hamper blood flow in capillaries.[12] In this study we aim to investigate whether pericytes exhibit a constrictive phenotype after SAH and are thereby involved in the formation of early cerebral ischemia.

Therefore we investigate the response of pericytes after SAH *in vivo*. By making use of the transgenic pericyte reporter mouse line NG2 DsRed[13] we want to elucidate the contribution of pericytes in the formation of microvasospasm. Data obtained after cerebral ischemia indicate that pericytes exhibit a migratory phenotype towards the ischemic lesion and contribute to scar formation.[14] Therefore we also aim to investigate migratory and cell death behavior of pericytes in response to SAH.

The identification of the role of pericytes will help to further characterize the pathophysiology of early cerebral ischemia after SAH.

Material and Methods:

Animals and experimental groups

In this study a transgenic reporter mouse line was investigated in an experimental setup for two-photon microscopy after SAH. The NG2 DsRed mouse line[13] is used for the visualization of pericytes and vascular smooth muscle cells (VSMC). Mice were obtained from the Jackson Laboratory and thereafter bred heterozygously on a C57Bl6 background. Experiments are approved by the Government of Upper Bavaria.

Histological analysis

Brains of heterozygous transgenic NG2 DsRed mice were extracted after perfusion and incubated in 4% PFA at 4°C over night. Brains were embedded in 2% agarose and sectioned with a vibratome (Leica, Germany) in 50 µm thick slices. Slices were collected in a cryoprotectant solution (50% 0.1 phosphate buffered saline (PBS), 25% glycerol, 25% polyethylenglycol) for long-term storage at -20°C. Before staining the sections were washed for three days in PBS at 4°C to remove cryoprotectant solution. Staining was performed for NeuN (MAB377 Millipore,

Darmstadt, Germany), glial fibrillary acidic protein (GFAP) (3670, Cell Signaling, USA), aquaporine 4 (AB 2218 Millipore, Darmstadt, Germany), platelet endothelial cell adhesion molecule (CD31) (BM4086 Acris, Germany), α smooth muscle actin (αSMA) (CP47 Novus, USA), desmin (MAP3430 Millipore, Darmstadt, Germany) and platelet derived growth factor receptorβ (PDGF Rβ) (3169 NEB, USA). Sections were blocked for one hour at room temperature in a blocking solution (3% bovine serum albumin, 0.5% glycine, 0.5% triton). Incubation of primary antibody was at 4°C over night in blocking solution. Sections were washed and incubated in the secondary antibody in blocking solution for two hours at room temperature. Alexa Fluor 488 and Cy3 conjugated AffiniPure (Jackson) secondary antibodies were chosen according to the species of the primary antibody. Sections were mounted in Vectashield DAPI mounting medium (Vector Labs, USA) for histological analysis. Microscopy of free-floating sections was performed with an Imager 7 fluorescent microscope (Zeiss, Germany). Confocal microscopy was performed with a LSM 7 confocal microscope (Zeiss, Germany).

Pericyte count after SAH

Free floating sections of NG2 DsRed mice three hours after SAH or sham surgery were stained according to the protocol described above for PDGF Rβ. Images for cell counts were captured with a 20x objective. Four regions of interest (ROI) in the cortex, two ROI in the hippocampus and two ROI in the striatum were analyzed in two coronal slices of each animal. Cells were counted with Image J software (NIH, USA).

Two coronal slices of free floating sections of C57Bl6 mice 24 hours after SAH or sham surgery were collected. The vasculature was stained with FITC lectin and pericytes with PDGF Rβ according to the protocol described above. Pericyte cell counts were performed as described for the three hour group.

SAH/sham surgery

SAH and sham surgery was performed as described previously.[15] After anesthesia induction with isoflurane mice were anesthetized with a mixture of 0.05 mg/kg fentanyl (Janssen-Cilac, Neuss, Germany), 0.5 mg/kg medetomidine (Pfizer, USA) and 5 mg/kg midazolam (Braun, Germany). Mice received a preoperative analgesia of 4 mg/kg carprofen (Pfizer, USA) subcutaneously. They were intubated and placed on a feedback regulated heating pad. A laser Doppler probe (Periflux 5000, Perimed, Sweden) was glued on the temporal bone. An ICP sensor (Codman, Johnson & Johnson, UK) was implanted under the temporal bone in the epidural space. For SAH/sham induction a stiff prolene 5-0 filament was inserted into the external carotid artery and advanced to the Circle of Willis via the internal carotid artery. At the bifurcation of the middle cerebral artery the Circle of Willis was perforated and a bleeding into the subarachnoid space was induced. Sham surgery was performed accordingly except that the vessel wall was not perforated. Animals were monitored for physiologic parameters 20 minutes post hemorrhage. After suturing anesthesia was antagonized by subcutaneous injection of 1.2 mg/kg naloxone (Actavis, Ireland, USA), 0.5 mg/kg flumazenil (Inresa, Germany) and 2.5 mg/kg atipamezol (Pfizer, USA).

Two-photon microscopy

First a thinned skull window preparation was performed as described previously.[16] Therefore the left hemisphere of the skull was exposed and major branches of the MCA were identified. After topic application of lidocaine (2% HCl) the skull over the parietal cortex was thinned. During drilling the bone was cooled continuously to prevent heat damage.

Two-photon microscopy was performed with a LSM 7 (Zeiss, Germany), equipped with a Li:Ti laser (Chameleon, Coherent, USA), as described previously.[17] Briefly anesthetized animals were intubated and mechanically ventilated (Minivent 845, Hugo Sachs, Germany). The endexpiratory

pCO_2 was measured by microcapnography (Model 340, Hugo Sachs, Germany). Animals were placed on a feedback controlled heating pad to maintain a body temperature of 37°C. Heart rate and peripheral oxygen saturation were measured on the hind paw by a pulsoximeter (MouseSAT, Kent Scientific, USA). The mouse was mounted in a nose clamp (David Kopf instruments, USA) and transferred to the microscope. Z stacks of 4 randomly chosen ROI were performed as follows: Fluorescence emission was captured with 20x water immersion objective (Plan Apochromat, NA 1.0 Zeiss, Germany) and GaAsP-NDD detectors for green (500-550 nm band pass) and red fluorescence (565-610 nm band pass). Z stacks of vessels and pericytes were obtained by scanning an area of 609 x 609 µm with a step distance of 1 µm. The depth of z-stacks varied due to window preparation and ranged from 250 to 400 µm. Laser power did not exceed 10% at the brain surface and was adjusted in deeper brain areas.

For the second imaging session the left femoral artery was catheterized using standard techniques. Fluoreszeinisothiocynate (FITC) dextran (0.5% in saline, Sigma Aldrich, USA) was injected to visualize the perfused vasculature. Imaging of the four ROIs was performed as described above.

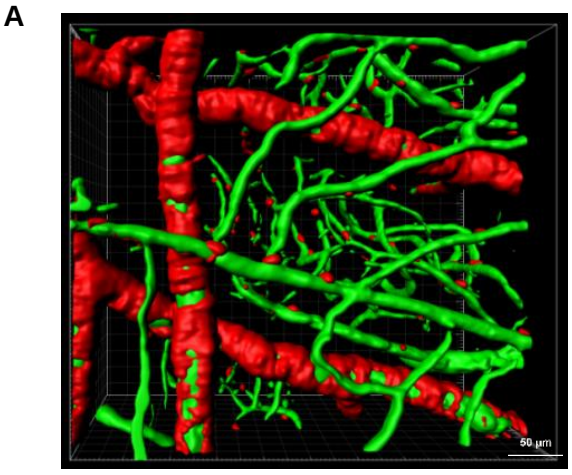

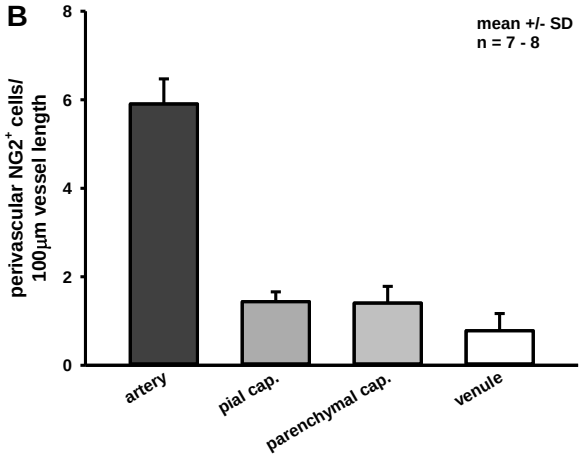

Figure 1

A *3D vessel reconstruction of two-photon microscopy. Superficial arteries are completely covered with NG2⁺ cells. 42% of perivascular NG2⁺ cells in the parenchymal microcirculation are associated to capillary bifurcations.* ***B*** *Quantification of NG2⁺ cells in arteries, venules, pial and parenchymal capillaries. Data represent mean number of NG2⁺ cell bodies along vessel segments of 100 µm length.*

Data analysis

Images of NG2 DsRed mice were analyzed for vessel diameter with Image J software (NIH, USA) as follows: Vessels were categorized in five different groups depending on their size before SAH induction (artery diameter 40-30µm, artery diameter 30-20 µm, arteriole diameter 20-15 µm). Vessels with a diameter of 40-15 µm were defined as arteries and arterioles. These vessels exhibited a confluent coverage with $NG2^+$ cells. Venules were not measured. Vessels with a diameter of 15-5 µm have intermittent coverage with $DsRed^+$ cells and were regarded as capillaries. The outer diameter of vessels represented by red signal was measured randomly at nine locations within each ROI before and after SAH. The diameter of capillaries was measured three times along two vessel segments in each ROI after SAH. The first measurement was proximal to the pericyte, the second was at the location of the pericyte and the third was distal to the pericyte (Fig. 7B).

Statistical analysis

Data are given in mean ± standard deviation (SD). Statistical tests were performed with SigmaPlot 12.0 software package (Systat Software Inc, USA).

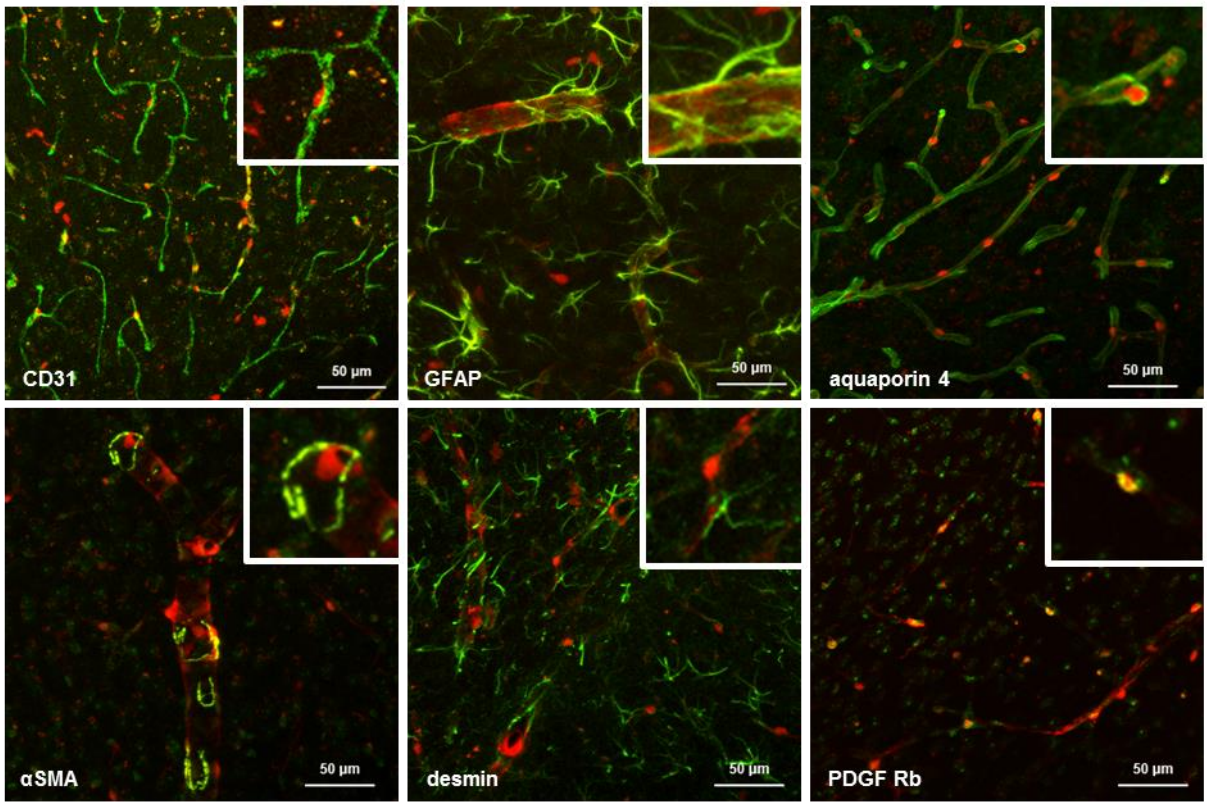

Figure 2

Immunohistological characterization of NG2⁺ cells. Red fluorescent signal shows transgene expression in heterozygous animals. Green staining depicts immunohistochemical staining of different cell markers. Pericytes are located at the parenchymal side of CD31⁺ endothelial cells. There is no colocalization with NeuN (data not shown), desmin or GFAP. Astrocytic endfeet (aquaporin 4) are covering NG2⁺ cells from the parenchymal side. NG2⁺ cells around arteries co-localize with αSMA. NG2⁺ cells in the microcirculation co-localize with PDGF Rβ.

For normally distributed data the paired t-test was used to test differences between groups. Differences between groups were interpreted statistically significant at a p value < 0.05.

Results

Histological characterization NG2 DsRed

The perivascular expression of NG2 in the transgenic mouse line NG2 DsRed has not been described in detail. Therefore we counted NG2⁺ cells along a vessel distance of 100 µm. Cell counts were performed in z stacks obtained by two-photon microscopy. Venules, arterioles and capillaries can easily be distinguished by blood flow direction and vessel branching pattern. Arteries have the highest coverage with NG2⁺ cells. The vessels are encompassed with a confluent red fluorescent signal. In order to count single cells, free floating sections were stained with DAPI for visualization of nuclei. Nuclei of red fluorescent cells were counted along a vessel length of 100 µm. Coverage of NG2⁺ cells was highest in arterioles with an average of 5.9 cells per 100 µm vessel length. Penetrating arterioles were similarly covered with NG2⁺ cells. Pial and parenchymal capillaries had a comparable coverage with NG2⁺ cells of 1.4 cells per 100 µm vessel length. 42% of parenchymal NG2⁺ cells were located at capillary bifurcations. NG2⁺ cells were rarely associated to venules; a vessel segment of 100 µm exhibits in average 0.8 NG2⁺ cells (Fig 1A and B).

In order to identify the cell types which are expressing NG2, co-staining with established markers of the neurovascular unit were performed in NG2 DsRed sections. NG2⁺ cells were negative for CD31, NeuN, GFAP, aquaporin 4 and desmin (Fig 2). αSMA co-localized with

$NG2^+$ cells that surround bigger vessels. We regard them as VSMC due to their location along the vascular tree and co-localization with αSMA. $NG2^+$ cells associated to capillaries consistently expressed PDGF Rβ. The immunohistological characterization indicates that $NG2^+$ cells associated to capillaries are mid-capillary pericytes.

Pericyte survival after SAH

Pericyte survival was investigated histologically three and 24 hours after SAH. Sections from SAH/sham experimental animals were stained for vessel lumen, PDGF Rβ and DAPI (Fig 3A). PDGF $R\beta^+$ and $DAPI^+$ cells were counted in the cortex, hippocampus and striatum. In average 15 to 30 cells per ROI expressed PDGF $R\beta^+$. Cell counts did not differ significantly between the SAH and sham surgery group (Fig 3B and C). The data shows that pericytes do not undergo apoptosis or necrosis within the first 24 hours after SAH. Furthermore pericytes at 24 hours after SAH are still associated to vessels, indicating that pericytes do not migrate away from vessels early after SAH.

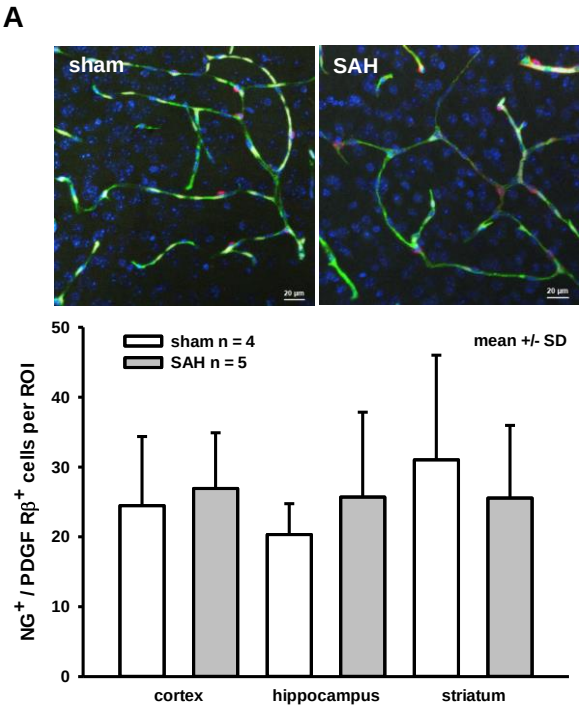

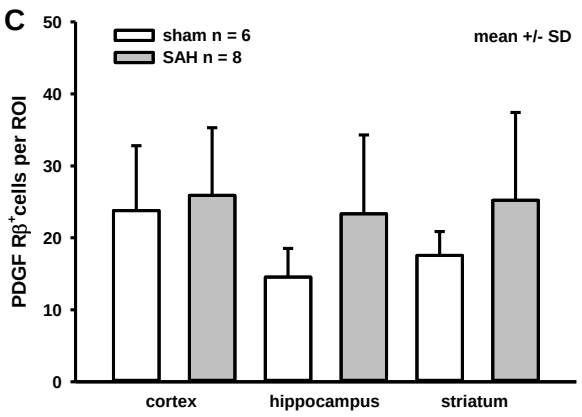

Figure 3
A *Representative PDGF Rβ, FITC lectin and DAPI staining of free floating sections 24 hours after SAH and sham surgery. PDGF $R\beta^+$ and $DAPI^+$ cells were regarded as pericytes.* ***B*** *Quantification of pericytes in the cortex, hippocampus and striatum 3 h after SAH/sham surgery. Data points represent mean number of PDGF $R\beta^+$, $NG2^+$ and $DAPI^+$ cells per ROI. There is no statistically significant difference between the SAH and sham surgery group.* ***C*** *Quantification of pericytes (PDGF $R\beta^+$ cells) in the cortex, hippocampus and striatum 24 hours after SAH/sham surgery. There is no statistically significant difference between the SAH and sham surgery group.*

Physiological monitoring

The ICP was recorded during SAH/sham induction and 20 minutes thereafter to confirm standardized SAH induction (Fig 4A). During SAH the ICP rose to values close to the systemic blood pressure and declined within five minutes after the bleeding to values between 20 and 30 mmHg. In the sham surgery group ICP stayed at four mmHg during the observation time. Cerebral blood flow was measured by laser Doppler flowmetry (Fig 4B). Regional cerebral blood flow (rCBF) values showed a severe drop in cerebral blood flow during bleeding induction. Reperfusion was variable. rCBF stayed constant in the sham surgery group for the observation time of 20 minutes. This indicates that SAH/sham surgery was performed in a standardized way and that the potentially variant genetic background of the transgenic mouse line does not have an impact on the SAH model.

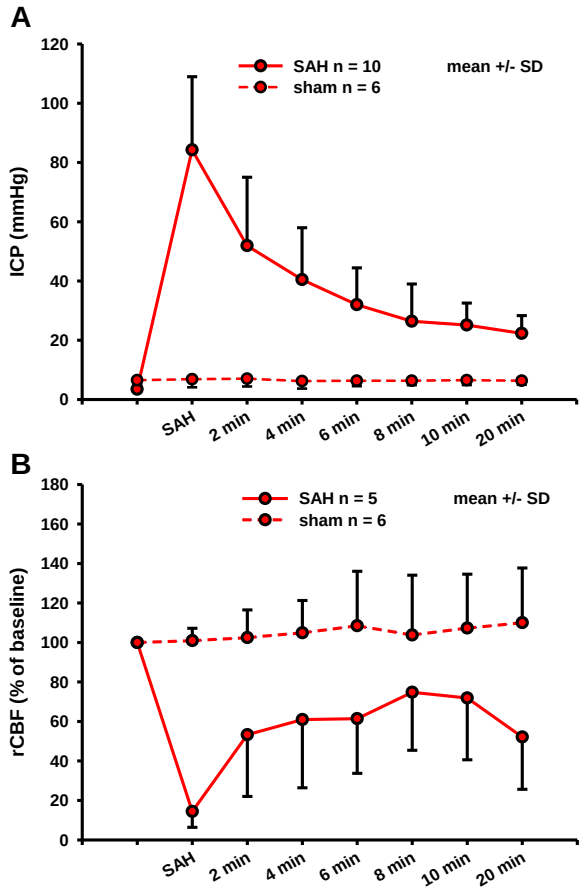

Figure 4
A *ICP values during SAH/sham surgery are depicted in mmHg. SAH induction induces mean peak ICP values of 84 mmHg. In sham operated animals the ICP stays at four mmHg throughout the procedure.* ***B*** *rCBF is depicted in % of initial values. Vessel perforation induces a reduction of cerebral blood flow to 14% whereas sham surgery does not induce a drop of rCBF.*

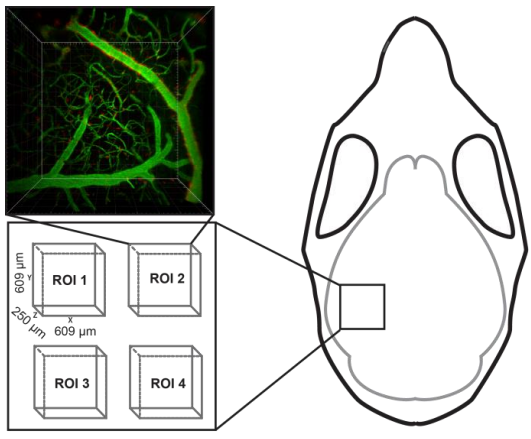

Figure 5
Schematic sketch shows the area where two-photon microscopy is performed. Example of z stack of a NG2 DsRed mouse with intravascular FITC dextran.

Microvasospasm and pericytes

The outer vessel diameter was measured in z stacks before and after SAH and sham surgery (Fig 6A). Arterioles have a mean vessel diameter reduction of 8% (Fig 6B). Arterioles that constricted were covered continuously with NG2$^+$ cells. This finding supports that VSMC play a role in the formation of superficial microvasospasm after SAH. Capillaries revealed a mean vessel diameter reduction of 5% compared to baseline (Fig 6B). The data on capillary diameter shows for the first time that also capillaries constrict in response to SAH. The degree of constriction is less pronounced than in arterioles. A differential measurement of vessel diameter after SAH at locations where pericyte cell bodies were located compared to vessel segments between pericytes elucidated the role of pericytes in capillary narrowing (Fig 7A). Vessel diameter did not differ between locations where pericyte cell bodies were located compared to vessel segments proximal or distal to that pericyte (Fig 7B). This finding indicates that capillary narrowing after SAH is not induced by pericyte constriction.

Discussion

In this study we studied the role of pericytes in early cerebral ischemia after SAH. In order to visualize pericytes we investigated the transgenic pericyte reporter mouse strain NG2 DsRed. Expression of DsRed under the NG2 promoter was characterized by immunohistochemistry of perivascular cells, indicating that VSMC and pericytes express NG2. Furthermore pericyte survival was investigated at three and 24 hours after SAH. PDGF Rβ$^+$ cell numbers did not differ significantly between SAH and sham surgery. Importantly PDGF Rβ$^+$ cells were still located in vessel proximity at 24 hours after the bleeding indicating that pericytes do not migrate in response to SAH. The involvement of VSMC and pericytes in the formation of microvasospasm after SAH was investigated *in vivo*. Arteries as well as capillaries showed a significant reduction in vessel diameter three hours after SAH. Constricted arterioles were continuously covered

with NG2$^+$ cells. Therefore NG2$^+$, αSMA$^+$ perivascular cells probably mediate arteriolar constriction. Constriction of capillaries however was not restricted to locations where pericyte cell bodies were located. We conclude that pericytes do not induce capillary microvasospasm after SAH.

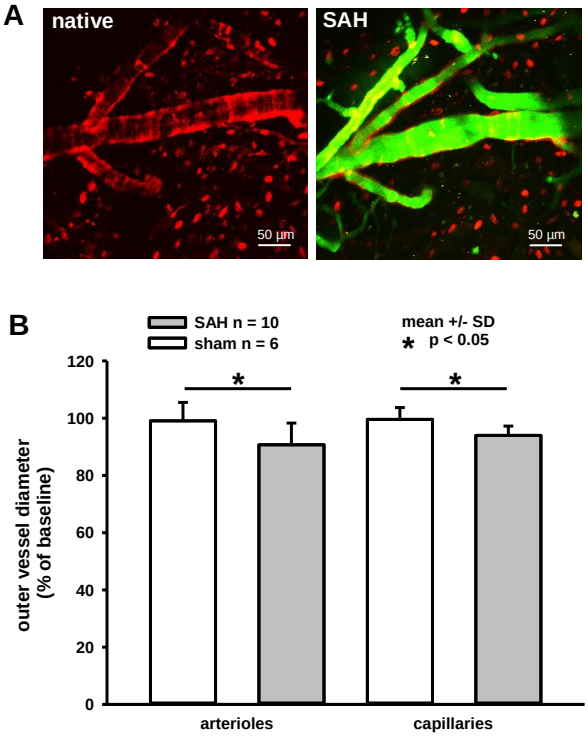

Figure 6

A *Representative 3D projection of a two-photon microscopy z stack. The left image shows a native picture. The diameter of the vessel is clearly outlined. Big solitary superficial NG2$^+$ cells were associated to remaining bone. The right image shows the same ROI after SAH with green plasma dye (FITC dextran).* ***B*** *Quantification of the outer vessel diameter before and after SAH. The vessel diameter of arterioles and capillaries was measured before and after SAH. After SAH the vessel diameter was significantly reduced. Arterioles showed a mean vessel diameter reduction of 8% and capillaries show mean vessel diameter reduction of 5%.*

Role of genetic background

The NG2 DsRed transgenic mouse line was used for investigations of pericyte involvement in the formation of vessel spasm after SAH. The mouse line was bred heterozygously on a C57Bl6 background; however a genetic shift can always induce an altered phenotype compared to wild type animals. Therefore it is important that the animal model produces robust and stable findings also in genetically modified mouse strains. Physiological data that were captured during SAH surgery were comparable to physiological data obtained from C57Bl6 animals.[18] This supports that the obtained data are valid and can be interpreted in conjunction with previously obtained results. Furthermore the data suggest that the pathophysiology of vessel spasm is robust and alike in different transgenic mouse lines.

Characterization of NG2$^+$ cells

The identification of pericytes based on immunohistochemical staining is difficult because none of the known pericyte markers is specific.[19] The definition of a pericyte is mainly morphological: pericytes are perivascular cells that are located in the same basement membrane with the endothelium.[20] This characteristic feature however can only be studied on a structural level by electron microscopy. In this study the identification problem is circumvented by looking at cell localization within the vascular tree in combination with expression of cell markers. A confluent layer of VSMC surrounds arteries and arterioles which consistently express αSMA.[21] At the capillary level the so called mid-capillary pericytes are located which are known to express PDGF Rβ and NG2.[19] Therefore co-staining in combination with perivascular vessel localization makes the identification of cerebral pericytes and VSMC possible. We regard NG2$^+$ cells that cover arterioles and express αSMA as VSMC and NG2$^+$ cells that are associated to capillaries and express PDGF Rβ as pericytes.

Pericyte numbers after SAH

A study that investigated the reaction of pericytes to hypoxic condition showed that pericytes migrate away from vessels immediately after onset of hypoxia.[22] In a stroke model pericytes were found to detach from the vessel and migrate toward the ischemic injury. These cells gather a microglial phenotype and are suspected to be involved in scar formation.[14] Similarly in the spinal cord pericytes have been shown to migrate and participate in scar formation.[23] In order to investigate the migratory behavior of pericytes

after SAH vessel lumen and pericytes were stained 24 hours after SAH and sham surgery. No significant difference in pericyte numbers along cerebral vessels was found when comparing SAH and sham condition. This indicates that pericytes do not migrate in significant numbers away from the capillaries within 24 hours after SAH. The finding however does not confirm previous findings that showed early pericyte migration in hypoxic condition. One explanation for this conflicting finding might be that the resolution of the obtained images was too low to detect small changes in pericyte position. Therefore pericyte location in relation to vessels after SAH might be reinvestigated by electron microscopy or high resolution microscopy techniques.

Another suggested reaction of pericytes to cerebral ischemia is early cell death.[11] In order to investigate pericyte survival following cerebral hemorrhage we counted the numbers of PDGF Rβ$^+$ cells three and 24 hours after SAH. Pericyte survival was not affected within 24 hours after the bleeding. This finding can be explained by the different pathophysiology of ischemic and hemorrhagic stroke. In the ischemic core of focal ischemia energy depletion is much more pronounced and leads to widespread apoptosis and necrosis. In SAH however apoptosis is sporadic and distributed in hippocampus and cortex.[24] The metabolic derangement is milder than in ischemic tissue. This difference might explain the differential findings on pericyte migration and survival between stroke and SAH.

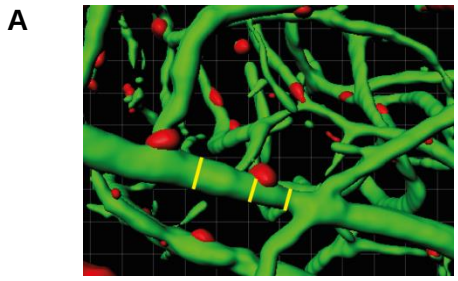

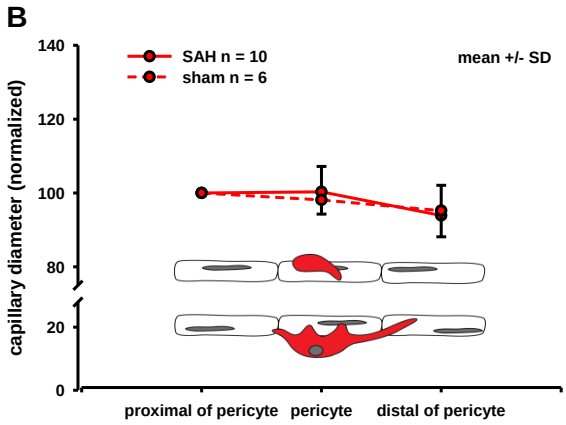

Figure 7
A *Representative measurement of capillary diameter at locations where pericytes are present compared to locations where no pericyte is present.* ***B*** *Quantification of vessel diameter in relation to pericyte location. There is no statistically significant difference between the capillary lumen at sites of pericytes compared to vessel segments which are devoid of pericytes.*

Pericytes and microvasospasm

After ischemia pericytes have been shown to constrict and thereby narrow capillary lumen.[12] The pathophysiologic assumption was that energy depletion induces passive pericyte constriction in analogy to rigor mortis observed in skeletal muscle.[11] Pericyte constriction was shown to induce a narrowing of the vessel lumen at sites where pericyte bodies are located. The narrowing may hamper blood flow and leads to microcirculatory perfusion deficits. Subsequently pericytes are suspected to undergo cell death. We investigated pericyte constriction after SAH, because metabolic derangement also occurs in the hemorrhagic subtype of stroke.[25] However no focal constrictions of capillaries at sites where pericytes were located were found. This finding supports that pericytes do not directly induce capillary narrowing after SAH. Therefore we could not confirm constriction of pericytes in hemorrhagic stroke. Long processes of mid-capillary pericytes may make the correct identification of cell dimensions difficult. However in NG2 DsRed mice also the processes of

pericytes contain red fluorescent dye. Thus we specifically identified vessel segments that were devoid of pericyte cell bodies as well as their processes. In summary our data show that pericytes do not play a significant role in the pathophysiology of early cerebral ischemia after SAH. VSMC however, are probably the cells which induce microvasospasm of arteries on the brain surface.

References

1. Pobereskin, L.H. Influence of premorbid factors on survival following subarachnoid hemorrhage. *J Neurosurg* **95**, 555-9 (2001).
2. Sehba, F.A., Pluta, R.M. & Zhang, J.H. Metamorphosis of subarachnoid hemorrhage research: from delayed vasospasm to early brain injury. *Mol Neurobiol* **43**, 27-40 (2011).
3. Bederson, J.B. et al. Acute vasoconstriction after subarachnoid hemorrhage. *Neurosurgery* **42**, 352-60; discussion 360-2 (1998).
4. Frontera, J.A. et al. Acute ischaemia after subarachnoid haemorrhage, relationship with early brain injury and impact on outcome: a prospective quantitative MRI study. *J Neurol Neurosurg Psychiatry* **86**, 71-8 (2015).
5. Uhl, E., Lehmberg, J., Steiger, H.J. & Messmer, K. Intraoperative detection of early microvasospasm in patients with subarachnoid hemorrhage by using orthogonal polarization spectral imaging. *Neurosurgery* **52**, 1307-15; disacussion 1315-7 (2003).
6. Pennings, F.A., Bouma, G.J. & Ince, C. Direct observation of the human cerebral microcirculation during aneurysm surgery reveals increased arteriolar contractility. *Stroke* **35**, 1284-8 (2004).
7. Friedrich, B., Muller, F., Feiler, S., Scholler, K. & Plesnila, N. Experimental subarachnoid hemorrhage causes early and long-lasting microarterial constriction and microthrombosis: an in-vivo microscopy study. *J Cereb Blood Flow Metab* **32**, 447-55 (2012).
8. Sun, B.L. et al. Dynamic alterations of cerebral pial microcirculation during experimental subarachnoid hemorrhage. *Cell Mol Neurobiol* **29**, 235-41 (2009).
9. Schubert, G.A., Seiz, M., Hegewald, A.A., Manville, J. & Thome, C. Acute hypoperfusion immediately after subarachnoid hemorrhage: a xenon contrast-enhanced CT study. *J Neurotrauma* **26**, 2225-31 (2009).
10. Sehba, F.A., Ding, W.H., Chereshnev, I. & Bederson, J.B. Effects of S-nitrosoglutathione on acute vasoconstriction and glutamate release after subarachnoid hemorrhage. *Stroke* **30**, 1955-61 (1999).
11. Hall, C.N. et al. Capillary pericytes regulate cerebral blood flow in health and disease. *Nature* **508**, 55-60 (2014).
12. Yemisci, M. et al. Pericyte contraction induced by oxidative-nitrative stress impairs capillary reflow despite successful opening of an occluded cerebral artery. *Nat Med* **15**, 1031-7 (2009).
13. Zhu, X., Bergles, D.E. & Nishiyama, A. NG2 cells generate both oligodendrocytes and gray matter astrocytes. *Development* **135**, 145-57 (2008).
14. Fernandez-Klett, F. et al. Early loss of pericytes and perivascular stromal cell-induced scar formation after stroke. *J Cereb Blood Flow Metab* **33**, 428-39 (2013).
15. Schuller, K., Buhler, D. & Plesnila, N. A murine model of subarachnoid hemorrhage. *J Vis Exp*, e50845 (2013).
16. Nakamura, T. et al. Acute CO2-independent vasodilatation of penetrating and pre-capillary arterioles in mouse cerebral parenchyma upon hypoxia revealed by a thinned-skull window method. *Acta Physiol (Oxf)* **203**, 187-96 (2011).
17. Schwarzmaier, S.M. et al. *In vivo* temporal and spatial profile of leukocyte adhesion and migration after experimental traumatic brain injury in mice. *J Neuroinflammation* **10**, 32 (2013).
18. Buhler, D., Schuller, K. & Plesnila, N. Protocol for the induction of subarachnoid hemorrhage in mice by perforation of the Circle of Willis with an endovascular filament. *Transl Stroke Res* **5**, 653-9 (2014).
19. Armulik, A., Genove, G. & Betsholtz, C. Pericytes: developmental, physiological, and pathological perspectives, problems, and promises. *Dev Cell* **21**, 193-215 (2011).
20. Sims, D.E. The pericyte--a review. *Tissue Cell* **18**, 153-74 (1986).

21. Boado, R.J. & Pardridge, W.M. Differential expression of alpha-actin mRNA and immunoreactive protein in brain microvascular pericytes and smooth muscle cells. *J Neurosci Res* **39**, 430-5 (1994).
22. Gonul, E. et al. Early pericyte response to brain hypoxia in cats: an ultrastructural study. *Microvasc Res* **64**, 116-9 (2002).
23. Goritz, C. et al. A pericyte origin of spinal cord scar tissue. *Science* **333**, 238-42 (2011).
24. Park, S. et al. Neurovascular protection reduces early brain injury after subarachnoid hemorrhage. *Stroke* **35**, 2412-7 (2004).
25. Prunell, G.F., Mathiesen, T. & Svendgaard, N.A. Experimental subarachnoid hemorrhage: cerebral blood flow and brain metabolism during the acute phase in three different models in the rat. *Neurosurgery* **54**, 426-36; discussion 436-7 (2004).

In vivo Ca^{2+}- imaging in cerebral endothelial cells

Aim of the study:

In order to investigate functional Ca^{2+} levels in endothelial cells we used a transgenic mouse line that expresses the ratiometric Ca^{2+} probe TN-XXL under the promotor of chicken β-actin.[216] The probe is composed of the two fluorescent proteins: the yellow fluorescent protein citrine and cyan fluorescent protein (CFP) that are coupled by a Ca^{2+} sensitive peptide derived from troponin C. A change of Ca^{2+} concentration leads to a conformation change that induces a Föster resonance energy transfer between both fluorescent proteins and thereby a change of their fluorescence intensity.[217] In the brain the sensor is primarily expressed in the vasculature. We confirmed expression of TN-XXL in endothelial cells by immunohistochemistry for different cell markers. Functional two-photon microscopy was performed under baseline condition and three hours after SAH or sham surgery. Citrine to CFP ratio revealed a small standard deviation under baseline condition. No bleaching or diffusion of the sensor was detected between the imaging sessions. Three hours after SAH the ratio of citrine to CFP was reduced indicating decreased Ca^{2+} concentration in endothelial cells.

A reduction of blood flow velocity may lead to reduced intracellular Ca^{2+} concentration mediated by a drop of shear stress on the endothelium. Shear stress triggers a certain level of intracellular Ca^{2+} concentration[218] that might mediate physiological vascular tone via nitric oxide signaling.

However the finding needs to be interpreted cautiously because two potential confounding factors were identified: The ratio may artificially be shifted by auto fluorescence of subarachnoid blood that is located around superficial vessels after SAH. A second confounding factor is that pH in endothelial cells may be decreased in ischemic condition, which may induce a selective quenching of citrine fluorescence.[219]

In vivo Ca^{2+}- imaging in cerebral endothelial cells

Kathrin Schüller[1,2], Farida Hellal[1,3], Arne Fabritius[4], Oliver Griesbeck[2,4], Nikolaus Plesnila[1,2,3]

[1] Institute for Stroke and Dementia Research, University of Munich Medical Center, Munich, Germany

[2] Graduate School of Systemic Neurosciences, Ludwig-Maximilians-Universität, Munich, Germany

[3] Cluster of Systems Neurology (Synergy), Munich, Germany

[4] Max Planck Institute of Neurobiology, Munich, Germany

Author contributions: KS and NP planned experiments, AF and OG provided animals, KS and FH acquired data, KS and AF analyzed data, KS and NP wrote manuscript

Key words: endothelial cell, calcium sensor, calcium signaling, nitric oxide, shear stress, subarachnoid hemorrhage

Abstract

Introduction

Cytosolic Ca^{2+} concentration is an important component of intracellular signaling and a sensitive marker for cell activation. Repetitive *in vivo* measurements of cytosolic Ca^{2+} concentration is challenging and therefore not studied in detail in cerebrovascular cells. Therefore the aim of this study was to investigate whether a transgenic mouse line expressing the ratiometric Ca^{2+} dye TN-XXL under the promotor of chicken β-actin can be used for this purpose.

Methods

Cellular expression of TN-XXL in the brain was characterized by immunohistochemistry. Cytosolic Ca^{2+} concentration was measured by two-photon microscopy under native condition and three hours after subarachnoid hemorrhage or sham surgery.

Results

Expression of TN-XXL was highest in cerebral endothelial cells and also detectable in cortical neurons. The citrine to cyan fluorescent protein ratio was robust under native condition and after sham surgery. Cerebral endothelial cells exhibited a decreased citrine to cyan fluorescent protein ratio three hours after subarachnoid hemorrhage, suggesting decreased intracellular Ca^{2+} levels in endothelial cells.

Conclusion

The TN-XXL transgenic mouse line is suitable to measure cytosolic Ca^{2+} in cerebrovascular endothelial cells *in vivo* under physiological and pathological conditions. Endothelial dysfunction after subarachnoid hemorrhage may be induced by reduced intracellular Ca^{2+} levels.

Introduction

The transgenic mouse line CAG TN-XXL was designed for chronic *in vivo* studies of functional Ca^{2+} imaging. Mice express the ratiometric Ca^{2+} probe TN-XXL under the promotor of chicken β-actin (CAG).[1] The Ca^{2+} probe is composed of the yellow fluorescent protein citrine cp174, which is coupled to a cyan fluorescent protein (CFP) by a troponin C analogue that has been optimized for physiological Ca^{2+} concentrations.[2] Changes in intracellular Ca^{2+} levels lead to a conformation change of the sensor thereby inducing a Förster resonance energy transfer (FRET) from CFP to citrine.[3] Shift of fluorescence intensity is independent of the concentration of the probe, a prerequisite for reliable repetitive measurements *in vivo*.[2] CAG TN-XXL mice express the Ca^{2+} probe theoretically in all cells of the body. So far, however, the vascular expression of TN-XXL in the brain has not been characterized in detail. Investigations of TN-XXL fluorescence in the brain suggest that the probe is predominantly found in the vasculature and to a lesser extent in neurons.[1] Which cells of the vessel wall express TN-XXL is of particular importance since repetitive measurements of intracellular Ca^{2+} concentrations in cerebrovascular cells have not been possible *in vivo*.

In order to study changes of cerebrovascular Ca^{2+} concentrations under pathological conditions we investigated the CAG TN-XXL mouse line in a model of subarachnoid hemorrhage (SAH). Cerebral ischemia is an important component of the early pathophysiology after SAH.[4] The mechanism that is causing cerebral ischemia after SAH is not known to date; suggested pathomechanisms for early cerebral ischemia after SAH are microvasospasm[5] and endothelial dysfunction;[6] both conditions that are associated with changes in intracellular Ca^{2+}.

Therefore the aim of the current study was to identify the vascular cell type which expresses TN-XXL in the brain and to investigate functional Ca^{2+} signaling in the vasculature in a mouse model of SAH.

Methods

Animals and experimental groups

In this study we investigated the CAG TN-XXL mouse strain by two-photon microscopy. Mice express the ratiometric Ca^{2+} probe TN-XXL under the chicken β-actin promoter with broad expression.[1] Experimental animals were randomly chosen and assigned to the sham and SAH group during surgery. Mice were group housed and always had access to food and water. Experiments are approved by the Government of Upper Bavaria.

Free floating immunohistochemistry

Paraformaldehyde (PFA) perfused and postfixed (24 hours) brains were sectioned with a vibratome (Leica, Germany). 50 µm sections were collected and stored in cryoprotectant solution (50% 0.1 phosphate buffered saline (PBS), 25% glycerol, 25% polyethylenglycol) until immunohistochemical staining. CAG TN-XXL sections were stained for NeuN (MAB377 Millipore, Darmstadt, Germany), aquaporine 4 (AB 2218 Millipore, Darmstadt, Germany), platelet endothelial cell adhesion molecule 1 (CD31) (BM4086 Acris, Germany), α smooth muscle actin (αSMA) (CP47 Novus, USA), desmin (MAP3430 Millipore, Darmstadt, Germany) and platelet derived growth factor beta (PDGF Rβ) (3169 NEB, USA). Sections were washed in PBS three days for removal of cryoprotectant. After incubation in blocking solution (3% bovine serum albumine, 0.5% glycine, 0.5% triton) for one hour the primary antibody was incubated at 4°C over night. After washing with PBS the respective secondary antibody (Alexa Fluor 488 and Cy3 conjugated AffiniPure, Jackson) was incubated at room temperature for two hours. Sections were mounted on slides and embedded in Vectashield DAPI mounting medium (Vector Labs, USA). Microscopy of free floating sections was performed with a LSM 7 (Zeiss, Germany) confocal microscope.

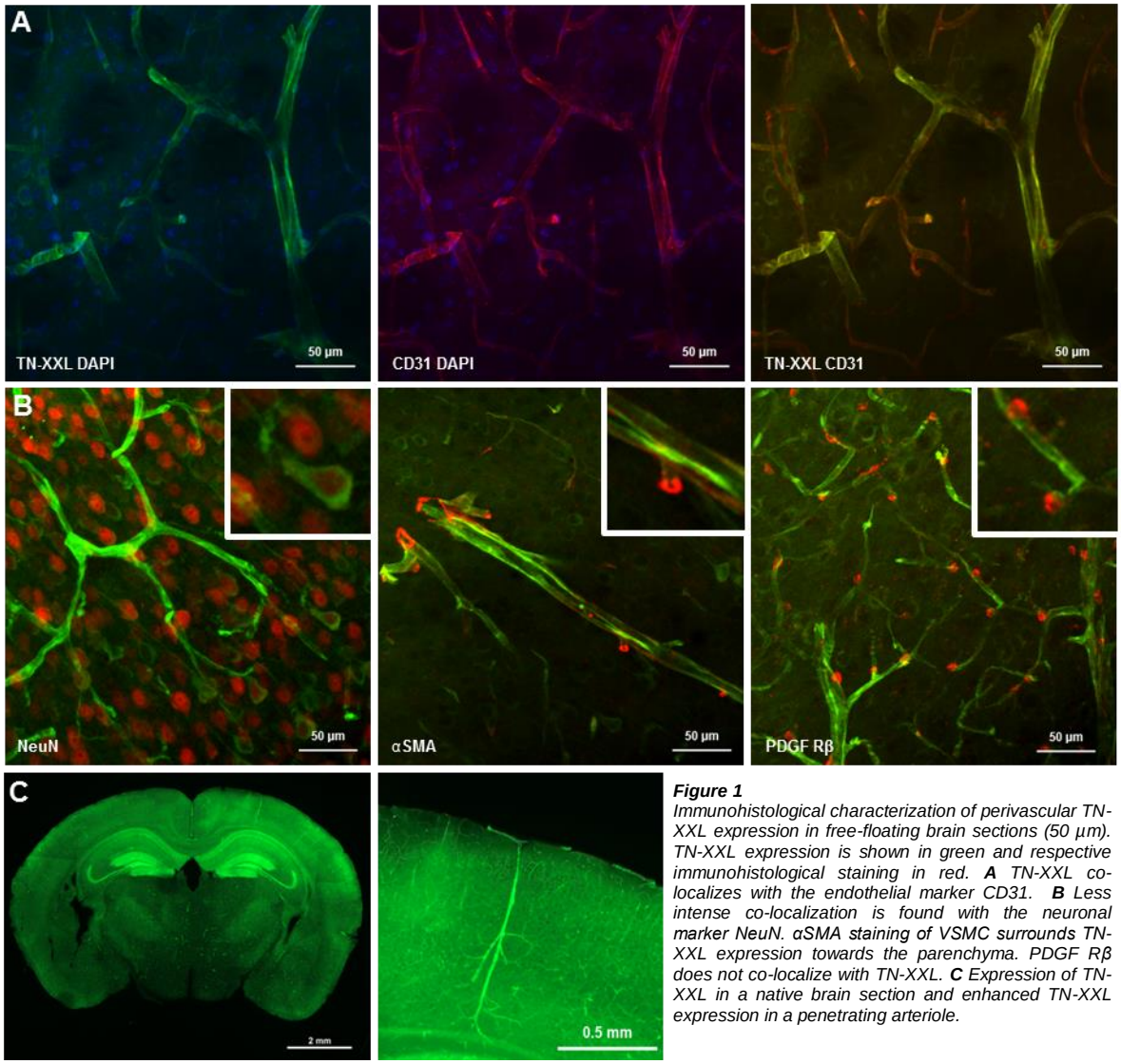

Figure 1
Immunohistological characterization of perivascular TN-XXL expression in free-floating brain sections (50 µm). TN-XXL expression is shown in green and respective immunohistological staining in red. ***A*** *TN-XXL co-localizes with the endothelial marker CD31.* ***B*** *Less intense co-localization is found with the neuronal marker NeuN. αSMA staining of VSMC surrounds TN-XXL expression towards the parenchyma. PDGF Rβ does not co-localize with TN-XXL.* ***C*** *Expression of TN-XXL in a native brain section and enhanced TN-XXL expression in a penetrating arteriole.*

SAH and respective sham surgery

SAH and respective sham surgery were performed as described previously.[7] After isoflurane induction animals were anesthetized with a combination of 0.05 mg/kg fentanyl (Janssen-Cilac, Neuss, Germany), 0.5 mg/kg medetomidine (Pfizer, USA) and 5 mg/kg midazolam (Braun, Germany). Animals received preoperative analgesia of 4 mg/kg carprofen (Pfizer, Germany). They were intubated, ventilated and placed on a feedback controlled heating pad. Peripheral oxygen saturation and heart rate were measured on the hind paw. SAH was induced by endovascular vessel perforation at the Circle of Willis. A prolene 5-0 filament was inserted into the external carotid artery and advanced to the skull base via the internal carotid artery. Vessel perforation at the skull base was indicated by a sharp rise of intracranial pressure (ICP) and a simultaneous drop of cerebral blood flow (CBF). After vessel perforation animals were monitored for another 20 minutes before they received antagonisation of anesthesia (s.c. 1.2 mg/kg naloxone (Actavis, Ireland, USA), 0.5

mg/kg flumazenil (Inresa, Germany) and 2.5 mg/kg atipamezol (Pfizer, USA)).

Two-photon microscopy

After topic application of lidocaine (2% HCl) a thinned skull window preparation was performed as described previously.[8] Z stacks (1 µm step distance) of four randomly chosen regions of interest (ROI) (609 x 609 µm) were obtained with a fixed laser power that did not exceed 20% (Fig 2). The initial scan and vessel imaging three hours after SAH were obtained with the same settings in each ROI. Excitation wavelength was 840 nm and fluorescence was detected with GaAsP-NDD detectors for yellow (520-560 nm band pass) and blue (460-500 nm band pass) fluorescence. After microscopy mice were transcardially perfused with 20 ml natural saline and 20 ml 4% PFA and brains were kept for histological examinations.

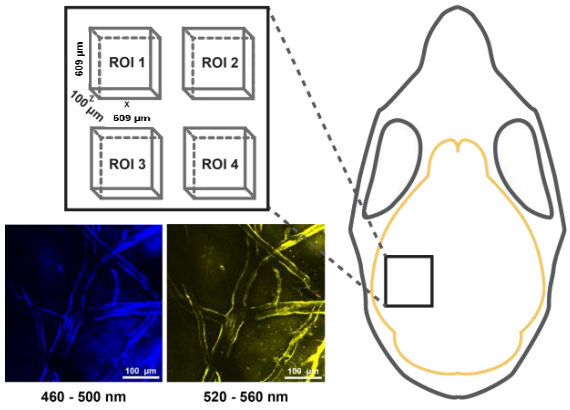

Figure 2
Experimental setup in vivo imaging. The area where vessels were investigated is indicated in a schematic skull drawing. 4 ROI were imaged before and after SAH. Pictures show examples of citrine and CFP fluorescence in the vasculature.

Data analysis

Images of CAG TN-XXL were analyzed for intensity of citrine and CFP with Image J software (NIH, USA) as follows: In each ROI three different vessel locations were chosen for analysis. Grey value measurements were selected by free hand drawing. If applicable the same shape of measurement was used before and after SAH/sham surgery. The mean grey value of the chosen region was measured in the blue and the yellow channel before and after SAH/sham. For background determination the vessel lumen was selected by free hand drawing when applicable. When vessel volume was too small a neighboring parenchymal area was chosen. The ratio of citrine to CFP signal was calculated for the same selected areas. A systematic bleed through of 30% from the yellow to the blue band pass filter was subtracted.

Statistical analysis

Data are given in mean ± standard deviation (SD). Statistical tests were performed with SigmaPlot 12.0 software package (Systat Software Inc, USA). For pairwise comparison the paired student t test was used. Differences between groups were interpreted as statistically significant at p values < 0.05.

Results

Histological characterization of CAG TN-XXL expression

The vascular and perivascular expression of TN-XXL in the brain has not been investigated in detail in the chicken β-actin TN-XXL mouse strain. In order to identify the cell type that is expressing the Ca^{2+} sensor free floating sections of CAG TN-XXL animals were stained with established cell markers. TN-XXL does not co-localize with αSMA and PDGF Rβ (Fig 1). Therefore it is not expressed by VSMC, pericytes or other vascular mural cells. Also the astrocytic endfeet marker aquaporin 4 does not co-localize with TN-XXL expression. TN-XXL is co-expressed with CD31, indicating high TN-XXL expression in endothelial cells (Fig 1A). Interestingly sensor expression is higher in arteries and arterioles than in venules (Fig 4A). $NeuN^+$ cells reveal weaker TN-XXL expression when compared to vascular expression. The findings show that TN-XXL is specifically expressed by endothelial cells and neurons.

Other cerebrovascular cell types do not exhibit TN-XXL expression.

Physiologic parameters during SAH induction

During SAH induction the ICP and the regional CBF were monitored. SAH led to a sharp increase of ICP which was accompanied by a severe reduction of regional CBF. ICP values stabilized at values around 30 mmHg within 5 min after the bleeding whereas cerebral reperfusion remained impaired (Fig 3A and B).

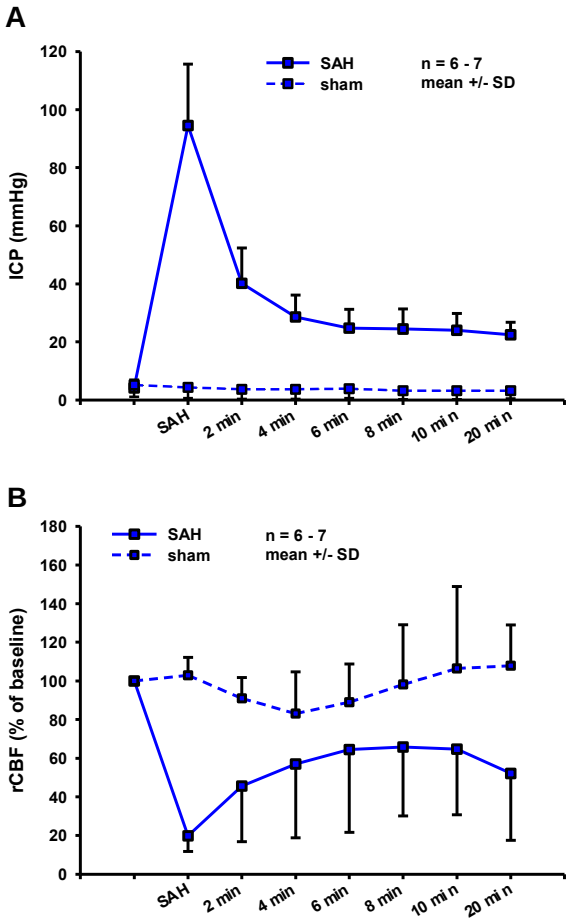

Figure 3
A *Intracranial pressure measurement during and 20 min after SAH or sham induction. SAH leads to an increase of ICP to a mean value of 95 mmHg. ICP values stabilize at values around 30 mmHg within 5 min after the bleeding. Sham surgery does not induce a rise of ICP.*
B *Regional cerebral blood flow (rCBF) during SAH induction. SAH leads to a sharp decrease of cerebral perfusion and reperfusion is variable between animals. Sham surgery does not induce a drop of rCBF.*

Ca^{2+} signals after SAH

The citrine to CFP ratio was compared between the native condition and after sham or SAH surgery (Fig 4A). In native condition the mean citrine to CFP ratio was ~0.6. We assume that this ratio corresponds with physiologic Ca^{2+} levels. The standard deviation of the ratio was small indicating a robust measurement. The citrine to CFP ratio after sham surgery did not significantly differ from the native condition even though the variance was slightly increased. After SAH the citrine to CFP ratio was significantly decreased compared to the native condition (Fig 4B). This decrease indicates a low free intracellular Ca^{2+} concentration in endothelial cells. However other explanations for this result are discussed below.

Discussion

Expression of TN-XXL

The TN-XXL Ca^{2+} probe is expressed under the chicken β-actin promoter. β-actin is a gene that is theoretically expressed by all cells in the body. However TN-XXL expression in this transgenic mouse line is abundant in some tissues and other tissues and cell types are devoid of the sensor. Direnberger et al. report that lymphatic tissues including spleen and circulating immune cells do not express the sensor. The underlying reasons for the differential expression of a transgene under the same promotor are not fully understood. Expression levels are probably not only dependent on the promotor which is flanking the transgene but also the insertion site with its surrounding transcription factors. Furthermore the number of integrated copies of the construct influences its expression pattern. Another β-actin reporter mouse strain shows little expression in neuronal tissue but strong expression in cerebral pericytes.[9] In the CAG TN-XXL mouse line however the sensor is largely confined to endothelial cells; weaker expression is found in neurons. This makes the CAG TN-XXL mouse

line the first model for functional Ca^{2+} imaging in endothelial cells.

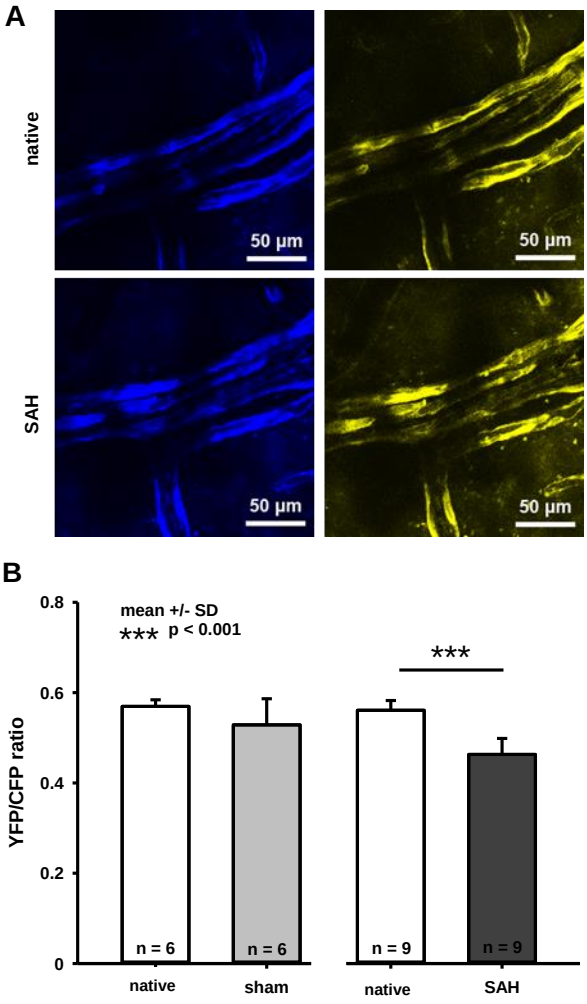

Figure 4

A *Representative pictures show two-photon microscopy 3D projections of TN-XXL before and after SAH. TN-XXL is expressed primarily in arteries and arterioles. Ratiometric change of fluorescence intensity is not detectable by eye.* ***B*** *Quantification of citrine to CFP ratio in native condition, after sham and SAH surgery. After SAH but not after sham surgery the citrine to CFP ratio is significantly reduced compared to the native situation. A reduced citrine to CFP ratio indicates low intracellular Ca^{2+} concentration.*

In vivo Ca^{2+} imaging

Native scans between different animals and also imaging after sham surgery exhibit a small standard deviation of citrine to CFP ratio, indicating that endothelial Ca^{2+} concentrations are stable under physiologic conditions (Fig 4B). During intravital microscopy neither bleaching of the signal during repetitive scans nor leaking of the sensor out of endothelial cells was detected. These findings show that ratiometric Ca^{2+} measurements under physiologic conditions are stable and robust.

Functional Ca^{2+} imaging after SAH indicates a reduction of endothelial Ca^{2+} concentration. This finding is somewhat surprising and needs to be interpreted carefully. However endothelial pathophysiology after SAH is potentially linked to decreased intracellular Ca^{2+} levels. The reason for decreased endothelial Ca^{2+} levels may be a reduction of blood flow velocity that has been shown in superficial arteries after SAH. Under physiologic conditions blood flow in vessels induces shear stress on the endothelium. Shear stress is important for the physiologic vasodilatory function of the endothelium and is associated with a certain level of intracellular Ca^{2+}.[10] Increased shear stress induces increased intracellular Ca^{2+} levels.[10] Therefore one can assume that a reduction of blood flow velocity will in turn lead to decreased intracellular Ca^{2+} levels.

Decreased intracellular Ca^{2+} values directly interfere with the endothelium mediated vasodilation. Endothelial vasodilatory function is mediated by the vasodilatory substance nitric oxide (NO) which induces dilation of surrounding vascular smooth muscle cells (VSMC). NO levels have been shown to be reduced early after SAH.[11] Importantly also the downstream signaling pathway of NO, the cyclic guanylatcyclase which mediates the vasodilatory effect in VSMC is reduced.[12] The activity of endothelial nitric oxide synthase (eNOS) is Ca^{2+} dependent; therefore decreased Ca^{2+} levels may lead to a lack of NO after SAH. A study investigating the vasodilatory effect of tetramethylpyrazine after SAH finds a combination of amelioration of vasospasm, increased NO and eNOS levels as well as increased intracellular Ca^{2+} in endothelial cells upon treatment after SAH.[13] This study indicates that the NO signaling pathway may be impaired in conjunction with decreased Ca^{2+} levels in endothelial cells. This suggested pathomechanism will have to be investigated in

detail by application of modulators of the NO pathway after SAH.

In addition to changes in endothelial Ca^{2+} concentrations also experimental factors affecting the measurement itself may be responsible for the observed change in TN-XXL fluorescence. One potential confounder is that extravasated subarachnoid blood that is located around superficial cerebral vessel exhibits autofluorescence which interferes with the fluorescence of the sensor. However no additional perivascular fluorescence was detected specifically after SAH during two-photon microscopy. Therefore it is not likely that extravasated subarachnoid blood directly interferes with the measurement.

A second potential confounding factor might be that especially the citrine fluorescence is pH sensitive,[14] e.g. a drop of pH from 7 to 6.8 reduces fluorescence emission by 5 to 10%. Because of acute energy depletion and acidosis after SAH[15] a decreased pH in endothelial cells is likely. Endothelial cells of parenchymal vessels have previously been shown to undergo cell death early after the bleeding.[16] Therefore the citrine to CFP ratio change could also be explained by early metabolic dysfunction and endothelial cell death early after SAH. Accordingly, endothelial viability needs to be carefully assessed when using the CAG TN-XXL mouse line.

In conclusion, we characterized cerebrovascular CAG TN-XXL expression and identified strong expression of the ratiometric Ca^{2+} sensor in endothelial cells in brain sections. These data suggest that CAG TN-XXL mice are suitable to measure intracellular Ca^{2+} in endothelial cells in the brain. Further experiments will allow to better understand the dynamics of endothelial signaling in healthy brain and during cerebral ischemia and hemorrhage.

References

1. Direnberger, S. et al. Biocompatibility of a genetically encoded calcium indicator in a transgenic mouse model. *Nat Commun* **3**, 1031 (2012).
2. Mank, M. et al. A genetically encoded calcium indicator for chronic in vivo two-photon imaging. *Nat Methods* **5**, 805-11 (2008).
3. Geiger, A. et al. Correlating calcium binding, Forster resonance energy transfer, and conformational change in the biosensor TN-XXL. *Biophys J* **102**, 2401-10 (2012).
4. Frontera, J.A. et al. Acute ischaemia after subarachnoid haemorrhage, relationship with early brain injury and impact on outcome: a prospective quantitative MRI study. *J Neurol Neurosurg Psychiatry* **86**, 71-8 (2015).
5. Friedrich, B., Muller, F., Feiler, S., Scholler, K. & Plesnila, N. Experimental subarachnoid hemorrhage causes early and long-lasting microarterial constriction and microthrombosis: an in-vivo microscopy study. *J Cereb Blood Flow Metab* **32**, 447-55 (2012).
6. McGirt, M.J. et al. Simvastatin increases endothelial nitric oxide synthase and ameliorates cerebral vasospasm resulting from subarachnoid hemorrhage. *Stroke* **33**, 2950-6 (2002).
7. Schuller, K., Buhler, D. & Plesnila, N. A murine model of subarachnoid hemorrhage. *J Vis Exp*, e50845 (2013).
8. Nakamura, T. et al. Acute CO2-independent vasodilatation of penetrating and pre-capillary arterioles in mouse cerebral parenchyma upon hypoxia revealed by a thinned-skull window method. *Acta Physiol (Oxf)* **203**, 187-96 (2011).
9. Fernandez-Klett, F., Offenhauser, N., Dirnagl, U., Priller, J. & Lindauer, U. Pericytes in capillaries are contractile in vivo, but arterioles mediate functional hyperemia in the mouse brain. *Proc Natl Acad Sci U S A* **107**, 22290-5 (2010).
10. Yamamoto, K., Korenaga, R., Kamiya, A. & Ando, J. Fluid shear stress activates Ca(2+) influx into human endothelial cells via P2X4 purinoceptors. *Circ Res* **87**, 385-91 (2000).
11. Sehba, F.A., Schwartz, A.Y., Chereshnev, I. & Bederson, J.B. Acute decrease in cerebral nitric oxide levels after subarachnoid hemorrhage. *J Cereb Blood Flow Metab* **20**, 604-11 (2000).
12. Nishizawa, S., Yamamoto, S. & Uemura, K. Interrelation between protein kinase C and nitric oxide in the development of vasospasm after subarachnoid hemorrhage. *Neurol Res* **18**, 89-95 (1996).
13. Shao, Z. et al. Effects of tetramethylpyrazine on nitric oxide/cGMP signaling after cerebral vasospasm in rabbits. *Brain Res* **1361**, 67-75 (2010).
14. Griesbeck, O., Baird, G.S., Campbell, R.E., Zacharias, D.A. & Tsien, R.Y. Reducing the environmental sensitivity of yellow fluorescent protein. Mechanism and applications. *J Biol Chem* **276**, 29188-94 (2001).
15. Brooke, N.S. et al. Phosphorus-31 magnetic resonance spectra reveal prolonged intracellular acidosis in the brain following subarachnoid hemorrhage. *Proc Natl Acad Sci U S A* **91**, 1903-7 (1994).
16. Park, S. et al. Neurovascular protection reduces early brain injury after subarachnoid hemorrhage. *Stroke* **35**, 2412-7 (2004).

D Conclusion

1. Aims of the study

Cerebral ischemia is an important component of the pathophysiology after subarachnoid hemorrhage (SAH), a subtype of stroke with a particularly bad prognosis.[3] For decades it was believed that the mechanisms causing cerebral ischemia after SAH were related to delayed spasm of large intracranial arteries, however, within the past few years experimental data suggested that disturbance on the level of the cerebral microcirculation could be the real source of post-hemorrhagic ischemia.[97] The underlying pathomechanisms that are causing early cerebral ischemia in SAH patients are not fully characterized to date. Among others pearl-string like constrictions of pial arteries have been suggested to be causative for early cerebral ischemia after SAH.[150]
The first aim of this thesis was to characterize how and to which extent blood flow dynamics in the parenchymal microcirculation are affected after SAH. We tested if superficial artery constrictions have implications on parenchymal brain perfusion. One hypothesis was that vessels in the cortical parenchyma namely penetrating arterioles and capillaries constrict in the same manner as pial arteries after SAH. Another potential cause for reduced parenchymal vessel perfusion is the plugging of vessels by leukocytes that interact with the endothelium.[127] Therefore parenchymal vessel diameter and leukocyte-endothelium interactions as triggers for reduced parenchymal perfusion after SAH were investigated.
The second aim of the study was to elucidate the role of pericytes in the formation of vessel spasm after SAH. The main hypothesis was that vascular smooth muscle cells (VSMC) and pericytes are contracting upon SAH and thereby narrow the vessel lumen. Another hypothesis was that pericytes die or migrate after SAH and thereby contribute to capillary perfusion deficits and the formation of brain edema. These questions were addressed by investigating constrictive and migratory behavior of pericytes after SAH.
The third aim of the study was to characterize the underlying functional pathomechanism of vessel spasm after SAH. Therefore the activation status of cerebrovascular cells was measured by comparing free intracellular Ca^{2+} concentration before and after SAH.

2. Methodological contribution

To better understand the pathophysiology of SAH a variety of animal models have been developed.[56] Ideally, these models should resemble SAH in patients as good as possible, should be standardized and reproducible. The model which resembles the human situation best is the endovascular filament perforation model.[213] Since SAH induction is microsurgically demanding the adaptation of the perforation model to mice, the most commonly used species in SAH research, was challenging. Especially the small body size in combination with a small blood volume were obstacles that had to be

taken. Thus the endovascular perforation model remained variable and was not frequently used in the field. In our laboratory we optimized the endovascular perforation model in mice.[67, 118] In the first part of the current thesis the SAH mouse model was further standardized.[64] The JoVE video publication "A murine model of subarachnoid hemorrhage" gives instructions for surgical procedures, emphasizes critical steps during surgery and gives recommendations for the use of monitoring devices that are prerequisites to perform the model in a standardized way. Monitoring of intracranial pressure (ICP) and regional cerebral blood flow (CBF) are important to control bleeding induction and to make sure that neuronal tissue is not damaged by the intravascular filament. When crucial points during surgical SAH induction are considered the model is highly reproducible and standardized. In this thesis we report robust physiological findings during SAH induction in different transgenic mouse strains. Therefore we conclude that the employed SAH mouse model is a standardized and reproducible animal model that reveals robust findings in the early phase of SAH.[67]

For *in vivo* investigations of cortical microvessels the preparation of a cranial window is required. Different techniques for cerebral window preparation have been described:[220] The preparation with the deepest insight into the brain is the glass window preparation. A piece of bone is removed and replaced by a glass window. A less invasive cranial window preparation technique is the thinned-skull window preparation.[221] Here the bone is not separated but merely thinned at the imaging position. The bone stays intact and the physiologic shape towards the brain surface is preserved. Therefore the anatomical unit of bone, dura mater and subarachnoid space is not altered. By this cranial window preparation the physiologic pressure situation in the subarachnoid space is preserved which allows the normal distribution of subarachnoid blood in a situation of elevated ICP. The optimized cranial window allows to image vessels in a native situation as well as a comparison of vessel morphology and functional imaging before and after hemorrhage.

In previous intravital microscopy studies on blood flow and vascular function after SAH pial vessels were visualized by epifluorescence microscopy.[150] This technique does not enable investigations of parenchymal vessels because of its limited penetration depth. Therefore the parenchymal microcirculation could not be studied in detail. The beauty of the current experimental setup is that we employed *in vivo* two-photon microscopy to investigate microcirculatory disturbances after SAH. Two-photon microscopy allows looking down more than 1mm into the brain tissue.[222] Optical sections within a brain column are obtained by the scanning of layers. For analysis the image stack can be reconstructed in three dimensions to identify large structures like the cerebral vasculature. Therefore vessel shape, perfused vessel volume and blood flow velocity in the parenchyma can be measured and quantified.

Another methodological improvement is that transgenic animal lines were used to

investigate the pathophysiology of SAH. So far SAH studies were only rarely performed in transgenic animals because they tend to have a higher standard deviation or may reveal a different disease phenotype. The experiments of this thesis were performed in mouse lines that were backcrossed to a C57Bl6 background, which means that data were obtained from the same genetic background and should therefore be comparable. However, especially when animals are bred homozygously for generations without refreshment of the background line a genetic shift can occur.[223] We therefore obtained additional physiological data in order to be able to compare results across different experimental groups. No differences neither in the induction of SAH nor in the formation of microvasospasm and early cerebral ischemia after SAH were detected. Therefore we are confident that results can be interpreted in conjunction across different lines.

3. Discussion of relevant findings

The distribution of extravasated subarachnoid blood after SAH has never been investigated in detail in the endovascular perforation mouse model. However the extravasated blood in the subarachnoid space is thought to be involved in the early pathophysiology after SAH.[133] It is suspected to be causative for pearl-string constrictions of superficial arteries after the bleeding. Subarachnoid blood stretches along brain supplying arteries from the base of the brain to the dorsal cortices. This finding is especially crucial for imaging experiments because the region of interest for intravital microscopy is located at the dorsal cortex. Therefore *in vivo* microscopy was performed at a location where superficial arteries were covered with subarachnoid blood.

By comparing the vessel morphology before and after SAH the identification of a global and a bottleneck constriction type in addition to the previously described pearl-string constrictions of superficial arteries was possible. These newly identified vessel constriction types have implications on the blood flow dynamics after SAH. Measurement of blood flow velocity before and after SAH show that blood flow is reduced after SAH compared to the sham situation. In combination with a reduced vessel diameter it leads to reduced blood volume flowing into the parenchyma via penetrating arterioles. When regarding the Hagen Poiseuille law, which takes the radius of a tube into the forth power to determine the flow volume, the observed reduction of vessel diameter has a big influence on blood flow volume through superficial arteries and arterioles. A diameter reduction of 20% is therefore associated with a 60% reduction of flow-through-volume. The Hagen Poiseuille law is primarily valid for laminar flow through a tube, in a turbulent flow situation the reduction of flow volume is expected to be even larger.
While superficial cerebral vessels reveal several collaterals that can take over tissue perfusion in case of vessel narrowing or occlusion penetrating arterioles represent a bottleneck in cortical perfusion.[131] Even the occlusion of one single penetrating arteriole

cannot be fully compensated by collateral blood flow in adjacent penetrating arterioles. Subsequently blood flow in parenchymal capillaries that are supplied by the affected penetrating arteriole is significantly reduced.[131]
Besides blood flow restrictions on the brain surface also dysfunction on the capillary level may be responsible for early ischemia after SAH. A potential pathomechanism for cerebral perfusion deficits may be the plugging of capillaries by leukocytes that interact with the endothelium.[127] The number of sticking leukocytes increased five-fold after SAH, but the absolute number of sticking leukocytes in the investigated tissue volume was too low to explain the observed perfusion deficits in the parenchyma.
It is likely that the observed reduction of blood flow in the parenchyma is severe enough to cause ischemia in brain tissue. Under ischemic conditions oxygen and glucose supply is not sufficient to provide cells with metabolites. The result is a metabolic derangement which manifests in increased lactate and pyruvate levels after SAH.[96] Cells in a metabolic stress condition may initiate apoptosis or undergo necrosis. Apoptosis after SAH is mainly detected in hippocampal neurons and endothelial cells and to a lesser extent in cortical neurons.[109] Similarly necrosis is found after SAH but brain infarction does not occur.[224] However a long lasting reduction of cerebral perfusion down to values around 30% of initial perfusion would cause widespread brain infarction.[225] Therefore it is likely that severe cerebral ischemia is not persistent in the employed SAH model. Acute ischemia after SAH has probably functional reasons and resolves subsequently. Microvasospasm have been shown to be most pronounced three hours after the bleeding and become less frequent and severe at 24 and 72 hours.[150] This finding is important for the discussion of potential therapeutic strategies of microvasospasm. Treatment has to be initiated early after the bleeding in order to prevent neuronal tissue damage. We suggest a therapeutic time frame of maximal 24 hours after SAH for the resolution of vasospasm and early cerebral ischemia. Our data indicate that the therapeutic resolution of superficial artery constriction will also promote brain perfusion in the parenchyma.

For the identification of new therapeutic targets in the treatment of acute cerebral ischemia after SAH we attempted to identify the cell type that is initiating vessel constriction and in a second step to reveal the underlying functional pathophysiology.
In this thesis a pericyte reporter mouse line was used for investigations on the role of pericytes after SAH. Transgenic mice express a red fluorescent protein (DsRed) in pericytes, which can therefore be visualized *in vivo*. One challenge of reporter mouse lines is a potential aggregation of a fluorescent dye[226] that may disturb the physiology of dye expressing cells. In NG2 DsRed mice no aggregation of DsRed in pericytes was found. The distribution of the fluorophore was homogeneous in the cytoplasm and stretched into cell processes. Another potential problem which may arise when using reporter mouse lines is that the expression of the reporter is sometimes unspecific. The NG2 DsRed mouse line expresses DsRed under the neural/glial antigen 2 (NG2) promoter, which is transcribed in oligodendrocytes, VSMC and pericytes.[215] Therefore

reporter mice express red fluorescent protein in those three cell types. Since a differentiation of the cell types *in vivo* is challenging expression characteristics have to be further identified in histological slices. The information that is obtained by histological staining can then be used for the interpretation of *in vivo* data. A detailed analysis of the same ROI *in vivo* and histologically is not possible with currently available experimental techniques. In the future whole brain clearing in combination with light sheet microscopy [227] will help to investigate fluorescence expression patterns in situ and histologically.

In the NG2 DsRed mouse line the differentiation between VSMC and pericytes is especially challenging because both cell types express essentially the same cell markers and none of the commercially available antibodies is specific for either cell type.[159] In order to solve this issue we investigated a combination of cell characteristics: The first criterion was the localization of the cell along the vascular tree. VSMC confluently cover arteries and arterioles whereas pericytes are located solitary close to capillaries and capillary bifurcations.[157] The second criterion was cell morphology. Smooth muscle cells are wrapping the vessel whereas pericytes are spindle shaped cells with long primary and short secondary processes. The cell localization and their morphology can be assessed by *in vivo* microscopy. The third criterion was the expression of different antigens that were examined by immunohistological staining. Platelet derived growth factor receptor ß (PDGF Rß) was used as a rather specific marker for pericytes and αSMA as a marker for VSMC. A combination of localization, morphology and marker expression allows the differentiation of VSMC and pericytes in the NG2 DsRed mouse line.

Vessel diameter after SAH in pericyte reporter mice was investigated to make a potential pericyte or VSMC contraction visible. Superficial artery and arteriole spasm co-localized with VSMC, indicating that VSMC are inducing formation of microvasospasm. However the finding that VSMC co-localize with sites where vasospasm occur does not yet prove that they are actively inducing vessel constrictions. In order to show VSMC contraction along superficial microvasospasm functional Ca^{2+} imaging will have to be performed.

In the microcirculation pericyte localization was investigated in relation to capillary narrowing after SAH. Vessel narrowing specifically at sites where pericytes are present would indicate that pericytes are constricting and thereby reducing the capillary lumen.[203] However no co-localization of capillary narrowing and pericyte location was detected. Therefore pericytes do not seem to be involved in capillary narrowing after SAH. This finding is not in line with previous publications on pericyte constriction in ischemic conditions.[198, 203] Yemisci et. al. show that pericyte constrict upon oxidative stress and narrow capillary lumen thereby hampering blood flow.[203] Hall et. al. report similar reactions of pericytes to oxygen glucose deprivation suggesting that pericytes die in rigor mortis upon ischemia.[198] The conflicting results are probably caused by the different pathophysiology of SAH and ischemic stroke. Presumably energy depletion is much more pronounced in the ischemic core of a focal stroke as compared to cortical perfusion deficits after SAH. A more severe metabolic derangement presumably

induces more widespread pericyte dysfunction. Furthermore the studies that investigated the role of pericytes in ischemic conditions have some limitations. The publication which shows pericytes constriction upon oxidative stress is a histological study. Whether capillary diameter can be investigated in histological sections is debatable.[228] The publication suggesting that pericytes die in “rigor mortis” was performed in *ex vivo* brain slice preparations. However the condition of oxygen glucose deprivation reveals differences to cerebral ischemia *in vivo*. Aspects like blood flow and circulation, systemic inflammatory responses and edema formation cannot be mimicked in brain slice cultures. In this setup the cerebral pathophysiology of stroke is narrowed down to oxygen and energy depletion. Therefore studies on pericyte constriction in ischemic condition will have to be confirmed by making use of functional imaging to clarify the role of pericytes in ischemia.

As the sole localization of a cell type in relation to vessel spasm is a rather weak indicator for its involvement in the pathophysiology we went one step further and performed functional Ca^{2+} imaging after SAH *in vivo*. A transgenic mouse line expressing the Ca^{2+} sensor TN-XXL under the promotor of chicken β-actin was used.[216] We expected expression in cerebral perivascular cells as described from a GFP β-actin reporter mouse.[199] Therefore we aimed to visualize the activation status of pericytes and VSMC before and after SAH. In the CAG TN-XXL mouse line however the cerebrovascular expression of the Ca^{2+} sensor is largely confined to endothelial cells. With this mouse line changes in endothelial intracellular Ca^{2+} concentration may be specifically addressed. Since investigations on Ca^{2+} changes in endothelial cells have to date primarily been performed in cell culture,[229, 230] our approach allows for the first time to investigate cerebral endothelial Ca^{2+} signaling *in vivo*. Measurements in the baseline condition and after sham surgery revealed robust Ca^{2+} concentrations in endothelial cells. No bleaching or leaking of the sensor from endothelial cells was observed. After SAH the ratio change indicates decreased Ca^{2+} levels in endothelial cells. This finding can be explained by decreased blood flow velocity in cerebral vessels after SAH. Shear stress, which is imposed on endothelial cells by blood flow, has an impact on the activation status of endothelial cells. High blood flow velocity induces high endothelial Ca^{2+} concentration.[218] High Ca^{2+} concentration in endothelial cells in turn activates endothelial nitric oxide synthase (eNOS), which leads to increased nitric oxide (NO) production and vasodilation. After SAH the activity of eNOS is reduced, leading to decreased NO levels and subsequent vasoconstriction. Low endothelial Ca^{2+} concentration could therefore be a trigger for endothelial dysfunction after SAH.
The CAG TN-XXL mouse line provides an excellent tool to further investigate functional Ca^{2+} concentration in endothelial cells in response to changes of neural activity or cerebral blood flow. These investigations might further elucidate neurovascular coupling and blood flow dynamics in the brain, principle mechanisms which are important in health and disease.

4. Summary

With our imaging setup we were able to investigate the cerebral microcirculation after SAH in detail. New vessel constriction patterns and reduced blood flow velocity in superficial arteries were identified. Perfused vessel volume was significantly reduced after SAH, indicating parenchymal ischemia. Leukocyte plugging occurred in capillaries, but low numbers made significant contribution to perfusion deficits after SAH unlikely. Microvasospasm of superficial arteries occurred at locations where VSMC confluently cover the vessel, however capillary narrowing did not co-localize with pericyte location. This finding supports the assumption that pericytes do not play a major role in the formation of early ischemia after SAH. Furthermore neither migration of pericytes nor cell death were observed acutely after SAH. Free intracellular Ca^{2+} concentration in endothelial cells was reduced after SAH. The reduction of endothelial Ca^{2+} may explain reduced NO levels and thereby endothelial dysfunction and vasoconstriction. Taken together these results further characterize early cerebral ischemia after SAH and suggest new key players in the formation of vessel spasm.

5. Outlook

This thesis investigates different aspects on the formation of microvasospasm after SAH but cannot provide a definite answer on the pathomechanism. It gives rise to more questions that may be addressed in this context.

Perfusion deficits of the brain parenchyma early after SAH should be investigated in more detail. Especially the distribution of perfusion deficits in different brain structures and its severity close to the bleeding site will be interesting to examine. The current experimental setup allows perfusion measurement in the cortex, either by laser Doppler flowmetry on the temporal bone or by assessment of perfused vessel volume with two-photon microscopy. The technique of autoradiography determines absolute perfusion values in whole brain slices.[231] If this technique is applied after SAH induction, early deficits in parenchymal perfusion will be detectable. The knowledge, which brain areas are severely undersupplied after SAH, if applicable to patients, will help to explain neurological deficits early after SAH.

Our data on the involvement of pericytes in the early pathophysiology after SAH indicate that pericytes are not causative for early cerebral ischemia. However this finding should be confirmed by investigations in a pericyte deficient mouse model. Mice that are devoid of pericytes, e.g. PDGF Rß full knockouts die during gestation.[183] Therefore pericyte deficient mouse models have been created that exhibit a reduced number of pericytes. Heterozygous PDGF Rβ knockouts exhibit only 35% functional pericytes.[173] Another frequently used mouse model for the investigation of pericytes is the PDGF b $^{ret/ret}$ mouse line which specifically lack the retention motive of PDGF b. As

the retention motive is important for the creation of a steep gradient of PDGF b around the vessel, a knockout leads to wider diffusion of PDGF b. The steep gradient, however, is needed for the proper attachment of pericytes to the endothelium. PDGF b $^{ret/ret}$ knockout mice exhibit pericytes that are not associated to vessels and are therefore not functional.[183] A broad phenotype can primarily be seen in retinal and renal vasculature although also BBB disruption has been reported.[183] We intend to investigate the PDGF b $^{ret/ret}$ mouse line to confirm that pericytes are indeed not involved in the formation of early cerebral ischemia after SAH.

More studies especially on the functional changes after SAH will have to be conducted in order to gain comprehensive insight into the processes of early ischemia after SAH. Because always an interplay of different cerebral cell types is defining a pathophysiology we plan to investigate functional changes in the whole neurovascular unit after SAH. Only a broad approach can ensure to elucidate the interplay between cells and the consequences for each cell type. As mentioned above functional *in vivo* investigations of specific cell types are not easy to perform. Maybe in the future mice that express Ca^{2+} dyes under cell-specific promotors will be available. Such functional transgenic mouse model would enable researchers to investigate, similarly to the CAG TN-XXL strain for endothelial cells, the different components of the neurovascular unit. In the pathology of vasospasm after SAH VSMC will be the first target because strong indication on their contribution to the formation of vessel spasm exists. Functional Ca^{2+} imaging in these cells will reveal the dynamics and extent of VSMC activation and constriction after SAH. Another important target for functional imaging is the crosstalk between neurons and the vasculature. The cells of the neurovascular unit that are probably involved in this communication are astrocytes and specifically astrocytic endfeet. It has already been shown in brain slices that Ca^{2+} sparks increase in frequency and intensity after SAH.[146] In this context it will be interesting to carry out a detailed characterization of neuronal activity after SAH. A specific targeting of neurons with Ca^{2+} probes may be performed by selective transfer by adenovirus.[232] Viral labeling of cells allows making use of the newest generation of Ca^{2+} sensitive dyes with a high specificity. Further functional *in vivo* investigation will elucidate the communication between astrocytes, neurons and the vasculature in health and disease. Only when the crosstalk between the involved cell types is comprehensively understood the identification of reasonable therapeutic targets for early ischemia after SAH will be possible.

E References

1. Kleindorfer, D.O. et al. Stroke incidence is decreasing in whites but not in blacks: a population-based estimate of temporal trends in stroke incidence from the Greater Cincinnati/Northern Kentucky Stroke Study. *Stroke* **41**, 1326-31 (2010).
2. Hop, J.W., Rinkel, G.J., Algra, A. & van Gijn, J. Case-fatality rates and functional outcome after subarachnoid hemorrhage: a systematic review. *Stroke* **28**, 660-4 (1997).
3. Pobereskin, L.H. Influence of premorbid factors on survival following subarachnoid hemorrhage. *J Neurosurg* **95**, 555-9 (2001).
4. Lovelock, C.E., Rinkel, G.J. & Rothwell, P.M. Time trends in outcome of subarachnoid hemorrhage: Population-based study and systematic review. *Neurology* **74**, 1494-501 (2010).
5. Dodel, R. et al. Cost of illness in subarachnoid hemorrhage: a German longitudinal study. *Stroke* **41**, 2918-23 (2010).
6. van Gijn, J., Kerr, R.S. & Rinkel, G.J. Subarachnoid haemorrhage. *Lancet* **369**, 306-18 (2007).
7. Vlak, M.H., Algra, A., Brandenburg, R. & Rinkel, G.J. Prevalence of unruptured intracranial aneurysms, with emphasis on sex, age, comorbidity, country, and time period: a systematic review and meta-analysis. *Lancet Neurol* **10**, 626-36 (2011).
8. Alfano, J.M. et al. Intracranial aneurysms occur more frequently at bifurcation sites that typically experience higher hemodynamic stresses. *Neurosurgery* **73**, 497-505 (2013).
9. Van Calenbergh, F., Plets, C., Goffin, J. & Velghe, L. Nonaneurysmal subarachnoid hemorrhage: prevalence of perimesencephalic hemorrhage in a consecutive series. *Surg Neurol* **39**, 320-3 (1993).
10. Linn, F.H., Rinkel, G.J., Algra, A. & van Gijn, J. Headache characteristics in subarachnoid haemorrhage and benign thunderclap headache. *J Neurol Neurosurg Psychiatry* **65**, 791-3 (1998).
11. Claassen, J. et al. Global cerebral edema after subarachnoid hemorrhage: frequency, predictors, and impact on outcome. *Stroke* **33**, 1225-32 (2002).
12. Laun, A. & Tonn, J.C. Cranial nerve lesions following subarachnoid hemorrhage and aneurysm of the circle of Willis. *Neurosurg Rev* **11**, 137-41 (1988).
13. Butzkueven, H. et al. Onset seizures independently predict poor outcome after subarachnoid hemorrhage. *Neurology* **55**, 1315-20 (2000).
14. Schievink, W.I. Intracranial aneurysms. *N Engl J Med* **336**, 28-40 (1997).
15. Suarez-Rivera, O. Acute hydrocephalus after subarachnoid hemorrhage. *Surg Neurol* **49**, 563-5 (1998).
16. Dupont, S. & Rabinstein, A.A. Extent of acute hydrocephalus after subarachnoid hemorrhage as a risk factor for poor functional outcome. *Neurol Res* **35**, 107-10 (2013).

17. Medele, R.J., Stummer, W., Mueller, A.J., Steiger, H.J. & Reulen, H.J. Terson's syndrome in subarachnoid hemorrhage and severe brain injury accompanied by acutely raised intracranial pressure. *J Neurosurg* **88**, 851-4 (1998).
18. Di Pasquale, G. et al. Holter detection of cardiac arrhythmias in intracranial subarachnoid hemorrhage. *Am J Cardiol* **59**, 596-600 (1987).
19. Toussaint, L.G., 3rd et al. Survival of cardiac arrest after aneurysmal subarachnoid hemorrhage. *Neurosurgery* **57**, 25-31; discussion 25-31 (2005).
20. Ohkuma, H., Tsurutani, H. & Suzuki, S. Incidence and significance of early aneurysmal rebleeding before neurosurgical or neurological management. *Stroke* **32**, 1176-80 (2001).
21. Brilstra, E.H., Algra, A., Rinkel, G.J., Tulleken, C.A. & van Gijn, J. Effectiveness of neurosurgical clip application in patients with aneurysmal subarachnoid hemorrhage. *J Neurosurg* **97**, 1036-41 (2002).
22. Hijdra, A., Braakman, R., van Gijn, J., Vermeulen, M. & van Crevel, H. Aneurysmal subarachnoid hemorrhage. Complications and outcome in a hospital population. *Stroke* **18**, 1061-7 (1987).
23. Brilstra, E.H., Rinkel, G.J., Algra, A. & van Gijn, J. Rebleeding, secondary ischemia, and timing of operation in patients with subarachnoid hemorrhage. *Neurology* **55**, 1656-60 (2000).
24. Rabinstein, A.A. et al. Predictors of cerebral infarction in aneurysmal subarachnoid hemorrhage. *Stroke* **35**, 1862-6 (2004).
25. Backes, D., Rinkel, G.J., Kemperman, H., Linn, F.H. & Vergouwen, M.D. Time-dependent test characteristics of head computed tomography in patients suspected of nontraumatic subarachnoid hemorrhage. *Stroke* **43**, 2115-9 (2012).
26. Opeskin, K. & Silberstein, M. False positive diagnosis of subarachnoid haemorrhage on computed tomography scan. *J Clin Neurosci* **5**, 382-6 (1998).
27. Mitchell, P. et al. Detection of subarachnoid haemorrhage with magnetic resonance imaging. *J Neurol Neurosurg Psychiatry* **70**, 205-11 (2001).
28. White, P.M., Teasdale, E.M., Wardlaw, J.M. & Easton, V. Intracranial aneurysms: CT angiography and MR angiography for detection prospective blinded comparison in a large patient cohort. *Radiology* **219**, 739-49 (2001).
29. Delgado Almandoz, J.E. et al. Diagnostic yield of catheter angiography in patients with subarachnoid hemorrhage and negative initial noninvasive neurovascular examinations. *AJNR Am J Neuroradiol* **34**, 833-9 (2013).
30. Eskey, C.J. & Ogilvy, C.S. Fluoroscopy-guided lumbar puncture: decreased frequency of traumatic tap and implications for the assessment of CT-negative acute subarachnoid hemorrhage. *AJNR Am J Neuroradiol* **22**, 571-6 (2001).
31. Shah, K.H. & Edlow, J.A. Distinguishing traumatic lumbar puncture from true subarachnoid hemorrhage. *J Emerg Med* **23**, 67-74 (2002).
32. Zhang, H., Zhang, B., Li, S., Liang, C. & Xu, K. Whole brain CT perfusion combined with CT angiography in patients with subarachnoid hemorrhage and cerebral vasospasm. *Clin Neurol Neurosurg* **115**, 2496-501 (2013).

33. Aaslid, R., Huber, P. & Nornes, H. Evaluation of cerebrovascular spasm with transcranial Doppler ultrasound. *J Neurosurg* **60**, 37-41 (1984).
34. Brown, R.J., Kumar, A., Dhar, R., Sampson, T.R. & Diringer, M.N. The relationship between delayed infarcts and angiographic vasospasm after aneurysmal subarachnoid hemorrhage. *Neurosurgery* **72**, 702-7; discussion 707-8 (2013).
35. Steiner, T. et al. European Stroke Organization guidelines for the management of intracranial aneurysms and subarachnoid haemorrhage. *Cerebrovasc Dis* **35**, 93-112 (2013).
36. Guglielmi, G., Vinuela, F., Sepetka, I. & Macellari, V. Electrothrombosis of saccular aneurysms via endovascular approach. Part 1: Electrochemical basis, technique, and experimental results. *J Neurosurg* **75**, 1-7 (1991).
37. Molyneux, A.J. et al. International subarachnoid aneurysm trial (ISAT) of neurosurgical clipping versus endovascular coiling in 2143 patients with ruptured intracranial aneurysms: a randomised comparison of effects on survival, dependency, seizures, rebleeding, subgroups, and aneurysm occlusion. *Lancet* **366**, 809-17 (2005).
38. Uozumi, Y. et al. Decompressive craniectomy in patients with aneurysmal subarachnoid hemorrhage: a single-center matched-pair analysis. *Cerebrovasc Dis* **37**, 109-15 (2014).
39. Ramakrishna, R. et al. Intraventricular tissue plasminogen activator for the prevention of vasospasm and hydrocephalus after aneurysmal subarachnoid hemorrhage. *Neurosurgery* **67**, 110-7; discussion 117 (2010).
40. Dorhout Mees, S.M. et al. Calcium antagonists for aneurysmal subarachnoid haemorrhage. *Cochrane Database Syst Rev*, CD000277 (2007).
41. Velly, L.J. et al. Anaesthetic and ICU management of aneurysmal subarachnoid haemorrhage: A survey of European practice. *Eur J Anaesthesiol* **32**, 168-76 (2015).
42. Vajkoczy, P. et al. Clazosentan (AXV-034343), a selective endothelin A receptor antagonist, in the prevention of cerebral vasospasm following severe aneurysmal subarachnoid hemorrhage: results of a randomized, double-blind, placebo-controlled, multicenter phase IIa study. *J Neurosurg* **103**, 9-17 (2005).
43. Macdonald, R.L. et al. Clazosentan to overcome neurological ischemia and infarction occurring after subarachnoid hemorrhage (CONSCIOUS-1): randomized, double-blind, placebo-controlled phase 2 dose-finding trial. *Stroke* **39**, 3015-21 (2008).
44. McGirt, M.J. et al. Simvastatin increases endothelial nitric oxide synthase and ameliorates cerebral vasospasm resulting from subarachnoid hemorrhage. *Stroke* **33**, 2950-6 (2002).
45. Tseng, M.Y., Czosnyka, M., Richards, H., Pickard, J.D. & Kirkpatrick, P.J. Effects of acute treatment with pravastatin on cerebral vasospasm, autoregulation, and

delayed ischemic deficits after aneurysmal subarachnoid hemorrhage: a phase II randomized placebo-controlled trial. *Stroke* **36**, 1627-32 (2005).
46. Kramer, A.H. & Fletcher, J.J. Statins in the management of patients with aneurysmal subarachnoid hemorrhage: a systematic review and meta-analysis. *Neurocrit Care* **12**, 285-96 (2010).
47. Wong, G.K. et al. High-dose simvastatin for aneurysmal subarachnoid hemorrhage: multicenter randomized controlled double-blinded clinical trial. *Stroke* **46**, 382-8 (2015).
48. van den Bergh, W.M. et al. Magnesium sulfate in aneurysmal subarachnoid hemorrhage: a randomized controlled trial. *Stroke* **36**, 1011-5 (2005).
49. Sen, J. et al. Triple-H therapy in the management of aneurysmal subarachnoid haemorrhage. *Lancet Neurol* **2**, 614-21 (2003).
50. Bauer, A.M. & Rasmussen, P.A. Treatment of intracranial vasospasm following subarachnoid hemorrhage. *Front Neurol* **5**, 72 (2014).
51. Zubkov, Y.N., Nikiforov, B.M. & Shustin, V.A. Balloon catheter technique for dilatation of constricted cerebral arteries after aneurysmal SAH. *Acta Neurochir (Wien)* **70**, 65-79 (1984).
52. Milburn, J.M. et al. Increase in diameters of vasospastic intracranial arteries by intraarterial papaverine administration. *J Neurosurg* **88**, 38-42 (1998).
53. Pluta, R.M. et al. Cerebral vasospasm following subarachnoid hemorrhage: time for a new world of thought. *Neurol Res* **31**, 151-8 (2009).
54. Hansen-Schwartz, J., Vajkoczy, P., Macdonald, R.L., Pluta, R.M. & Zhang, J.H. Cerebral vasospasm: looking beyond vasoconstriction. *Trends Pharmacol Sci* **28**, 252-6 (2007).
55. Macdonald, R.L., Pluta, R.M. & Zhang, J.H. Cerebral vasospasm after subarachnoid hemorrhage: the emerging revolution. *Nat Clin Pract Neurol* **3**, 256-63 (2007).
56. Titova, E., Ostrowski, R.P., Zhang, J.H. & Tang, J. Experimental models of subarachnoid hemorrhage for studies of cerebral vasospasm. *Neurol Res* **31**, 568-81 (2009).
57. Solomon, R.A., Antunes, J.L., Chen, R.Y., Bland, L. & Chien, S. Decrease in cerebral blood flow in rats after experimental subarachnoid hemorrhage: a new animal model. *Stroke* **16**, 58-64 (1985).
58. Jackowski, A., Crockard, A., Burnstock, G., Russell, R.R. & Kristek, F. The time course of intracranial pathophysiological changes following experimental subarachnoid haemorrhage in the rat. *J Cereb Blood Flow Metab* **10**, 835-49 (1990).
59. Sabri, M. et al. Anterior circulation mouse model of subarachnoid hemorrhage. *Brain Res* **1295**, 179-85 (2009).
60. Altay, T. et al. A novel method for subarachnoid hemorrhage to induce vasospasm in mice. *J Neurosci Methods* **183**, 136-40 (2009).

61. Schwartz, A.Y., Masago, A., Sehba, F.A. & Bederson, J.B. Experimental models of subarachnoid hemorrhage in the rat: a refinement of the endovascular filament model. *J Neurosci Methods* **96**, 161-7 (2000).
62. Bederson, J.B., Germano, I.M. & Guarino, L. Cortical blood flow and cerebral perfusion pressure in a new noncraniotomy model of subarachnoid hemorrhage in the rat. *Stroke* **26**, 1086-91; discussion 1091-2 (1995).
63. Veelken, J.A., Laing, R.J. & Jakubowski, J. The Sheffield model of subarachnoid hemorrhage in rats. *Stroke* **26**, 1279-83; discussion 1284 (1995).
64. Schuller, K., Buhler, D. & Plesnila, N. A murine model of subarachnoid hemorrhage. *J Vis Exp*, e50845 (2013).
65. Kamii, H. et al. Amelioration of vasospasm after subarachnoid hemorrhage in transgenic mice overexpressing CuZn-superoxide dismutase. *Stroke* **30**, 867-71; discussion 872 (1999).
66. Parra, A. et al. Mouse model of subarachnoid hemorrhage associated cerebral vasospasm: methodological analysis. *Neurol Res* **24**, 510-6 (2002).
67. Buhler, D., Schuller, K. & Plesnila, N. Protocol for the induction of subarachnoid hemorrhage in mice by perforation of the Circle of Willis with an endovascular filament. *Transl Stroke Res* **5**, 653-9 (2014).
68. Ecker, A. & Riemenschneider, P.A. Arteriographic demonstration of spasm of the intracranial arteries, with special reference to saccular arterial aneurysms. *J Neurosurg* **8**, 660-7 (1951).
69. Tani, E. & Matsumoto, T. Continuous elevation of intracellular Ca2+ is essential for the development of cerebral vasospasm. *Curr Vasc Pharmacol* **2**, 13-21 (2004).
70. Kim, I. et al. Thin and thick filament regulation of contractility in experimental cerebral vasospasm. *Neurosurgery* **46**, 440-6; discussion 446-7 (2000).
71. Bauer, V. & Sotnikova, R. Nitric oxide--the endothelium-derived relaxing factor and its role in endothelial functions. *Gen Physiol Biophys* **29**, 319-40 (2010).
72. Kasuya, H. et al. Nitric oxide synthase and guanylate cyclase levels in canine basilar artery after subarachnoid hemorrhage. *J Neurosurg* **82**, 250-5 (1995).
73. Knott, A.B. & Bossy-Wetzel, E. Nitric oxide in health and disease of the nervous system. *Antioxid Redox Signal* **11**, 541-54 (2009).
74. Aladag, M.A. et al. Melatonin ameliorates cerebral vasospasm after experimental subarachnoidal haemorrhage correcting imbalance of nitric oxide levels in rats. *Neurochem Res* **34**, 1935-44 (2009).
75. Seifert, V., Loffler, B.M., Zimmermann, M., Roux, S. & Stolke, D. Endothelin concentrations in patients with aneurysmal subarachnoid hemorrhage. Correlation with cerebral vasospasm, delayed ischemic neurological deficits, and volume of hematoma. *J Neurosurg* **82**, 55-62 (1995).
76. Ahn, Y.M. et al. Sustained arterial narrowing after prolonged exposure to perivascular endothelin. *Neurosurgery* **50**, 843-8; discussion 848-9 (2002).

77. Kasuya, H., Weir, B.K., White, D.M. & Stefansson, K. Mechanism of oxyhemoglobin-induced release of endothelin-1 from cultured vascular endothelial cells and smooth-muscle cells. *J Neurosurg* **79**, 892-8 (1993).
78. Fassbender, K. et al. Endothelin-1 in subarachnoid hemorrhage: An acute-phase reactant produced by cerebrospinal fluid leukocytes. *Stroke* **31**, 2971-5 (2000).
79. Alabadi, J.A. et al. Changes in the cerebrovascular effects of endothelin-1 and nicardipine after experimental subarachnoid hemorrhage. *Neurosurgery* **33**, 707-14; discussion 714-5 (1993).
80. Vergouwen, M.D., Vermeulen, M., Coert, B.A., Stroes, E.S. & Roos, Y.B. Microthrombosis after aneurysmal subarachnoid hemorrhage: an additional explanation for delayed cerebral ischemia. *J Cereb Blood Flow Metab* **28**, 1761-70 (2008).
81. Ostergaard, L. et al. The role of the microcirculation in delayed cerebral ischemia and chronic degenerative changes after subarachnoid hemorrhage. *J Cereb Blood Flow Metab* **33**, 1825-37 (2013).
82. Ayata, C. Spreading depression and neurovascular coupling. *Stroke* **44**, S87-9 (2013).
83. Busija, D.W., Bari, F., Domoki, F., Horiguchi, T. & Shimizu, K. Mechanisms involved in the cerebrovascular dilator effects of cortical spreading depression. *Prog Neurobiol* **86**, 379-95 (2008).
84. Dreier, J.P. et al. Products of hemolysis in the subarachnoid space inducing spreading ischemia in the cortex and focal necrosis in rats: a model for delayed ischemic neurological deficits after subarachnoid hemorrhage? *J Neurosurg* **93**, 658-66 (2000).
85. Dreier, J.P. et al. Cortical spreading ischaemia is a novel process involved in ischaemic damage in patients with aneurysmal subarachnoid haemorrhage. *Brain* **132**, 1866-81 (2009).
86. Bosche, B. et al. Recurrent spreading depolarizations after subarachnoid hemorrhage decreases oxygen availability in human cerebral cortex. *Ann Neurol* **67**, 607-17 (2010).
87. Woitzik, J. et al. Delayed cerebral ischemia and spreading depolarization in absence of angiographic vasospasm after subarachnoid hemorrhage. *J Cereb Blood Flow Metab* **32**, 203-12 (2012).
88. Iadecola, C. Bleeding in the brain: Killer waves of depolarization in subarachnoid bleed. *Nat Med* **15**, 1131-2 (2009).
89. Sehba, F.A., Pluta, R.M. & Zhang, J.H. Metamorphosis of subarachnoid hemorrhage research: from delayed vasospasm to early brain injury. *Mol Neurobiol* **43**, 27-40 (2011).
90. Cahill, J. & Zhang, J.H. Subarachnoid hemorrhage: is it time for a new direction? *Stroke* **40**, S86-7 (2009).
91. Nornes, H. The role of intracranial pressure in the arrest of hemorrhage in patients with ruptured intracranial aneurysm. *J Neurosurg* **39**, 226-34 (1973).

92. Arutiunov, A.I., Baron, M.A. & Majorova, N.A. The role of mechanical factors in the pathogenesis of short-term and prolonged spasm of the cerebral arteries. *J Neurosurg* **40**, 459-72 (1974).
93. Nornes, H. & Magnaes, B. Intracranial pressure in patients with ruptured saccular aneurysm. *J Neurosurg* **36**, 537-47 (1972).
94. Zoerle, T. et al. Intracranial pressure after subarachnoid hemorrhage. *Crit Care Med* **43**, 168-76 (2015).
95. Buhler, D., Azghandi, S., Schuller, K. & Plesnila, N. Effect of Decompressive Craniectomy on Outcome Following Subarachnoid Hemorrhage in Mice. *Stroke* (2015).
96. Prunell, G.F., Mathiesen, T. & Svendgaard, N.A. Experimental subarachnoid hemorrhage: cerebral blood flow and brain metabolism during the acute phase in three different models in the rat. *Neurosurgery* **54**, 426-36; discussion 436-7 (2004).
97. Tso, M.K. & Macdonald, R.L. Acute microvascular changes after subarachnoid hemorrhage and transient global cerebral ischemia. *Stroke Res Treat* **2013**, 425281 (2013).
98. Plesnila, N. Pathophysiological Role of Global Cerebral Ischemia following Subarachnoid Hemorrhage: The Current Experimental Evidence. *Stroke Res Treat* **2013**, 651958 (2013).
99. Bederson, J.B. et al. Acute vasoconstriction after subarachnoid hemorrhage. *Neurosurgery* **42**, 352-60; discussion 360-2 (1998).
100. Schubert, G.A., Seiz, M., Hegewald, A.A., Manville, J. & Thome, C. Acute hypoperfusion immediately after subarachnoid hemorrhage: a xenon contrast-enhanced CT study. *J Neurotrauma* **26**, 2225-31 (2009).
101. Honda, M. et al. Early cerebral circulatory disturbance in patients suffering subarachnoid hemorrhage prior to the delayed cerebral vasospasm stage: xenon computed tomography and perfusion computed tomography study. *Neurol Med Chir (Tokyo)* **52**, 488-94 (2012).
102. Frontera, J.A. et al. Acute ischaemia after subarachnoid haemorrhage, relationship with early brain injury and impact on outcome: a prospective quantitative MRI study. *J Neurol Neurosurg Psychiatry* **86**, 71-8 (2015).
103. Nicotera, P. & Leist, M. Energy supply and the shape of death in neurons and lymphoid cells. *Cell Death Differ* **4**, 435-42 (1997).
104. Crompton, M.R. The Pathogenesis of Cerebral Infarction Following the Rupture of Cerebral Berry Aneurysms. *Brain* **87**, 491-510 (1964).
105. Kim, J.B. et al. HMGB1, a novel cytokine-like mediator linking acute neuronal death and delayed neuroinflammation in the postischemic brain. *J Neurosci* **26**, 6413-21 (2006).
106. Nakahara, T. et al. High-mobility group box 1 protein in CSF of patients with subarachnoid hemorrhage. *Neurocrit Care* **11**, 362-8 (2009).

107. Elmore, S. Apoptosis: a review of programmed cell death. *Toxicol Pathol* **35**, 495-516 (2007).
108. Cheng, G., Wei, L., Zhi-Dan, S., Shi-Guang, Z. & Xiang-Zhen, L. Atorvastatin ameliorates cerebral vasospasm and early brain injury after subarachnoid hemorrhage and inhibits caspase-dependent apoptosis pathway. *BMC Neurosci* **10**, 7 (2009).
109. Park, S. et al. Neurovascular protection reduces early brain injury after subarachnoid hemorrhage. *Stroke* **35**, 2412-7 (2004).
110. Friedrich, V., Flores, R. & Sehba, F.A. Cell death starts early after subarachnoid hemorrhage. *Neurosci Lett* **512**, 6-11 (2012).
111. Prunell, G.F., Svendgaard, N.A., Alkass, K. & Mathiesen, T. Delayed cell death related to acute cerebral blood flow changes following subarachnoid hemorrhage in the rat brain. *J Neurosurg* **102**, 1046-54 (2005).
112. Westermaier, T., Jauss, A., Eriskat, J., Kunze, E. & Roosen, K. The temporal profile of cerebral blood flow and tissue metabolites indicates sustained metabolic depression after experimental subarachnoid hemorrhage in rats. *Neurosurgery* **68**, 223-9; discussion 229-30 (2011).
113. Liang, D., Bhatta, S., Gerzanich, V. & Simard, J.M. Cytotoxic edema: mechanisms of pathological cell swelling. *Neurosurg Focus* **22**, E2 (2007).
114. Mocco, J., Prickett, C.S., Komotar, R.J., Connolly, E.S. & Mayer, S.A. Potential mechanisms and clinical significance of global cerebral edema following aneurysmal subarachnoid hemorrhage. *Neurosurg Focus* **22**, E7 (2007).
115. Scholler, K. et al. Characterization of microvascular basal lamina damage and blood-brain barrier dysfunction following subarachnoid hemorrhage in rats. *Brain Res* **1142**, 237-46 (2007).
116. Sehba, F.A., Mostafa, G., Knopman, J., Friedrich, V., Jr. & Bederson, J.B. Acute alterations in microvascular basal lamina after subarachnoid hemorrhage. *J Neurosurg* **101**, 633-40 (2004).
117. Dzwonek, J., Rylski, M. & Kaczmarek, L. Matrix metalloproteinases and their endogenous inhibitors in neuronal physiology of the adult brain. *FEBS Lett* **567**, 129-35 (2004).
118. Feiler, S., Plesnila, N., Thal, S.C., Zausinger, S. & Scholler, K. Contribution of matrix metalloproteinase-9 to cerebral edema and functional outcome following experimental subarachnoid hemorrhage. *Cerebrovasc Dis* **32**, 289-95 (2011).
119. Thal, S.C. et al. Brain edema formation and neurological impairment after subarachnoid hemorrhage in rats. Laboratory investigation. *J Neurosurg* **111**, 988-94 (2009).
120. Fassbender, K. et al. Inflammatory cytokines in subarachnoid haemorrhage: association with abnormal blood flow velocities in basal cerebral arteries. *J Neurol Neurosurg Psychiatry* **70**, 534-7 (2001).

121. Jiang, Y. et al. Neuroprotective effects of anti-tumor necrosis factor-alpha antibody on apoptosis following subarachnoid hemorrhage in a rat model. *J Clin Neurosci* **19**, 866-72 (2012).
122. Prunell, G.F., Svendgaard, N.A., Alkass, K. & Mathiesen, T. Inflammation in the brain after experimental subarachnoid hemorrhage. *Neurosurgery* **56**, 1082-92; discussion 1082-92 (2005).
123. Kubota, T., Handa, Y., Tsuchida, A., Kaneko, M. & Kobayashi, H. The kinetics of lymphocyte subsets and macrophages in subarachnoid space after subarachnoid hemorrhage in rats. *Stroke* **24**, 1993-2000; discussion 2000-1 (1993).
124. Friedrich, V. et al. Reduction of neutrophil activity decreases early microvascular injury after subarachnoid haemorrhage. *J Neuroinflammation* **8**, 103 (2011).
125. Yoshimoto, Y., Tanaka, Y. & Hoya, K. Acute systemic inflammatory response syndrome in subarachnoid hemorrhage. *Stroke* **32**, 1989-93 (2001).
126. Asano, T. & Sano, K. Pathogenetic role of no-reflow phenomenon in experimental subarachnoid hemorrhage in dogs. *J Neurosurg* **46**, 454-66 (1977).
127. del Zoppo, G.J., Schmid-Schonbein, G.W., Mori, E., Copeland, B.R. & Chang, C.M. Polymorphonuclear leukocytes occlude capillaries following middle cerebral artery occlusion and reperfusion in baboons. *Stroke* **22**, 1276-83 (1991).
128. Ames, A., 3rd, Wright, R.L., Kowada, M., Thurston, J.M. & Majno, G. Cerebral ischemia. II. The no-reflow phenomenon. *Am J Pathol* **52**, 437-53 (1968).
129. Herz, D.A., Baez, S. & Shulman, K. Pial microcirculation in subarachnoid hemorrhage. *Stroke* **6**, 417-24 (1975).
130. Nishimura, N. & Schaffer, C.B. Big effects from tiny vessels: imaging the impact of microvascular clots and hemorrhages on the brain. *Stroke* **44**, S90-2 (2013).
131. Nishimura, N., Schaffer, C.B., Friedman, B., Lyden, P.D. & Kleinfeld, D. Penetrating arterioles are a bottleneck in the perfusion of neocortex. *Proc Natl Acad Sci U S A* **104**, 365-70 (2007).
132. Sehba, F.A., Friedrich, V., Jr., Makonnen, G. & Bederson, J.B. Acute cerebral vascular injury after subarachnoid hemorrhage and its prevention by administration of a nitric oxide donor. *J Neurosurg* **106**, 321-9 (2007).
133. Sehba, F.A. & Bederson, J.B. Mechanisms of acute brain injury after subarachnoid hemorrhage. *Neurol Res* **28**, 381-98 (2006).
134. Zheng, R., Qin, L., Li, S., Xu, K. & Geng, H. CT perfusion-derived mean transit time of cortical brain has a negative correlation with the plasma level of Nitric Oxide after subarachnoid hemorrhage. *Acta Neurochir (Wien)* **156**, 527-33 (2014).
135. Sehba, F.A., Ding, W.H., Chereshnev, I. & Bederson, J.B. Effects of S-nitrosoglutathione on acute vasoconstriction and glutamate release after subarachnoid hemorrhage. *Stroke* **30**, 1955-61 (1999).

136. Sehba, F.A., Schwartz, A.Y., Chereshnev, I. & Bederson, J.B. Acute decrease in cerebral nitric oxide levels after subarachnoid hemorrhage. *J Cereb Blood Flow Metab* **20**, 604-11 (2000).
137. Nishizawa, S., Yamamoto, S., Yokoyama, T., Ryu, H. & Uemura, K. Chronological changes of arterial diameter, cGMP, and protein kinase C in the development of vasospasm. *Stroke* **26**, 1916-20; discussion 1920-1 (1995).
138. Said, S., Rosenblum, W.I., Povlishock, J.T. & Nelson, G.H. Correlations between morphological changes in platelet aggregates and underlying endothelial damage in cerebral microcirculation of mice. *Stroke* **24**, 1968-76 (1993).
139. Sabri, M. et al. Mechanisms of microthrombi formation after experimental subarachnoid hemorrhage. *Neuroscience* **224**, 26-37 (2012).
140. Sehba, F.A., Mostafa, G., Friedrich, V., Jr. & Bederson, J.B. Acute microvascular platelet aggregation after subarachnoid hemorrhage. *J Neurosurg* **102**, 1094-100 (2005).
141. Friedrich, V., Flores, R., Muller, A. & Sehba, F.A. Escape of intraluminal platelets into brain parenchyma after subarachnoid hemorrhage. *Neuroscience* **165**, 968-75 (2010).
142. Wang, Z. et al. Progesterone administration modulates cortical TLR4/NF-kappaB signaling pathway after subarachnoid hemorrhage in male rats. *Mediators Inflamm* **2011**, 848309 (2011).
143. Ishikawa, M. et al. Platelet and leukocyte adhesion in the microvasculature at the cerebral surface immediately after subarachnoid hemorrhage. *Neurosurgery* **64**, 546-53; discussion 553-4 (2009).
144. Attwell, D. et al. Glial and neuronal control of brain blood flow. *Nature* **468**, 232-43 (2010).
145. Filosa, J.A. et al. Local potassium signaling couples neuronal activity to vasodilation in the brain. *Nat Neurosci* **9**, 1397-1403 (2006).
146. Koide, M., Bonev, A.D., Nelson, M.T. & Wellman, G.C. Inversion of neurovascular coupling by subarachnoid blood depends on large-conductance Ca2+-activated K+ (BK) channels. *Proc Natl Acad Sci U S A* **109**, E1387-95 (2012).
147. Uhl, E., Lehmberg, J., Steiger, H.J. & Messmer, K. Intraoperative detection of early microvasospasm in patients with subarachnoid hemorrhage by using orthogonal polarization spectral imaging. *Neurosurgery* **52**, 1307-15; disacussion 1315-7 (2003).
148. Pennings, F.A., Bouma, G.J. & Ince, C. Direct observation of the human cerebral microcirculation during aneurysm surgery reveals increased arteriolar contractility. *Stroke* **35**, 1284-8 (2004).
149. Sun, B.L. et al. Dynamic alterations of cerebral pial microcirculation during experimental subarachnoid hemorrhage. *Cell Mol Neurobiol* **29**, 235-41 (2009).
150. Friedrich, B., Muller, F., Feiler, S., Scholler, K. & Plesnila, N. Experimental subarachnoid hemorrhage causes early and long-lasting microarterial

constriction and microthrombosis: an in-vivo microscopy study. *J Cereb Blood Flow Metab* **32**, 447-55 (2012).
151. Friedrich, B. et al. CO2 has no therapeutic effect on early microvasospasm after experimental subarachnoid hemorrhage. *J Cereb Blood Flow Metab* **34**, e1-6 (2014).
152. Krueger, M. & Bechmann, I. CNS pericytes: concepts, misconceptions, and a way out. *Glia* **58**, 1-10 (2010).
153. Sims, D.E. The pericyte--a review. *Tissue Cell* **18**, 153-74 (1986).
154. Allt, G. & Lawrenson, J.G. Pericytes: cell biology and pathology. *Cells Tissues Organs* **169**, 1-11 (2001).
155. Shepro, D. & Morel, N.M. Pericyte physiology. *FASEB J* **7**, 1031-8 (1993).
156. Frank, R.N., Dutta, S. & Mancini, M.A. Pericyte coverage is greater in the retinal than in the cerebral capillaries of the rat. *Invest Ophthalmol Vis Sci* **28**, 1086-91 (1987).
157. Zimmermann, K.W. Der feinere Bau der Blutkapillaren. *Z. Anat. Entwicklungsgesch*, 29–109 (1923).
158. Diaz-Flores, L., Gutierrez, R., Varela, H., Rancel, N. & Valladares, F. Microvascular pericytes: a review of their morphological and functional characteristics. *Histol Histopathol* **6**, 269-86 (1991).
159. Armulik, A., Genove, G. & Betsholtz, C. Pericytes: developmental, physiological, and pathological perspectives, problems, and promises. *Dev Cell* **21**, 193-215 (2011).
160. Wu, Z., Hofman, F.M. & Zlokovic, B.V. A simple method for isolation and characterization of mouse brain microvascular endothelial cells. *J Neurosci Methods* **130**, 53-63 (2003).
161. Nehls, V. & Drenckhahn, D. The versatility of microvascular pericytes: from mesenchyme to smooth muscle? *Histochemistry* **99**, 1-12 (1993).
162. Nehls, V. & Drenckhahn, D. Heterogeneity of microvascular pericytes for smooth muscle type alpha-actin. *J Cell Biol* **113**, 147-54 (1991).
163. Ozerdem, U., Grako, K.A., Dahlin-Huppe, K., Monosov, E. & Stallcup, W.B. NG2 proteoglycan is expressed exclusively by mural cells during vascular morphogenesis. *Dev Dyn* **222**, 218-27 (2001).
164. Murfee, W.L., Skalak, T.C. & Peirce, S.M. Differential arterial/venous expression of NG2 proteoglycan in perivascular cells along microvessels: identifying a venule-specific phenotype. *Microcirculation* **12**, 151-60 (2005).
165. Armulik, A., Abramsson, A. & Betsholtz, C. Endothelial/pericyte interactions. *Circ Res* **97**, 512-23 (2005).
166. Winkler, E.A., Bell, R.D. & Zlokovic, B.V. Pericyte-specific expression of PDGF beta receptor in mouse models with normal and deficient PDGF beta receptor signaling. *Mol Neurodegener* **5**, 32 (2010).

167. Chen, Y.T. et al. Platelet-derived growth factor receptor signaling activates pericyte-myofibroblast transition in obstructive and post-ischemic kidney fibrosis. *Kidney Int* **80**, 1170-81 (2011).
168. Fisher, M. Pericyte signaling in the neurovascular unit. *Stroke* **40**, S13-5 (2009).
169. Ballabh, P., Braun, A. & Nedergaard, M. The blood-brain barrier: an overview: structure, regulation, and clinical implications. *Neurobiol Dis* **16**, 1-13 (2004).
170. Wolburg, H., Noell, S., Mack, A., Wolburg-Buchholz, K. & Fallier-Becker, P. Brain endothelial cells and the glio-vascular complex. *Cell Tissue Res* **335**, 75-96 (2009).
171. Cuevas, P. et al. Pericyte endothelial gap junctions in human cerebral capillaries. *Anat Embryol (Berl)* **170**, 155-9 (1984).
172. Stratman, A.N., Malotte, K.M., Mahan, R.D., Davis, M.J. & Davis, G.E. Pericyte recruitment during vasculogenic tube assembly stimulates endothelial basement membrane matrix formation. *Blood* **114**, 5091-101 (2009).
173. Bell, R.D. et al. Pericytes control key neurovascular functions and neuronal phenotype in the adult brain and during brain aging. *Neuron* **68**, 409-27 (2010).
174. Armulik, A. et al. Pericytes regulate the blood-brain barrier. *Nature* **468**, 557-61 (2010).
175. Keller, A. Breaking and building the wall: the biology of the blood-brain barrier in health and disease. *Swiss Med Wkly* **143**, w13892 (2013).
176. Gaengel, K., Genove, G., Armulik, A. & Betsholtz, C. Endothelial-mural cell signaling in vascular development and angiogenesis. *Arterioscler Thromb Vasc Biol* **29**, 630-8 (2009).
177. Winkler, E.A., Bell, R.D. & Zlokovic, B.V. Central nervous system pericytes in health and disease. *Nat Neurosci* **14**, 1398-405 (2011).
178. Dohgu, S. et al. Brain pericytes contribute to the induction and up-regulation of blood-brain barrier functions through transforming growth factor-beta production. *Brain Res* **1038**, 208-15 (2005).
179. Sieczkiewicz, G.J. & Herman, I.M. TGF-beta 1 signaling controls retinal pericyte contractile protein expression. *Microvasc Res* **66**, 190-6 (2003).
180. Lindahl, P., Johansson, B.R., Leveen, P. & Betsholtz, C. Pericyte loss and microaneurysm formation in PDGF-B-deficient mice. *Science* **277**, 242-5 (1997).
181. Hellstrom, M., Kalen, M., Lindahl, P., Abramsson, A. & Betsholtz, C. Role of PDGF-B and PDGFR-beta in recruitment of vascular smooth muscle cells and pericytes during embryonic blood vessel formation in the mouse. *Development* **126**, 3047-55 (1999).
182. Hellstrom, M. et al. Lack of pericytes leads to endothelial hyperplasia and abnormal vascular morphogenesis. *J Cell Biol* **153**, 543-53 (2001).
183. Lindblom, P. et al. Endothelial PDGF-B retention is required for proper investment of pericytes in the microvessel wall. *Genes Dev* **17**, 1835-40 (2003).

184. Joyce, N.C., Haire, M.F. & Palade, G.E. Contractile proteins in pericytes. II. Immunocytochemical evidence for the presence of two isomyosins in graded concentrations. *J Cell Biol* **100**, 1387-95 (1985).
185. Joyce, N.C., Haire, M.F. & Palade, G.E. Contractile proteins in pericytes. I. Immunoperoxidase localization of tropomyosin. *J Cell Biol* **100**, 1379-86 (1985).
186. Bandopadhyay, R. et al. Contractile proteins in pericytes at the blood-brain and blood-retinal barriers. *J Neurocytol* **30**, 35-44 (2001).
187. Elfont, R.M., Sundaresan, P.R. & Sladek, C.D. Adrenergic receptors on cerebral microvessels: pericyte contribution. *Am J Physiol* **256**, R224-30 (1989).
188. van Zwieten, E.J., Ravid, R., Swaab, D.F. & Van de Woude, T. Immunocytochemically stained vasopressin binding sites on blood vessels in the rat brain. *Brain Res* **474**, 369-73 (1988).
189. Dehouck, M.P. et al. Endothelin-1 as a mediator of endothelial cell-pericyte interactions in bovine brain capillaries. *J Cereb Blood Flow Metab* **17**, 464-9 (1997).
190. Haefliger, I.O., Zschauer, A. & Anderson, D.R. Relaxation of retinal pericyte contractile tone through the nitric oxide-cyclic guanosine monophosphate pathway. *Invest Ophthalmol Vis Sci* **35**, 991-7 (1994).
191. Rucker, H.K., Wynder, H.J. & Thomas, W.E. Cellular mechanisms of CNS pericytes. *Brain Res Bull* **51**, 363-9 (2000).
192. Oishi, K., Kamiyashiki, T. & Ito, Y. Isometric contraction of microvascular pericytes from mouse brain parenchyma. *Microvasc Res* **73**, 20-8 (2007).
193. Lee, S. et al. Pericyte actomyosin-mediated contraction at the cell-material interface can modulate the microvascular niche. *J Phys Condens Matter* **22**, 194115 (2010).
194. Dai, M., Nuttall, A., Yang, Y. & Shi, X. Visualization and contractile activity of cochlear pericytes in the capillaries of the spiral ligament. *Hear Res* **254**, 100-7 (2009).
195. Hamilton, N.B., Attwell, D. & Hall, C.N. Pericyte-mediated regulation of capillary diameter: a component of neurovascular coupling in health and disease. *Front Neuroenergetics* **2** (2010).
196. Peppiatt, C.M., Howarth, C., Mobbs, P. & Attwell, D. Bidirectional control of CNS capillary diameter by pericytes. *Nature* **443**, 700-4 (2006).
197. Stefanovic, B. et al. Functional reactivity of cerebral capillaries. *J Cereb Blood Flow Metab* **28**, 961-72 (2008).
198. Hall, C.N. et al. Capillary pericytes regulate cerebral blood flow in health and disease. *Nature* **508**, 55-60 (2014).
199. Fernandez-Klett, F., Offenhauser, N., Dirnagl, U., Priller, J. & Lindauer, U. Pericytes in capillaries are contractile in vivo, but arterioles mediate functional hyperemia in the mouse brain. *Proc Natl Acad Sci U S A* **107**, 22290-5 (2010).
200. Webb, R.C. Smooth muscle contraction and relaxation. *Adv Physiol Educ* **27**, 201-6 (2003).

201. Kamouchi, M. et al. Calcium influx pathways in rat CNS pericytes. *Brain Res Mol Brain Res* **126**, 114-20 (2004).
202. Kamouchi, M., Ago, T., Kuroda, J. & Kitazono, T. The possible roles of brain pericytes in brain ischemia and stroke. *Cell Mol Neurobiol* **32**, 159-65 (2012).
203. Yemisci, M. et al. Pericyte contraction induced by oxidative-nitrative stress impairs capillary reflow despite successful opening of an occluded cerebral artery. *Nat Med* **15**, 1031-7 (2009).
204. Dalkara, T., Gursoy-Ozdemir, Y. & Yemisci, M. Brain microvascular pericytes in health and disease. *Acta Neuropathol* **122**, 1-9 (2011).
205. Fernandez-Klett, F. et al. Early loss of pericytes and perivascular stromal cell-induced scar formation after stroke. *J Cereb Blood Flow Metab* **33**, 428-39 (2013).
206. Melgar, M.A., Rafols, J., Gloss, D. & Diaz, F.G. Postischemic reperfusion: ultrastructural blood-brain barrier and hemodynamic correlative changes in an awake model of transient forebrain ischemia. *Neurosurgery* **56**, 571-81 (2005).
207. Gonul, E. et al. Early pericyte response to brain hypoxia in cats: an ultrastructural study. *Microvasc Res* **64**, 116-9 (2002).
208. Duz, B., Oztas, E., Erginay, T., Erdogan, E. & Gonul, E. The effect of moderate hypothermia in acute ischemic stroke on pericyte migration: an ultrastructural study. *Cryobiology* **55**, 279-84 (2007).
209. Liu, S., Agalliu, D., Yu, C. & Fisher, M. The role of pericytes in blood-brain barrier function and stroke. *Curr Pharm Des* **18**, 3653-62 (2012).
210. Renner, O. et al. Time- and cell type-specific induction of platelet-derived growth factor receptor-beta during cerebral ischemia. *Brain Res Mol Brain Res* **113**, 44-51 (2003).
211. Ozen, I. et al. Brain pericytes acquire a microglial phenotype after stroke. *Acta Neuropathol* **128**, 381-96 (2014).
212. Thomas, W.E. Brain macrophages: on the role of pericytes and perivascular cells. *Brain Res Brain Res Rev* **31**, 42-57 (1999).
213. Kooijman, E. et al. The rodent endovascular puncture model of subarachnoid hemorrhage: mechanisms of brain damage and therapeutic strategies. *J Neuroinflammation* **11**, 2 (2014).
214. Sabri, M., Kawashima, A., Ai, J. & Macdonald, R.L. Neuronal and astrocytic apoptosis after subarachnoid hemorrhage: a possible cause for poor prognosis. *Brain Res* **1238**, 163-71 (2008).
215. Zhu, X., Bergles, D.E. & Nishiyama, A. NG2 cells generate both oligodendrocytes and gray matter astrocytes. *Development* **135**, 145-57 (2008).
216. Direnberger, S. et al. Biocompatibility of a genetically encoded calcium indicator in a transgenic mouse model. *Nat Commun* **3**, 1031 (2012).
217. Geiger, A. et al. Correlating calcium binding, Forster resonance energy transfer, and conformational change in the biosensor TN-XXL. *Biophys J* **102**, 2401-10 (2012).

218. Yamamoto, K., Korenaga, R., Kamiya, A. & Ando, J. Fluid shear stress activates Ca(2+) influx into human endothelial cells via P2X4 purinoceptors. *Circ Res* **87**, 385-91 (2000).
219. Griesbeck, O., Baird, G.S., Campbell, R.E., Zacharias, D.A. & Tsien, R.Y. Reducing the environmental sensitivity of yellow fluorescent protein. Mechanism and applications. *J Biol Chem* **276**, 29188-94 (2001).
220. Holtmaat, A. et al. Long-term, high-resolution imaging in the mouse neocortex through a chronic cranial window. *Nat Protoc* **4**, 1128-44 (2009).
221. Nakamura, T. et al. Acute CO2-independent vasodilatation of penetrating and pre-capillary arterioles in mouse cerebral parenchyma upon hypoxia revealed by a thinned-skull window method. *Acta Physiol (Oxf)* **203**, 187-96 (2011).
222. Kobat, D. et al. Deep tissue multiphoton microscopy using longer wavelength excitation. *Opt Express* **17**, 13354-64 (2009).
223. Mutant mice and neuroscience: recommendations concerning genetic background. Banbury Conference on genetic background in mice. *Neuron* **19**, 755-9 (1997).
224. Feiler, S., Friedrich, B., Scholler, K., Thal, S.C. & Plesnila, N. Standardized induction of subarachnoid hemorrhage in mice by intracranial pressure monitoring. *J Neurosci Methods* **190**, 164-70 (2010).
225. Fujii, M. et al. Early brain injury, an evolving frontier in subarachnoid hemorrhage research. *Transl Stroke Res* **4**, 432-46 (2013).
226. Strack, R.L. et al. A noncytotoxic DsRed variant for whole-cell labeling. *Nat Methods* **5**, 955-7 (2008).
227. Erturk, A. et al. Three-dimensional imaging of solvent-cleared organs using 3DISCO. *Nat Protoc* **7**, 1983-95 (2012).
228. Vates, G.E., Takano, T., Zlokovic, B. & Nedergaard, M. Pericyte constriction after stroke: the jury is still out. *Nat Med* **16**, 959; author reply 960 (2010).
229. Stanimirovic, D.B., Nikodijevic, B., Nikodijevic-Kedeva, D., McCarron, R.M. & Spatz, M. Signal transduction and Ca2+ uptake activated by endothelins in rat brain endothelial cells. *Eur J Pharmacol* **288**, 1-8 (1994).
230. Scharbrodt, W. et al. Cytosolic Ca2+ oscillations in human cerebrovascular endothelial cells after subarachnoid hemorrhage. *J Cereb Blood Flow Metab* **29**, 57-65 (2009).
231. Ewing, J.R. et al. Direct comparison of local cerebral blood flow rates measured by MRI arterial spin-tagging and quantitative autoradiography in a rat model of experimental cerebral ischemia. *J Cereb Blood Flow Metab* **23**, 198-209 (2003).
232. Akli, S. et al. Transfer of a foreign gene into the brain using adenovirus vectors. *Nat Genet* **3**, 224-8 (1993).

Acknowledgement

I first would like to thank Prof. Nikolaus Plesnila for providing me the opportunity to perform research on subarachnoid hemorrhage in a translational context. He always supported my work and motivated me with his great enthusiasm.

I also want to thank the whole group AG Plesnila for the nice and inspiring working atmosphere. Special thanks go to Uta and Kathrin, who always supported me in solving minor and major problems. I want to thank our post docs Farida, Manuela and Lilja for their scientific and overall consultant support. Further Sepiede and Dominik were super-supportive during my time in the laboratory. Without the help of these people the completion of my thesis would hardly have been possible.

I am very grateful for my excellent Thesis Advisory Committee who was always eager to improve my work and provided important scientific input.

The Graduate School of Systemic Neurosciences provided the framework and money to discover neurosciences in a broader and exciting environment. Especially the organization of numerous social events and travels encouraged researcher from different fields to communicate and interact.

I want to thank my family and all my friends for their support and patience during the last couple of years.

Last but not least I want to thank my proofreaders Annette and Sepiede.

Current publications

- **Schuller, K**., Buhler, D. & Plesnila, N. A murine model of subarachnoid hemorrhage. *J Vis Exp*, e50845 (2013)
  doi: 10.3791/50845

- Buhler, D., **Schuller, K**. & Plesnila, N. Protocol for the induction of subarachnoid hemorrhage in mice by perforation of the Circle of Willis with an endovascular filament. *Transl Stroke Res* **5**, 653-9 (2014)
  doi: 10.1007/s12975-014-0366-6

- Buhler, D., Azghandi, S., **Schuller, K.** & Plesnila, N. Effect of Decompressive Craniectomy on Outcome Following Subarachnoid Hemorrhage in Mice. *Stroke* (2015)
  doi: 10.1161/STROKEAHA.114.007703

Eidesstattliche Versicherung

Hiermit versichere ich an Eides statt, dass ich die vorliegende Dissertation „The role of pericytes in microcirculatory dysfunction after subarachnoid hemorrhage“ selbstständig angefertigt habe, mich außer der angegebenen keiner weiteren Hilfsmittel bedient und alle Erkenntnisse, die aus dem Schrifttum ganz oder annähernd übernommen sind, als solche kenntlich gemacht und nach ihrer Herkunft unter Bezeichnung der Fundstelle einzeln nachgewiesen habe.

München, _____

Kathrin Nehrkorn (geb. Schüller)

Scientific contribution

1. **A murine model of subarachnoid hemorrhage**
   Authors: Kathrin Schüller (KS), Dominik Bühler (DB), Nikolaus Plesnila (NP)
   Plan experiments: KS and NP
   Acquire data: KS and DB
   Analyze data: KS and DB
   Write manuscript: KS and NP

2. **Impairment of the cerebral microcirculation after subarachnoid hemorrhage**
   Authors: Kathrin Schüller (KS), Uta Mamrak (UM), Nikolaus Plesnila (NP)
   Plan experiments: KS and NP
   Acquire data: KS and UM
   Analyze data: KS
   Write manuscript: KS and NP

3. **The role of pericytes on microcirculatory dysfunction after subarachnoid hemorrhage**
   Authors: Kathrin Schüller (KS), Matilde Balbi (MB), Nikolaus Plesnila (NP)
   Plan experiments: KS and NP
   Acquire data: KS and MB
   Analyze data: KS
   Write manuscript: KS and NP

4. ***In vivo* Ca^{2+}- imaging in cerebral endothelial cells**
   Authors: Kathrin Schüller (KS), Arne Fabritius (AF), Farida Hellal (FH), Oliver Griesbeck (OG), Nikolaus Plesnila (NP)
   Plan experiments: KS and NP
   Provide animals: AF and OG
   Acquire data: KS and FH
   Analyze data: KS
   Write manuscript: KS and NP

Munich, _____ _____
Prof. Nikolaus Plesnila

Munich, _____ _____
Kathrin Nehrkorn (geb. Schüller)